Mechanism of neuronal death in familial encephalopathy with neuroserpin inclusion bodies (FENIB)

Implications for mutant neuroserpin degradation – a study in *mus musculus*

Dissertation

Zur Erlangung der Würde des Doktors der Naturwissenschaften
des Fachbereichs Biologie, der Fakultät für Mathematik, Informatik und Naturwissenschaften,
der Universität Hamburg

vorgelegt von

Angela Schipanski
aus Ilmenau

Hamburg

Genehmigt vom Fachbereich Biologie
der Fakultät für Mathematik, Informatik und Naturwissenschaften
an der Universität Hamburg
auf Antrag von Prof. Dr. M. Glatzel
Weiterer Gutachter der Dissertation:
Prof. Dr. C. Voigt
Tag der Disputation: 23. Juni 2011

Hamburg, den 10. Juni 2011

Universität Hamburg
64
Fakultät
Mathematik, Informatik und Naturwissenschaften

Professor Dr. Axel Temming
Leiter des Fachbereichs Biologie

Language Certificate

Dr Stefan Marciniak PhD
MRC Clinician Scientist/Honorary Consultant Physician

Tel: 01223 762660
Fax: 01223 336827
E-mail: sjm20@cam.ac.uk

UNIVERSITY OF CAMBRIDGE
Cambridge Institute for Medical Research
Wellcome Trust/MRC Building
Hills Road
Cambridge CB2 0XY

21 April 2011

TO WHOM IT MAY CONCERN

Dear Sir/Madam

I am a native English speaker. I have read this PhD thesis and hereby confirm that it complies with the rules of the English language.

Yours sincerely

Stefan Marciniak

meinen Eltern

Index

1. Abstract

The inheritable dementia FENIB (familial encephalopathy with neuroserpin inclusion bodies) is caused by the accumulation of ordered polymers of mutant neuroserpin within the endoplasmic reticulum (ER) of neurons. Intracellular deposits of mutant neuroserpin challenge the fidelity of protein homeostasis, also proteostasis, which ensures a balanced interplay between protein synthesis, folding and clearance. Maintenance of cytosolic neuronal proteostasis is supported by the ubiquitin proteasome system (UPS) and the autophagy-lysosomal pathways. As mutant neuroserpin accumulates in the ER of neurons, we addressed how disturbance of ER proteostasis leads to neurodegeneration in a murine model of FENIB.

Specifically, we studied the role of ER associated degradation (ERAD) and autophagy on mutant neuroserpin degradation in mice expressing mutant *Tg*(NS^{S49P}) or wild-type *Tg*(NS) neuroserpin. We showed that mutant neuroserpin is specifically degraded by the proteasome via ERAD and non-specifically by autophagy. Only when the proteasomal activity is impaired, does autophagy contribute to mutant neuroserpin degradation. Further on, we studied the impact of the unfolded protein response (UPR) in regulating amounts of aggregated proteins. Transient induction of UPR in *Tg*(NS^{S49P}) mice controls polymeric protein formation and aggregation in young mice. With increasing age, the capacity to mount UPR ceases and the amount of polymeric proteins and aggregates rises exponentially.

Thus, our data support the concept of disturbed neuronal proteostasis in dementias and point towards age-related exhaustion of proteostasis maintaining mechanisms which are decisive for disease progression in dementias with intracellular protein depositions.

2. Introduction

2.1 Serpins

Serpins are a superfamily of serine protease inhibitors characterized by their common structure and their unique suicide inhibitory mechanism (Lomas et al., 2005; Silverman et al., 2001). They are highly conserved throughout species ranging from plants to viruses to humans (Irving et al., 2000; Silverman et al., 2001). Serpins are multifaceted, thus playing a central role in regulating enzymes involved in a diversity of biological functions (Lomas, 2002), like inflammation and blood pressure regulation (Silverman et al., 2001).

Members of the serpin superfamily controlling intra- and extra-cellular proteolytic pathways are well characterized (Lomas, 2002). For example, in human plasma: C1-inhibitor controls complement activation, α1-antitrypsin protects the connective tissue of the lungs from elastase released by leukocytes, antithrombin controls the destruction of released coagulation proteases, and the inhibitors of plasmin together with its activators control fibrinolysis (Carrell and Lomas, 2002; Huntington et al., 2000; Lomas, 2002). All family members share more than 30 % amino acid sequence homology with the archetypal α1-antitrypsin which is the most intense studied serpin (Gooptu and Lomas, 2009; Lomas and Mahadeva, 2002).

Neuroserpin is involved in synaptogenesis and synaptic plasticity (Hastings et al., 1997; Krueger et al., 1997; Osterwalder et al., 1996) as well as in neuroprotection (Wannier-Morino et al., 2003; Wu et al., 2010). It shares 33 % homology with α1-antitrypsin (Miranda and Lomas, 2006; Osterwalder et al., 1996; Schrimpf et al., 1997). It is expressed predominantly in neurons of the nervous system (Hastings et al., 1997; Osterwalder et al., 1996; Stoeckli et al., 1989) where it is axonally secreted and inhibits tissue type plasminogen activator (tPA) (Krueger et al., 1997; Osterwalder et al., 1998).

2.1.1. Structure and inhibitory mechanisms of Serpins

Serpins are composed of 350-450 amino acids (Silverman et al., 2001). They fold into a native metastable conformation rather than adopting the most stable state (Elliott et al., 1996; Whisstock and Bottomley, 2006). Their tertiary structure is in most cases composed of nine α-helices (hA to hI), three ß-sheets (A to C with A being the largest), and a mobile reactive centre loop (RCL) (Gettins, 2002; Loebermann et al., 1984; Silverman et al., 2001) (Fig. 1).

The basic structural elements are the central ß-sheet A (Fig. 1; in green) composed of five strands and the exposed mobile reactive centre loop (Fig. 1; in red) above the body of the serpin scaffold. The RCL contains 20-25 amino acids determining the serpins' specificity which functions as a pseudo-substrate for the target protease (Elliott et al., 1998; Elliott et al., 1996; Kim et al., 2001; Ryu et al., 1996). Once the serpin-protease complex is formed, the protease recognizes and cleaves the RCL at the P1-P1' peptide bond (Huntington et al., 2000; Loebermann et al., 1984; Wilczynska et al., 1997; Wilczynska et al., 1995). The cleavage of the RCL triggers an extensive conformational change in which the bound proteinase is translocated from the upper to the lower pole of the serpin molecule (Stratikos and Gettins, 1999). At the same time the RCL is incorporated into the ß-sheet A of the serpin (Huntington et al., 2000). This molecular rearrangement rigorously distorts the overall structure of the protease resulting in inactivation and targeting degradation (Huntington et al., 2000; Stratikos and Gettins, 1999; Wilczynska et al., 1997; Wilczynska et al., 1995). Concomitantly, the overall stability of the serpins is increased; typically the T_m for cleaved serpins is >100 °C, compared with less than 60 °C for the native state (Kaslik et al., 1997). The remarkable conformational change during inhibition explains the efficiency of serpins and may explain their ubiquitous appearance (Huntington et al., 2000; Lomas et al., 2005).

In addition to native and cleaved states, selective serpins adopt an inactive "latent" conformation harbouring physiological relevance (Whisstock and Bottomley, 2006). Latent serpins incorporate their intact RCL fully into ß-sheet A without a cleavage event (Whisstock and Bottomley, 2006). For example, plasminogen activator inhibitor-1 (PAI-1) is normally in its latent state until its activation by cofactor vitronectin (Declerck et al., 1988; Wiman et al., 1988).

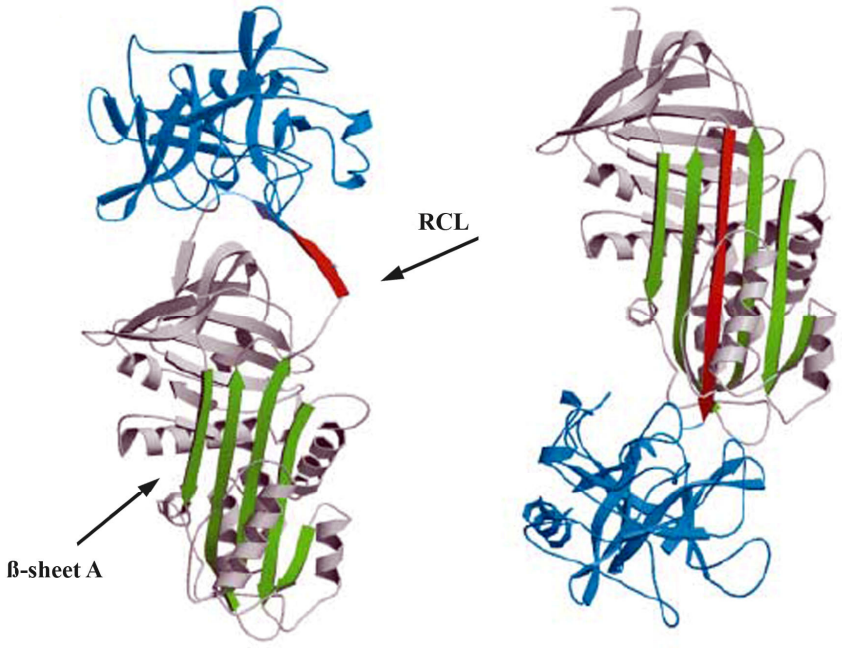

Figure 1: Serpins inhibit their target proteinase by a conformational transition

Serine proteinase inhibitors, such as the depicted α1-antitrypsin, are hallmarked by their central ß-sheet A (green) and an exposed reactive centre loop (red). The target protease, in this case neutrophile elastase (blue), docks to the RCL (left), thereby being inactivated by a translocation from the upper to the lower pole of the molecule (right). This is accompanied by an incorporation of the reactive centre loop as an additional strand into ß-sheet A of the serpin. Adapted and modified from (Gooptu and Lomas, 2009; Huntington et al., 2000; Lomas, 2002).

2.1.2. Serpinopathies – conformational diseases

Due to their high molecular flexibility, serpins are vulnerable to dysfunction (Carrell and Lomas, 1997; Lomas et al., 2005; Lomas, 2002). Point mutations in the mobile domains of serpin destabilize their already metastable conformation resulting in aberrant rearrangements and transitions leading to their retention (Lomas et al., 1992).

In the classical serpin polymerisation model, a point mutation destabilizes the central ß-sheet A (Fig. 2; orange circle) which leads to an opening of the five-stranded sheet, thus allowing the incorporation of the RCL of another serpin molecule to form a dimer (Fig. 2; D). Repeated cycles of RCL incorporation results in the formation of chains of loop-sheet polymers (Fig. 2; P) (Dafforn et al., 1999; Gooptu et al., 2000; Lomas et al., 1992; Mahadeva et al., 2002). This process was first described in detail for mutant Z α1-antitrypsin and was

then transferred to other serpin mutants causing disease through polymer formation (Davis et al., 1999b; Lomas et al., 1992).

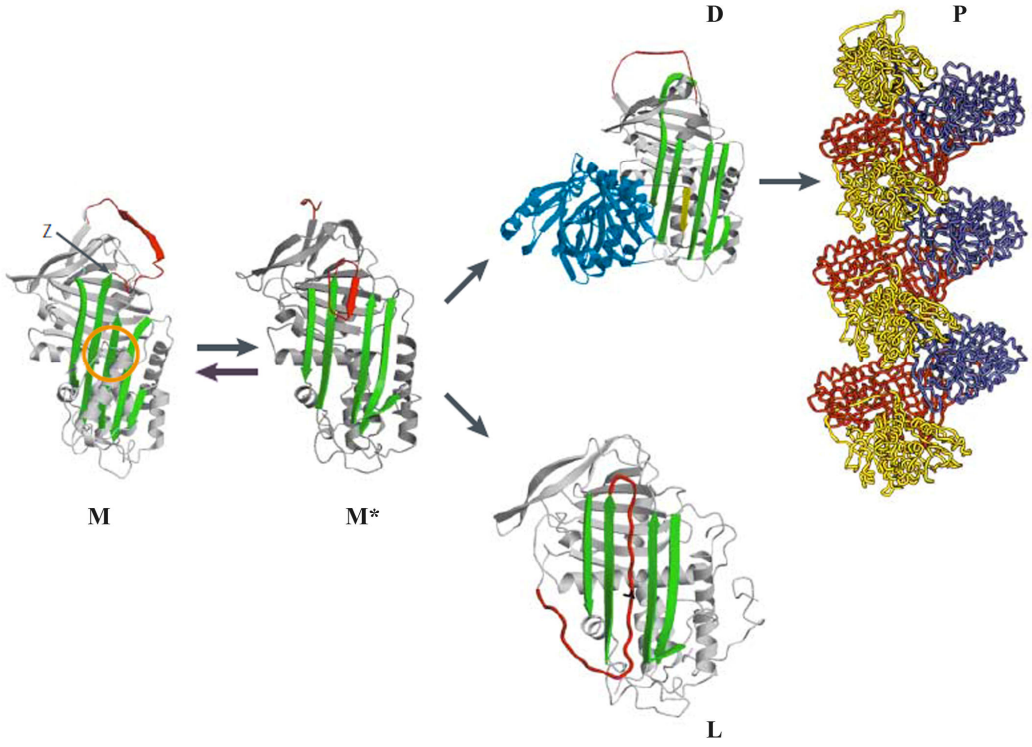

Figure 2: Classical serpin polymerisation model represented by α1-antitrypsin

Point mutations in the shutter domain (orange circle) or at the hinge region (between ß-sheet A (green) and the loop containing the reactive centre (red)) open ß-sheet A allowing partial loop insertion into the molecule to form an unstable intermediate M* (Dafforn et al., 1999; Gooptu et al., 2000; Mahadeva et al., 2002). Depicted here is the case for mutant Z α1-antitripysin (long thin black arrow). The open ß-sheet A can accept the loop of another molecule to form a dimer (D) which extends to form polymers (P) (Lomas et al., 2002; Sivasothy et al., 2000). Another possibility for the unstable intermediate M* is to insert its own RCL to form a latent conformation (L) (Lomas, 2005; Onda et al., 2005). The single α1-antitripysin molecules in the polymer (P) are highlighted in yellow, red and blue. Adapted and modified from (Gooptu and Lomas, 2008; Lomas, 2002).

Recently, a second polymerisation model based on the crystal structure of dimeric antithrombin was published (Yamasaki et al., 2008). This model proposes destabilising mutations at the top of ß-sheet A as well as in the shutter region causing partial extrusion of strand 5 of the central ß-sheet A (Yamasaki et al., 2008). Thereby an intermediate is formed with a hairpin domain out of the unfolded RCL and strand 5 (Fig. 3;M*) (Yamasaki et al., 2008). Polymers are built by insertion of the hairpin domain into another serpin molecule,

which also has an extruded strand 5 (Fig. 3;P) (Yamasaki et al., 2008). Although structure and origin of the intermediate M* is different in both models, the destabilizing effect of mutations to ß-sheet A and the propensity to form polymers are identical (Yamasaki et al., 2008). Nevertheless, recent studies favoured the classical polymerisation model as it best explains biochemical properties of polymerogenic intermediate and pathological polymers formed by mutant α1-antitrypsin (Ekeowa et al., 2010).

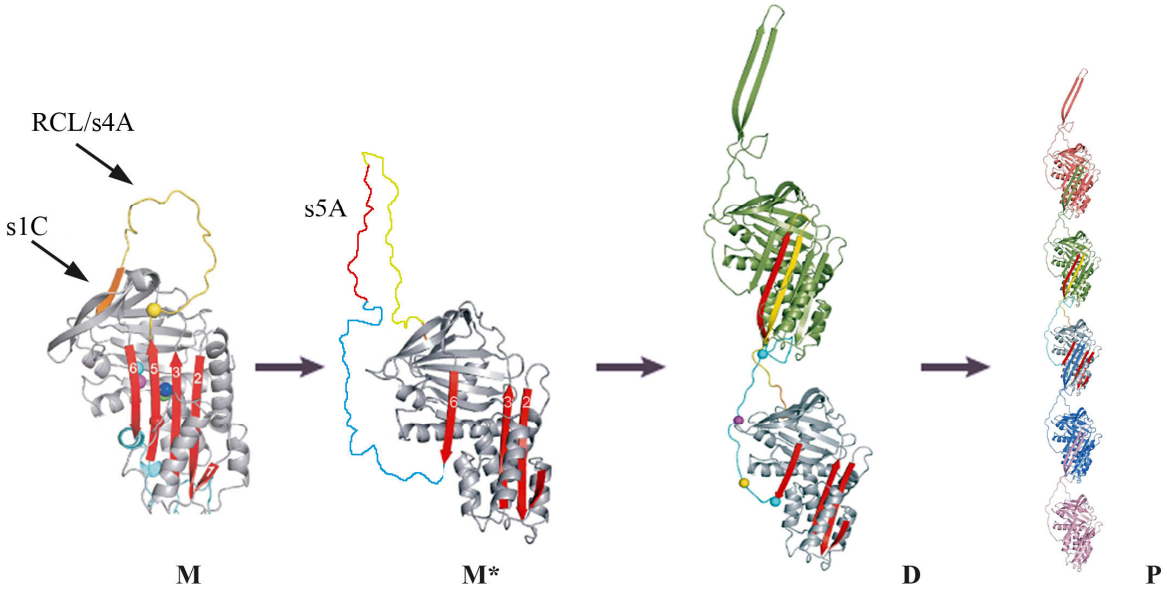

Figure 3: Newly suggested serpin polymerisation model represented by dimeric antithrombin

Point mutations destabilise the central ß-sheet A (red). This leads to an extrusion of strand 5 of ß-sheet A, whereby an intermediate M* with a protruding hairpin out of strand 5A (red), the reactive centre loop s4A (yellow) and the partial unfolded helix I (blue), is formed. The M* can donate the protruding hairpin into ß-sheet A of another extruded serpin to form dimers (D) and continue to form polymers (B). Adapted and modified from (Yamasaki et al., 2008).

As the formation of mutant polymers occurs during biosynthesis, the aggregates are deposited in the cell of synthesis. This evokes a damage of the tissue either by a toxic gain of function from the inclusions or loss of function due to insufficient protease inhibitors for regulating proteolytic activity (Lomas et al., 2005; Lomas, 2002). The clinical outcomes of such diseases are as diverse as cirrhosis, thrombosis, angio-oedema, emphysema, and dementia (Carrell and Lomas, 2002; Lomas, 2002). Due to their common underlying mechanism, these diseases are grouped together as serpinopathies (Carrell and Lomas, 2002; Lomas and Mahadeva, 2002; Lomas, 2002). This was first reported for mutant α1-antitrypsin

where accumulations in the ER of hepatocytes occur, causing plasma deficiency of the protein directly evoking liver damage (Lomas et al., 1992). It was also shown that mutant neuroserpin is retained within neurons of the brain, causing a severe dementia (Davis et al., 1999b; Miranda et al., 2004). Remarkably, mutations leading to a high protein-instability result in more intracellular retention causing earlier disease onset and more severe clinical manifestation, indicating a strong genotype-phenotype correlation (Carrell and Lomas, 2002).

2.2 Neuroserpin

Neuroserpin has been identified in a screen for neuronal proteins involved in axonal growth and synapse formation (Stoeckli et al., 1989). It is an axonally secreted serpin expressed by neurons of the central and peripheral nervous system (Osterwalder et al., 1996). The protein was purified from the ocular vitreous fluid of chicken embryo making an amino acid microsequencing possible (Osterwalder et al., 1996). A sequence analysis assigned neuroserpin as a new member of the serpin superfamily, termed Proteinase Inhibitor 12 (PI12, gene symbol SERPINI1) (Schrimpf et al., 1997; Silverman et al., 2001). The cDNA of chicken neuroserpin served as a template to isolate human and mouse counterparts, revealing an amino acid sequence homology of 80 % to human and 76 % to mouse neuroserpin (Krueger et al., 1997; Schrimpf et al., 1997). In addition, human neuroserpin shares 86 % amino acid sequence homology with mouse neuroserpin (Krueger et al., 1997; Schrimpf et al., 1997).

The human neuroserpin gene is mapped to chromosome 3q26 (Schrimpf et al., 1997). It is composed of nine exons (Berger et al., 1998), giving rise to an open reading frame spanning over 1230 nucleotides encoding a protein of 410 amino acids (Schrimpf et al., 1997). Neuroserpin has three predicted N-glycosylation sites (at position 157, 321, and 401) and the first 16 amino acids were assigned as a signal peptide for secretion. Thus, the mature protein has a molecular mass of approximately 55 kDa (Hastings et al., 1997; Schrimpf et al., 1997). As the amino acids arginine and methionine are at position P_1 and P_1', respectively, like scissile bonds in the RCL, neuroserpin could be identified as an inhibitory trypsin-like serine protease (Schrimpf et al., 1997). Additionally, a heparin-binding exosite was not identified, proposing an anti-proteolytic activity of neuroserpin without the support of heparin (Hastings et al., 1997; Schrimpf et al., 1997).

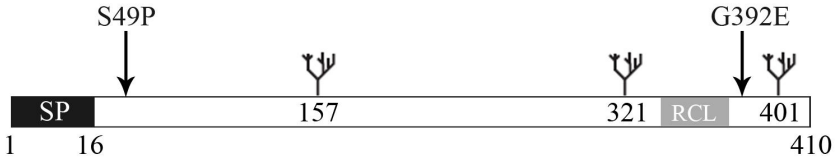

Figure 4: Schematic representation of human neuroserpin

Human neuroserpin is 410 amino acids long. It has three predicted N-linked glycosylation sites at positions 157, 321 and 401, a signal peptide (SP) (black), consisting of 16 amino acids, and a reactive centre loop (RCL) (grey) (Hastings et al., 1997; Schrimpf et al., 1997). Possible sites for amino acid substitutions are indicated at position 49 (S to P) and 392 (G to E) which cause a disease called familial encephalopathy with neuroserpin inclusion bodies (FENIB) (Davis et al., 2002).

Neuroserpin is expressed during the late stages of neurogenesis, when neurons migrate and synapse formation takes place. In the adult brain neuroserpin is found in areas where synaptic changes associated with learning and memory occurs, including the cerebral cortex and the hippocampus (Hastings et al., 1997; Krueger et al., 1997; Osterwalder et al., 1996). These features implicate neuroserpin to be a modulator for local extracellular proteolytic events involved in reorganization of the synaptic connectivity during development and synaptic plasticity in the adult nervous system (Osterwalder et al., 1996). The expression of neuroserpin is not solely restricted to brain. Protein levels of neuroserpin were detected in pancreas and testis, whereas only mRNA could be detected in heart and kidney (Hastings et al., 1997; Krueger et al., 1997; Schrimpf et al., 1997). Recently, neuroserpin was purified of dense-cored secretory vesicles of pituitary and adrenal glands (Hill et al., 2000).

The main target of neuroserpin is presumably tPA, but it also inhibits to a lesser extent urokinase-type plasminogen activator (uPA) and plasmin, but no inhibitory activity against thrombin was shown (Hastings et al., 1997; Krueger et al., 1997; Osterwalder et al., 1998). Primarily, tPA acts as a thrombolytic enzyme in the regulation of blood coagulation. Beyond that it is involved in neuronal development, motor learning and synaptogenesis (Yepes and Lawrence, 2004a, b). The highest levels of neuroserpin expression are found in regions of the brain where either tPA message or tPA protein has been found (Hastings et al., 1997; Krueger et al., 1997; Osterwalder et al., 1998; Schrimpf et al., 1997; Yepes and Lawrence, 2004a, b). The common tissue distribution of neuroserpin and tPA further indicates that neuroserpin is the selective inhibitor of tPA in the central nervous system (CNS) (Yepes and Lawrence, 2004a, b). Kinetic studies of the neuroserpin-tPA complex revealed a half-life of only minutes

compared to weeks observed for other serpin-cognate protease complexes (Ricagno et al., 2009).

2.2.1. Mutations in neuroserpin gene cause familial encephalopathy with neuroserpin inclusion bodies (FENIB)

Mutations in the neuroserpin gene give rise to polymeric protein aggregation causing a progressive pre-senile dementia called familial encephalopathy with neuroserpin inclusion bodies or FENIB (Bradshaw et al., 2001; Davis et al., 1999a; Davis et al., 1999b). Five different mutations in the gene coding for neuroserpin (serine 49 to proline (S49P), serine 52 to arginine (S52R), histidine 338 to arginine (H338R), glycine 392 to glutamic acid (G392E) and glycine 392 to arginine (G392R)) have been described in humans (Coutelier et al., 2008; Davis et al., 1999a; Davis et al., 2002; Davis et al., 1999b; Takao et al., 2000). All five mutations induce spontaneous formation of neuroserpin polymers that are retained as inclusion bodies (Collin bodies) within neurons (Table 1) (Davis et al., 2002; Davis et al., 1999b). The mechanism for neuroserpin polymerisation corresponds to serpin α1-antitrypsin as shown in 2.1.2 in Fig. 2 (Briand et al., 2001; Davis et al., 1999b; Gooptu and Lomas, 2009).

The first mutation identified to cause FENIB was S49P (Fig. 4) (Davis et al., 1999a; Davis et al., 1999b). Members of a Caucasian family living in the United States revealed unusual signs of dementia with seizures in their fifties to sixties (Table 1) (Davis et al., 1999a; Davis et al., 1999b). Post-mortem histological analysis of the brain exhibited eosinophilic neuronal inclusions in deep cortical layers consisting of mutant neuroserpin (Davis et al., 1999a; Davis et al., 1999b). DNA sequencing indicated a point mutation (T to C transition at nucleotide 226) resulting in a substitution of serine 49 to an uncharged small proline (S49P). As the S49P mutation was discovered in a family from Syracuse (New York), it is called Syracuse mutation. All affected members of the family were heterozygous for the mutation (Davis et al., 1999a; Davis et al., 1999b) indicating an autosomal dominant mood of inheritance. A second family, coming from Portland, described to carry the S52R mutation (Portland), where serine 52 is replaced by a bulky charged arginine. This mutation was characterized by an earlier disease onset in their thirties, more severe clinical symptoms (dementia with myoclonus) and at post-mortem a higher number of inclusions in the brain (Table 1) (Davis et al., 1999a; Davis et al., 1999b; Takao et al., 2000). Further investigations revealed two more disease-causing mutations in the neuroserpin gene: H338R and G392E

(Davis et al., 2002). Both of them are characterized by more severe symptoms (progressive myoclonus, epilepsy) and more inclusions in brain; and earlier disease onset (Table 1) (Davis et al., 2002). Recently, a fifth mutation (G392R) has been described (Fig. 4). This mutation results in the most severe type of FENIB with disease onset at eight years of age (Table 1) (Coutelier et al., 2008).

The different degrees of clinical presentations of FENIB (dementia, seizures, progressive myoclonic and epilepsy) depend on the type of mutation, displaying a close genotype-phenotype relationship (Davis et al., 2002). The predictable conformational instability of the different mutant proteins is as follow: G392R > G392E > H338R > S52R > S49P (Table 1) (Davis et al., 2002).

The two mild-polymerizing mutants of neuroserpin, S49P and S52R, have been well characterized biochemically and in a cell culture model (Belorgey et al., 2002; Belorgey et al., 2004; Miranda et al., 2008; Miranda et al., 2004; Onda et al., 2005). Recombinant human S49P neuroserpin is a poor proteinase inhibitor ($0.3 \times 10^4 M^{-1}s^{-1}$ versus $1.2 \times 10^4 M^{-1}s^{-1}$ for wild-type form at 25 °C), while S52R neuroserpin completely lost its inhibitory activity (Belorgey et al., 2002; Belorgey et al., 2004). Additionally, when incubated at 37 °C, wild-type protein does not polymerise, whereas both mutant neuroserpin showed an accelerated rate of polymerisation, with S52R polymerising 15 times faster than S49P (Belorgey et al., 2002; Belorgey et al., 2004; Onda et al., 2005).

Table 1: Striking genotype-phenotype correlation between mutations in neuroserpin and the severity of FENIB

mutation	rate of polymerisation	number of inclusions	age of disease onset (years)	clinical features
S49P	+	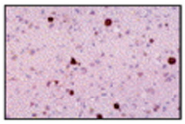	45-63	dementia, seizure
S52R	++	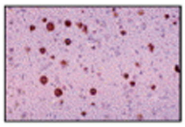	20-40	dementia, myoclonus
H338R	+++	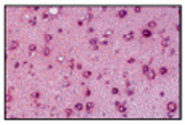	15	progressive myoclonus, epilepsy
G392E	++++	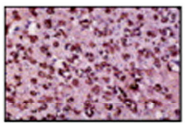	13	progressive myoclonus, epilepsy, chorea
G392R	+++++	N/A	8	dementia, epilepticus of slow-wave sleep

Mutants of neuroserpin clearly demonstrate the strong correlation between the amount of neuroserpin accumulations and the severity of the disease. Mutations leading to a high protein-instability result in more intracellular retention and an earlier disease onset. The destabilizing effects of all five mutations are underpinned by *in vitro* biochemical and cell culture analysis (Belorgey et al., 2002; Belorgey et al., 2004; Miranda et al., 2008; Miranda et al., 2004). Intracellular aggregates of mutant neuroserpin are depicted in cross sections of cerebral cortex stained for inclusions. The late-onset polymerizing mutant S49P shows smaller inclusions, with moderate disease progression associated with age of onset of the dementia at 48-63 years. The number of detectable inclusions increases with the instability of mutant protein. This is best demonstrated by G392E and G392R, where the disease shows the first symptoms in childhood. The + indicates relative rates of polymerization. Modified and adapted from (Coutelier et al., 2008; Davis et al., 2002; Lomas, 2002).

In a FENIB cell culture model it was shown that mutant neuroserpin (S49P and S52R) is retained in inclusion bodies within the ER (Miranda et al., 2008; Miranda et al., 2004). The polymeric nature of these inclusions became apparent by non-denaturating PAGE and immunoblotting (Miranda et al., 2008; Miranda et al., 2004). Further on, Miranda and co-workers showed by a pulse-chase assay that wild-type neuroserpin is readily secreted (half time for secretion is 1h) whereas neuroserpin mutants had a significant delay in their secretion as polymers (half time for secretion, 11h for S52R and 5h for S49P) (Miranda et al., 2004).

Galliciotti and co-workers came up with a mouse model for the Syracuse and Portland mutation causing FENIB. They generated mice over-expressing human wild-type, S49P and

S52R neuroserpin under the neuronal Thy-1 promoter (Galliciotti et al., 2007). These mice showed an increased accumulation of mutant neuroserpin aggregates in neurons, accompanied by clinical symptoms like ataxia, slow movements, seizure-like episodes and tremor, resembling those found in FENIB patients (Galliciotti et al., 2007). These data confirmed that the amount of neuroserpin inclusions correlates with the predicted instability of the protein (Galliciotti et al., 2007). Ultra structural analysis and sub-cellular fractionation suggested ER localization of mutant neuroserpin. Biochemical purification confirmed their mutant composition (Galliciotti et al., 2007). In addition, inclusions were present in brain long before the occurrence of clinical symptoms (Galliciotti et al., 2007).

Recently, a mouse model of FENIB expressing G392E neuroserpin has been described (Takasawa et al., 2008). This model demonstrated accumulation of mutant neuroserpin in the ER and in lysosomal-like compartments, which increased with age (Takasawa et al., 2008). Interestingly, the only phenotype specific for G392E mice was an increased susceptibility to kainite-induced seizures when compared to non-transgenic mice (Takasawa et al., 2008).

A yet unanswered question is how the intracellular retained mutant neuroserpin contributes to the clinical features of FENIB. The lack of functional neuroserpin in the extracellular space might lead to uncontrolled activation of proteolytic cascades (loss of function), or the retained neuroserpin might be cytotoxic due to polymer formation (toxic gain of function) or a combination of both (Davis et al., 1999a; Davis et al., 1999b; Lomas, 2002). For neuroserpin it is impossible to distinguish between the effects of loss or gain of function, as there is no physiological separation of the site of synthesis and the site of action. Madani and co-workers investigated the role of over-expression or knock-out of neuroserpin in mice (Madani et al., 2003). Both genetically modified mice showed a reduced locomotor activity in a new environment and, when novel objects were presented, demonstrated an anxiety-like behaviour (Madani et al., 2003). Such mild and similar phenotypes argue in favour of a cytotoxic gain of function effect of polymeric mutant neuroserpin. In addition, deficiency of neuroserpin at the synapse might lead to uncontrolled tPA activity being neurotoxic and thus might explain the seizure-like episodes seen in FENIB (Belorgey et al., 2004; Lebeurrier et al., 2008; Lebeurrier et al., 2005; Madani et al., 2003). Ergo, neuroserpin might have a neuroprotective function (Yepes et al., 2002). Moreover, this indicates that precise levels of neuroserpin expression are required to tightly control proteolysis at the synapse. Interestingly, in knock-out neuroserpin mice the level and distribution of tPA was not altered, suggesting neuroserpin independent functions of tPA (Madani et al., 2003).

2.3 Endoplasmic reticulum (ER)

The endoplasmic reticulum (ER) is an intracellular membranous network that is in contact with the outer nuclear membrane (Kaufman, 1999). It is part of the secretory pathway system (Palade, 1975). All membrane and secretory proteins are post or co-translationally translocated to the ER lumen, where they are modified, folded and assembled correctly before being transported to the Golgi compartment (Gething and Sambrook, 1992; Kaufman, 1999; Sitia and Braakman, 2003). The ER provides a unique oxidizing environment which supports disulphide bond formation during protein folding (Tu and Weissman, 2004). The majority of newly synthesised proteins undergo N-linked glycosylation (Hammond et al., 1994; Helenius and Aebi, 2004; Parodi, 2000). This unique covalent protein modification plays an important role in promoting correct protein folding, efficient quality control, and recognition for ER associated degradation (ERAD), as well as lysosomal trafficking and sorting of glycoproteins (Helenius and Aebi, 2001, 2004; Kato and Kamiya, 2007).

Therefore, the ER comprises quality control mechanisms to ensure that only mature and functionally active proteins are synthesised (Ellgaard and Helenius, 2003; Hegde and Ploegh, 2010; Zhang and Kaufman, 2008). ER quality control pathways are maintained by chaperones which facilitate protein folding (Ellgaard and Helenius, 2003; Helenius and Aebi, 2004; Kaufman, 2002). Proteins are retained in the ER until they are properly folded (Ellgaard and Helenius, 2003; Helenius and Aebi, 2004; Rutkevich and Williams, 2010).

2.4 Unfolded protein response (UPR)

The ER has evolved specific signalling pathways to sense an imbalance between the load of proteins in the ER and the protein-folding capacity. Thus, the ER ensures that proteins entering are efficiently folded and modified. These intracellular signalling pathways are collectively termed unfolded protein response (UPR) (Bernales et al., 2006; Kaufman, 1999; Ron and Walter, 2007; Schroder and Kaufman, 2005). Collectively they help the cell to maintain ER homeostasis (Kaufman, 2002; Ron and Walter, 2007; Schroder and Kaufman, 2005).

A number of biochemical and physiological stimuli, such as calcium depletion, elevated secretory protein syntheses or expression of mutant proteins, unbalance the ER and cause accumulation of unfolded or misfolded proteins (Kaufman, 1999; Ron and Walter, 2007; Schroder and Kaufman, 2005; Zhang and Kaufman, 2006, 2008). Specialised ER transmembrane proteins inositol-requiring kinase 1 (IRE1), activating transcription factor-6

(ATF6), double-stranded RNA-activated protein kinase (PKR)-like ER kinase (PERK)) sense these conditions by their luminal domains and convey the sensed signals by their effector portions to the cytosol and the nucleus (Bernales et al., 2006; Kohno, 2010; Mori, 2000; Schroder and Kaufman, 2005).

Firstly, the activated UPR leads to a general reduction in the protein load of the ER. This is a transient adaptation reached by attenuating protein synthesis and reducing translocation of new client proteins into the ER (Kaufman, 2002; Marciniak and Ron, 2006; Ron and Walter, 2007; Zhang and Kaufman, 2006). Secondly, UPR leads to an increase in the protein folding capacity of the ER, which is a longer term adaptation including transcriptional activation of UPR target genes. This leads to an increase in the ER content, expands ER protein folding capacity, and enhances retranslocation and degradation of ER-localized proteins (Kaufman, 2002; Ron and Walter, 2007; Shen et al., 2004). If ER homeostasis cannot be restored, a third mechanism, cell death, will be activated (Ron and Walter, 2007; Szegezdi et al., 2006b).

2.4.1. Sensing of ER stress

In resting cells, all three ER stress sensors are kept inactive by association of their luminal stress sensing domains with the ER chaperone BIP (Fig. 5) (Bertolotti et al., 2000; Okamura et al., 2000). BIP is an Hsp70 family protein located in the lumen of the ER (Haas and Wabl, 1983; Normington et al., 1989), which recognizes a hydrophobic amino acid motif on unfolded proteins (Flynn et al., 1991). As soon as ER stress is induced, BIP binds to unfolded proteins to prevent their translocation to the Golgi. Thereby, BIP is sequestered from the ER stress sensors leading to their activation and thus triggering UPR (Bertolotti et al., 2000; Okamura et al., 2000; Shen et al., 2002; Zhang and Kaufman, 2006).

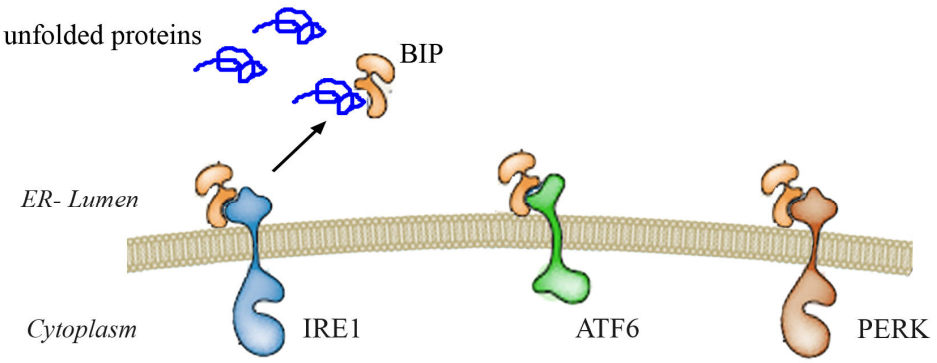

Figure 5: Stress sensing transmembrane proteins in the ER

The ER stress transducers inositol-requiring kinase 1 (IRE1), activating transcription factor-6 (ATF6), and double-stranded RNA-activated protein kinase (PKR)-like ER kinase (PERK) are transmembrane proteins with an ER luminal stress sensing domain and a cytoplasmic portion. Binding of the abundant ER chaperone BIP locks the stress sensors in an inactive state. ER stress leads to a dissociation of BIP, which binds unfolded proteins as a chaperone, thereby releasing and activating the stress sensor. Modified and adapted from (Ron and Walter, 2007).

2.4.2. Regulation of the UPR

2.4.2.1. IRE1-arm of the UPR

IRE1 is evolutionarily highly conserved (Iwawaki et al., 2001; Tirasophon et al., 1998; Wang et al., 1998). It is a type-1 transmembrane protein whose N-terminal part is located in the ER lumen to sense the protein-folding environment and the C-terminal part is situated in the cytosol (Fig. 6) (Cox et al., 1993; Mori et al., 1993; Tirasophon et al., 1998; Wang et al., 1998). The cytosolic portion is an effector domain with a dual enzymatic function, a protein kinase and a RNAse activity (Cox et al., 1993; Mori et al., 1993). In response to the accumulation of unfolded proteins, BIP dissociates from IRE1 permitting their dimerisation or oligomerisation (Liu et al., 2002), thus triggering trans-autophosphorylation of the kinase domain (Papa et al., 2003; Shamu and Walter, 1996). By a yet poorly understood mechanism, this in turn activates the unusual endonucleolytic activity of IRE1, which causes the precise cleavage of cytosolic XBP1 mRNA in mammals (Calfon et al., 2002; Yoshida et al., 2001) or Hac1 in yeast (Cox and Walter, 1996; Mori et al., 1996). This unconventional splicing event leads to the production of a stable and active transcription factor XBP1s, which up-regulates genes encoding components of the ERAD machinery and genes important for ER biogenesis (Fig. 6) (Calfon et al., 2002; Yoshida et al., 2003; Yoshida et al., 2001). This reduces the load

on the stressed ER and facilitates alteration in ER-associated protein synthesis. Interestingly, IRE1 promotes cleavage of several cellular mRNAs leading to their degradation, a process named regulated IRE-1 dependent decay (RIDD) (Fig. 6) (Hollien et al., 2009; Hollien and Weissman, 2006).

Both, the precursor and the spliced form of XBP1 mRNA are translated (Calfon et al., 2002; Yoshida et al., 2006), whereas the protein encoded by the unspliced mRNA (XBP1u) is labile and represses UPR target genes (Calfon et al., 2002). This probably serves to stop signalling by competition for binding sites and inhibitory hetrodimerisation between XBP1s and XBP1u mRNA (Ron and Walter, 2007; Schroder and Kaufman, 2005).

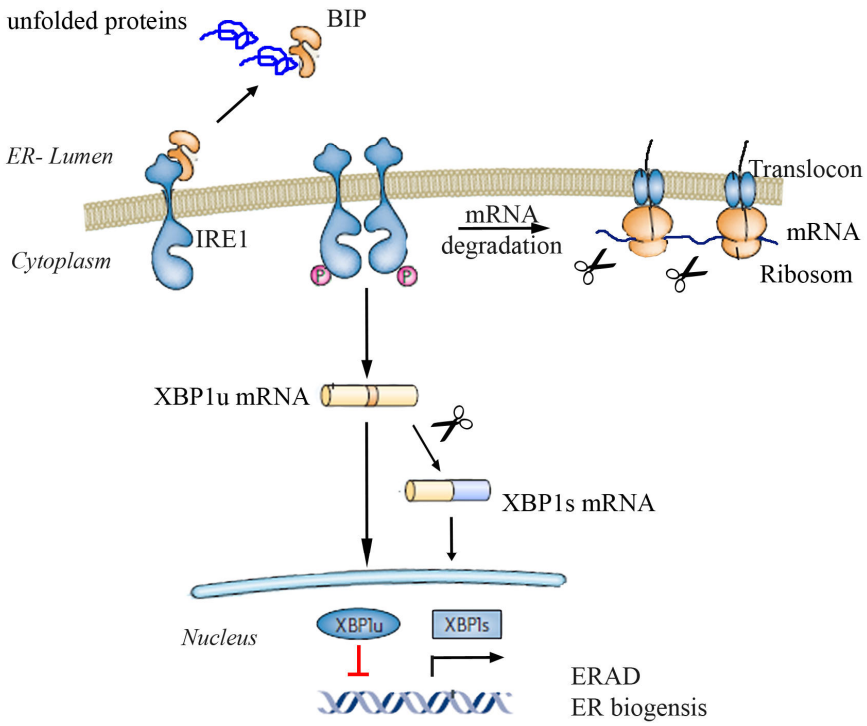

Figure 6: IRE1-arm of the UPR

On aggregation of misfolded proteins, BIP releases inositol-requiring kinase 1 (IRE1), allowing their oligomerisation in the plane of the ER membrane. Trans-autophosphorylation of the cytosolic kinase domain increases the affinity for nucleotides and induces the endoribonucleolytic activity. IRE1 mediates sequence specific splicing of XBP1 mRNA, which leads to a frame shift in the coding sequence. The unspliced as well as the spliced XBP1 mRNA are translated. XBP1s is stable and active transcription factor for UPR target genes promoting ERAD and ER biogenesis (Yoshida et al., 2003). XBP1u is a labile protein repressing UPR (Calfon et al., 2002; Yoshida et al., 2006). Interestingly, IRE1 can also act in an alternative way, by facilitating the degradation of various ER localized mRNAs (Hollien and Weissman, 2006). So far it is not known if IRE1 degrades these mRNAs directly or if it is an indirect effect by recruiting other RNases. Modified and adapted from (Ron and Walter, 2007).

2.4.2.2. ATF6-arm of the UPR

ATF6 is a type-2 transmembrane protein, with a C-terminal stress sensing portion in the ER lumen and an N-terminal effector domain, composed of a basic leucine zipper transcription factor region, in the cytosol (Haze et al., 1999). Upon ER stress, ATF6 is released from BIP allowing its transport from the ER to the Golgi compartment via COPII vesicles (Shen et al., 2002), where it is sequentially cleaved by Golgi-resident site specific proteases, S1P (site-1 protease) and S2P (site-2 protease) (Fig. 7) (Haze et al., 1999; Ye et al., 2000). The cleaved 50 kD cytosolic fragment migrates to the nucleus to activate transcription not only for ER chaperones and ERAD-related genes but also for the transcription factors CHOP and XBP1 (Adachi et al., 2008; Okada et al., 2002; Wu et al., 2007; Yoshida et al., 2001; Yoshida et al., 2000).

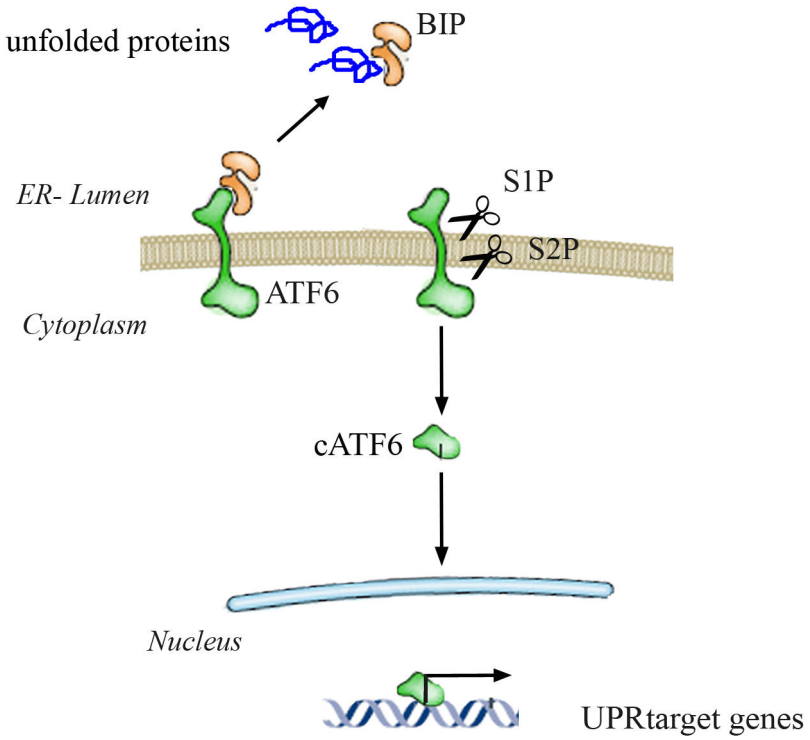

Figure 7: ATF6-arm of UPR

Activating transcription factor 6 (ATF6) resides in the ER membrane as its luminal domain is associated with BIP. ER stress disrupts BIP binding which allows the traffic of ATF6 to the Golgi compartment (Shen et al., 2002). ATF6 is sequentially cleaved by Golgi-resident enzymes, first by the luminal site-1 protease (S1P) and afterwards by the intra membrane site-2 protease (S2P). This releases the cytosolic effector domain of the protein from the membrane and allows their translocation into the nucleus. cATF6 activated transcription of UPR target genes including ER chaperones and XBP1. Modified and adapted from (Ron and Walter, 2007).

2.4.2.3. PERK-arm of the UPR

PERK is a type-1 transmembrane and shares a weak homology in their luminal stress sensing domain with IRE1 (Liu et al., 2000; Schroder and Kaufman, 2005). As soon as unfolded proteins accumulate, BIP dissociates from the luminal region of PERK permitting oligomerisation and trans-autophosphorylation of the cytoplasmic effector domain (Fig. 8) (Harding et al., 1999; Marciniak and Ron, 2006; Shi et al., 1998). PERK phosphorylates the α-subunit of the eukaryotic initiation factor 2α (eIF2 α) at Ser51, causing a general attenuation in protein translation (Harding et al., 1999). The phosphorylation blocks the guanine nucleotide exchange factor eIF2B that recycles eIF2α to its active GTP-bound form. Thereby, less eIF2α is available to initiate translation (Harding et al., 1999; Kozak, 2002). This block in protein translation helps the cell to survive by decreasing the load of nascent proteins arriving at the ER (Harding et al., 1999; Szegezdi et al., 2006b).

However, at the same time PERK-mediated eIF2α phosphorylation contributes to transcriptional activation of genes carrying certain regulatory sequences in their 5` untranslated regions (Scheuner et al., 2001). One of the best investigated of these genes in mammals is ATF4 encoding a cAMP response element-binding transcription factor (Harding et al., 2000; Ron and Walter, 2007; Scheuner et al., 2001); the homologue in yeast is Gcn4 (Hinnebusch and Natarajan, 2002). ATF4 mediates cell survival by activating genes involved in amino acid metabolism, stress response and protein secretion (Fig. 8) (Harding et al., 2003). However, at the same time ATF4 also promotes the expression of the transcription factor CHOP (C/EBP homologous protein), a protein well known to cause apoptotic cell death (Szegezdi et al., 2006a).

It is worth mentioning that several other signalling cascades unrelated to ER-stress also converge on eIF2α phosphorylation, activating a common set of genes. Due to this integrative feature, signalling downstream of phosphorylated eIF2α was termed the integrated stress response (ISR) (Harding et al., 2003).

PERK activation by ER stress is quickly reversible; soon after ER homeostasis is restored, activated PERK is dephosphorylated (Bertolotti et al., 2000; Jousse et al., 2003).

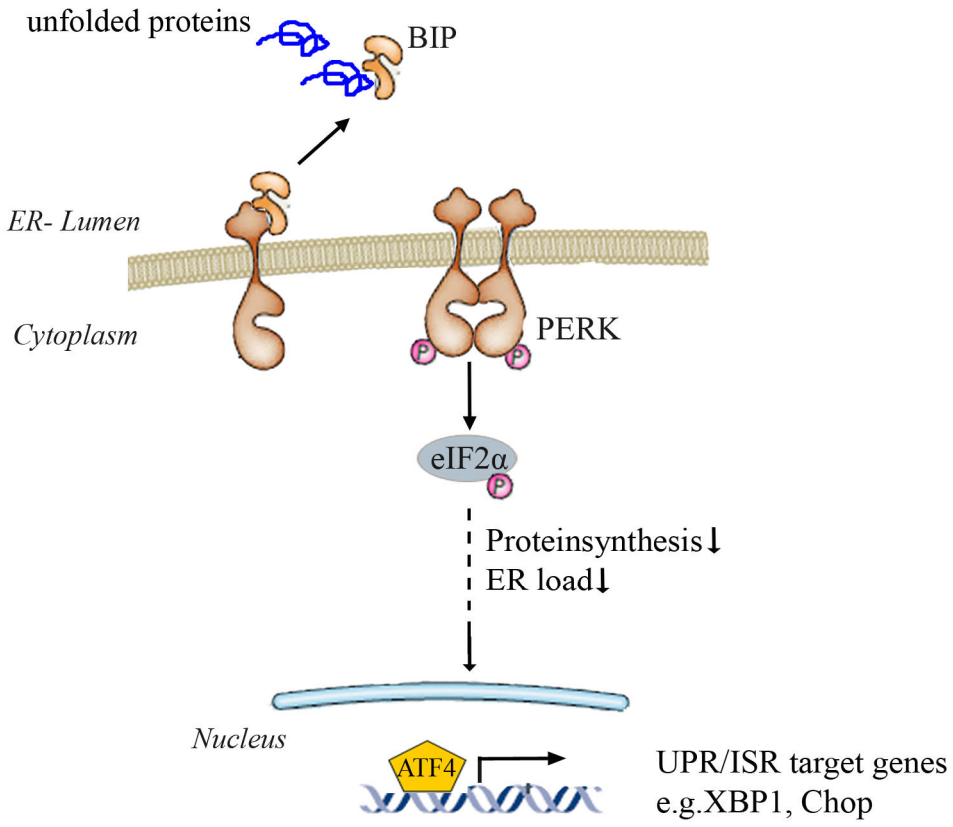

Figure 8: PERK-arm of the UPR

In response to the accumulation of unfolded proteins, BIP dissociates from the luminal part of protein kinase (PKR)-like ER kinase (PERK), thus permitting their oligomerisation in the plane of the ER membrane. This leads to extensive trans-autophosphorylation of the cytosolic kinase domain, which enhances substrate affinity (Marciniak and Ron, 2006). PERK phosphorylates the α-subunit of the eukaryotic initiation factor 2α (eIF2α) at Ser51, which blocks its recycling. The reduced availability of active eIF2α prevents initiation of translation causing a general decrease in protein synthesis, thereby reducing the unfolded protein load of the ER. Concomitantly, limited eIF2 levels affect gene transcription; for example translation of activating transcription factor 4 (ATF4) is increased. ATF4 induces the transcription of genes required to restore ER homeostasis. At the same time ATF4 activates gene expression of CHOP, which is involved in cell death signalling. Additionally, other signalling cascades unrelated to ER-stress converge on eIF2α phosphorylation. Due to this integrative feature, signalling downstream of phosphorylated eIF2α is termed the integrated stress response (ISR). Modified and adapted from (Ron and Walter, 2007).

2.4.2.4. ER stress induced apoptosis

If subjected to continuous ER stress, ER homeostasis cannot be maintained and cells die (Bernales et al., 2006; Ron and Walter, 2007; Szegezdi et al., 2006a). Apoptotic cascades are triggered by a combination of signals from each of the three UPR arms and by Ca^{2+} release from the ER (Scorrano et al., 2003; Zong et al., 2003). As already mentioned, activation of the

PERK- and ATF6-armes of the UPR contribute to the up-regulation of the pro-apoptotic transcription factor CHOP (Harding et al., 2000; Harding et al., 2003; Yoshida et al., 2000), which promotes mitochondrial cytochrome *c* release, apoptosome formation and caspase signalling (Ma et al., 2002; McCullough et al., 2001). In parallel, activated IRE1 can bind to TRAF2, which is thought to activate JNK cascade signalling (Urano et al., 2000) contributing to proteolytic activation of caspases, such as ER-localized Caspase-12 (Nakagawa et al., 2000).

Mutant neuroserpin polymers are retained within inclusion bodies in the ER of the cell, contributing decisively to the pathogenesis of FENIB. The mutant aggregated prone protein as well as the resulting inclusions present an additional burden to the normal protein folding capacity of the ER. This delicate situation leads inescapably to a disturbance of ER homeostasis. Therefore it is worth studying possible implications of UPR in FENIB to understand cellular processing of polymeric mutant neuroserpin.

2.5 ER associated degradation (ERAD)

Glycoproteins that fail to fold correctly in the ER are extracted from the folding machineries and subsequently dislocated across the ER membrane to the cytoplasm where they are degraded by the 26S proteasome in a series of strictly regulated events (Bonifacino and Weissman, 1998; Ellgaard and Helenius, 2003; Plemper et al., 1999). Terminally misfolded proteins are tagged for degradation by extensive demannosylation of the protein-bound oligosaccharide core (Hebert and Molinari, 2007; Nakatsukasa and Brodsky, 2008). This modification triggers association with ER luminal, transmembrane and cytosolic complexes formed around membrane-embedded E3 ubiquitin ligases to facilitate dislocation of the polypeptide across the ER membrane into the cytosol (Carvalho et al., 2006; Gardner et al., 2000; Gauss et al., 2006; Kanehara et al., 2010). Several ER-resident proteins that recognise misfolded proteins, such as ER degradation-enhancing α-mannosidase-like lectins (EDEMs) (Hosokawa et al., 2001), and lectins containing mannose-6-phosphat receptor-like domains, like OS9 and XTP3-B (Christianson et al., 2008; Hosokawa et al., 2008) have been characterized in yeast and mammals.

Before being hydrolysed, retranslocated polypeptides are ubiquitinated by the 26S proteasome in the cytosol (Fig. 9) (Gardner et al., 2001; Plemper et al., 1999). Ubiquitination is mediated by three cytosolic enzymes. First, E1 (ubiquitin-activating enzyme) activates

ubiquitin in an ATP dependent manner; then one of several E2 enzymes (ubiquitin-conjugating enzyme) transfers ubiquitin through a thiol-ester bond to its essential cystein residue and finally, the E3 ubiquitin ligase transfers ubiquitin onto lysine residues or the N-terminus of specifically bound target protein (Kerscher et al., 2006; Pickart, 2001). The ubiquitin chain is lengthened by E2 and E3 enzymes, sometimes with the help of an accessory factor (E4) (Koegl et al., 1999). Finally, the polyubiquitin chain is recognized by the proteasome (Thrower et al., 2000). The 26S proteasome is a multicatalytic protease composed of two subcomplexes, the 20S proteolytical core particle and the 19S regulatory particle, that contains a deubiquitinating enzyme, six different ATPase subunits and several other proteins of unknown function (Ciechanover and Brundin, 2003; Voges et al., 1999).

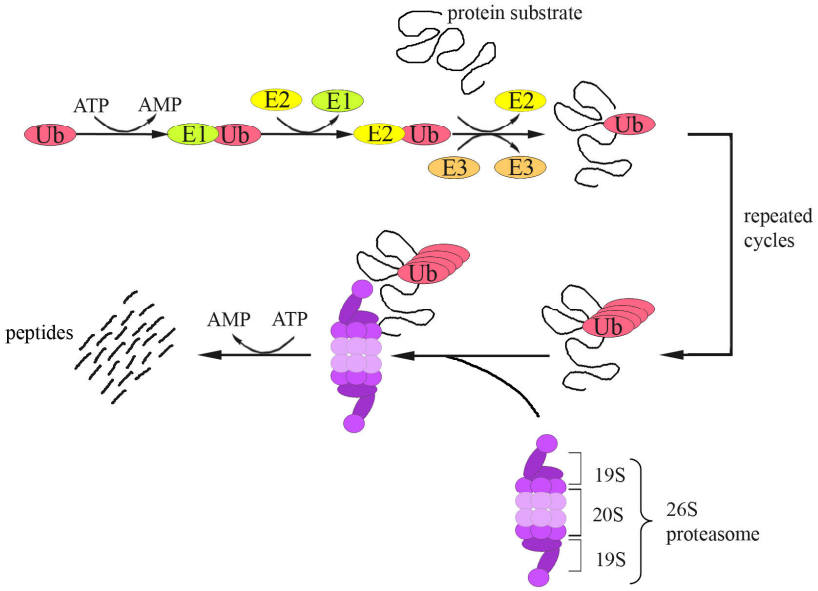

Figure 9: The ubiquitin-proteasome system (UPS)

The UPS system is required for the targeted degradation of short lived and misfolded proteins in the eukaryotic cell. ERAD substrates are targeted through ubiquitination. Ubiquitin is activated by an ubiquitin-activating enzyme E1, which forms a thiol-ester bond with ubiquitin. This reaction follows binding of ubiquitin to E2, an ubiquitin-conjugating enzyme. Ubiquitin-ligase E3 transfers the ubiquitin chain from E2 onto the specifically bound target protein substrate, by formation of an isopeptide bond between the carboxy terminus of the ubiquitin and a lysine residue on the substrate. Multiple cycles of ubiquitination extend the ubiquitin chain which targets the protein substrate to the 26S proteasome. The 26S proteasome is a multiple enzyme complex, which recognises, binds and degrades polyubiquitinated proteins into small peptides. Adapted and modified from (Welchman et al., 2005).

The intracellular accumulation of mutant serpin in the ER of the cell is the major cause of the cytotoxic “gain of function” phenotype in serpinopathies. Regardless of the detailed knowledge on protein folding mechanisms in the ER, it is so far a mystery what evokes the cytotoxic phenotype which leads to neurodegeneration in neuroserpin dementia. It could be the metastable folding intermediate M*, the dimerised mutant species or the polymers which account for cell death giving rise to disease. Therefore, it is necessary to investigate neuronal pathways involved in protein degradation to circumvent the cytotoxic effects.

2.6 Autophagy

Autophagy, or cellular self-digestion, is a strictly regulated degradation process through which parts of the cytoplasm containing organelles, including mitochondria, peroxisomes, the ER and the Golgi, or damaged proteins are delivered to the lysosomes to be degraded (Cuervo, 2004a; Knaevelsrud and Simonsen, 2010; Mizushima, 2005; Xie and Klionsky, 2007). In many organisms, autophagy is activated as an adaptation to starvation to recycle essential nutrients (Kuma et al., 2004; Mizushima and Klionsky, 2007). Autophagy is also important for protein turnover of cytoplasmic contents to maintain cellular homeostasis and differentiation (Cuervo, 2004a; Eskelinen et al., 2003; Klionsky and Emr, 2000; Mizushima and Hara, 2006). Moreover, it has been discovered that autophagy plays a critical role in immunity and prevention of diseases (Levine and Kroemer, 2008; Mizushima et al., 2008).

In yeast it was discovered that autophagy is regulated by phosphatidylinositol-3 kinase (PI3K) pathway (Cuervo and Dice, 1996) and by the protein kinase Target Of Rapamycin (TOR). It has been shown that an active TOR kinase inhibits autophagy (Noda and Ohsumi, 1998) and, vice versa, autophagy is induced upon inhibition of TOR kinase, for example under starvation or by treatment with rapamycin (Jung et al., 2010; Kamada et al., 2000). The TOR kinase as well as its pathway is conserved in mammals, although the regulation of the cascade is more complex (Chan et al., 2009; Klionsky, 2005; Meijer and Codogno, 2006).

There are three different kinds of autophagy, differing in their mechanism and functions: chaperone-mediated autophagy (CMA), microautophagy and macroautophagy (Cuervo, 2004a; Klionsky, 2005; Massey et al., 2006). During CMA, soluble proteins are selectively transported form the cytoplasm to the lysosomal lumen for degradation (Cuervo and Dice, 1996; Massey et al., 2006). In microautophagy, the lysosomal membrane itself sequesters a portion of the cytoplasm (Ahlberg et al., 1982). However, in macroautophagy, hereafter referred as autophagy, a double-membrane vesicle is formed around the cytoplasm

to be degraded, which then fuses with lysosomal vesicles (Fig. 10) (Arstila and Trump, 1968; Ravikumar et al., 2004; Xue et al., 2001).

Autophagy is an active process in which sub-cellular membranes undergo immense morphological changes (Kim and Klionsky, 2000; Klionsky and Ohsumi, 1999), which is accompanied by expression of specific autophagic genes (*atg*) (Klionsky and Emr, 2000). Upon induction of autophagy a double-layered membrane, the phagophore, is formed, engulfing parts of cytoplasmic content (Fig. 10A). The phagophore expands to form a vacuole, containing cytosol and/or organelles as well as aggregated proteins (Arstila and Trump, 1968). The sealed vacuole is termed autophagosome and it is free of any lysosomal proteins (Fig. 10B). Further on, the autophagosomes fuse with endosomes to from amphisomes prior to fusing with lysosomes or they fuse directly with lysosomes, which deliver lysosomal membrane proteins and enzymes for degradation (Fig. 10C and D) (Eskelinen, 2005; Fengsrud et al., 1995). In the autophagolysosome, the sequestered cytoplasm content is degraded by lysosomal hydrolases and proteases, the resulting macromolecules are released to be reused by the cell (Fig. 10C and D) (Arstila and Trump, 1968; Dunn, 1994; Eskelinen, 2005; Klionsky and Emr, 2000).

The origin of the phagophore is still controversial. Various organelles, such as the ER, the Golgi complex, and the plasma membrane have been proposed (Reggiori, 2006). Experimental evidence suggests that the autophagosomes are formed from ribosome-free regions of rough ER (Arstila and Trump, 1968; Ueno et al., 1991), a post Golgi compartment (Yamamoto et al., 1990) or from a novel compartment (Stromhaug et al., 1998). Recent works supports the ER and more generally the membrane flow through the secretory pathway as the main source of the sequestering membrane (Klionsky et al., 2008).

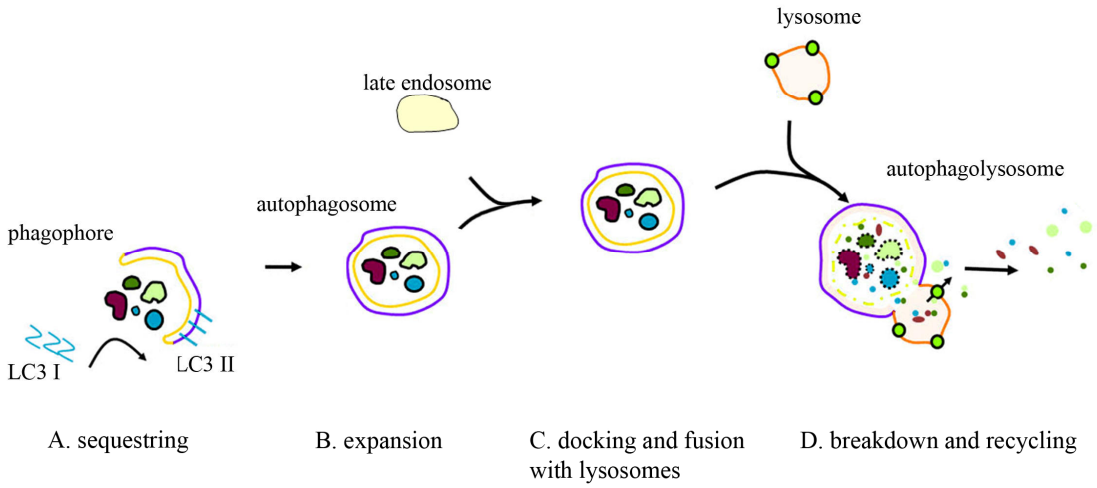

Figure 10: Schematic model describing macroautophagy in mammalian cells

Upon induction of autophagy a sequestering membrane, the phagophore (A.), expands to form an autophagosome (B.) thereby engulfing cytosolic proteins, organelles and aggregated proteins. Cytosolic LC3 I is lipidated to LC3 II, thus being bound to the membrane of the autophagosome. Fusion of the autophagosome with endosomes (to form amphisomes) increases acidification, which is required for the docking and fusion with the lysosome (C.). Lysis of the internalized contents occurs in autophagolysosomes and the resulting macromolecules are released back into the cytosol (D.). Modified and adapted from (Mizushima et al., 2008).

LC3 (microtubule-associated protein 1 light chain 3) is the first discovered mammalian marker protein for autophagy (Kabeya et al., 2000). It is one of the mammalian homologues of Atg-8 and it is necessary for the formation of autophagosomes (Kabeya et al., 2000; Kirisako et al., 1999). It was shown that upon induction of autophagy, cytosolic LC3 I (16 kD) is processed into another form, LC3 II (18 kD) which is associated with the inner and outer membrane of the autophagosome (Fig. 10) (Ichimura et al., 2000; Kabeya et al., 2000). Further analysis revealed that LC3 I is conjugated to phosphatidylethanolamine (LC3 II) (Kuma et al., 2002) thus being tightly bound to the autophagosome membrane (Kabeya et al., 2000; Mizushima et al., 2001; Tanida et al., 2004). These findings enriched the methodical repertoire in the autophagy research field. In addition to electron microscopy, where autophagosomes are monitored by double layered membranes (Klionsky et al., 2008; Mizushima, 2004), protein biochemistry by western blot analysis can now be performed (Klionsky et al., 2008; Klionsky et al., 2007; McLeland et al., 2011; Mizushima, 2004).

In conformational diseases, such as mutant α1-antitrypsin deficiency (Kamimoto et al., 2006; Kruse et al., 2006) and in dementias, such as Alzheimer's disease (Nixon et al., 2000),

or in trinucelotide diseases (e.g. Huntigton's disease) (Kegel et al., 2000; Ravikumar et al., 2002; Ravikumar et al., 2004) an increased number of autophagic vacuoles have been reported. The autophagy-mediated isolation and degradation of altered cytosolic contents, like aggregated proteins or damaged organelles, protects the cells from further damage (Lemasters et al., 2002; Webb et al., 2003). Thus, the cellular activation of autophagy might play a crucial role in cell protection during early stages of neurodegenerative diseases (Cuervo, 2004a).

2.7 Summary and objectives

Neuroserpin belongs to the superfamily of serpins. Point mutations in serpins destabilize their structure and favour protein polymerisation within the cell of synthesis giving rise to diseases. Little is known about the precise pathophysiology of such conformational diseases. Mutations in neuroserpin lead to the autosomal inherited dementia, FENIB. The accumulations of polymeric mutant neuroserpin within inclusions in the ER may lead to a deficiency of active protein (loss of function phenotype) in neurons of the brain. Conversely, aggregated mutant neuroserpin polymers themselves might have toxic influence on neurons (toxic gain of function phenotype). Therefore, neuroserpin dementia is a suitable model system to elucidate signals generated by neurons in response to protein aggregation within the ER. This allows us to gain more insights into cellular signal processing to eliminate or to handle protein aggregates.

For my thesis, my team and me set out to investigate neuronal pathways involved in mutant neuroserpin degradation. As mutant neuroserpin inclusions occur in the ER, we focused on ER resident stress sensing pathways, such as UPR, as well as associated degradative paths, such as ER associated degradation (ERAD) and autophagy.

We demonstrated that mutant neuroserpin is specifically degraded by the proteasome via ERAD and non-specifically by autophagy. Only when the proteasomal capacity is overwhelmed does autophagy gain importance in mutant neuroserpin degradation. We went on to investigate the role of UPR in neuroserpin protein turnover. Thereby, it became apparent, that transient induction of the ATF6-arm of UPR promotes transient decrease in polymeric neuroserpin formation. This raises the exciting possibility that activation of UPR-pathways may have therapeutic potential.

3. Material

3.1 Equipment

All equipment used in this study is listed in an alphabetical order in table 2.

Table 2: Equipment

product	company, city
8-channel pipette 10-100 µl	Eppendorf, Hamburg
8-channel pipette 1-10 µl	Eppendorf, Hamburg
ASP300S tissue processor	Leica, Wetzlar
autoclave	Memmert, Schwabach
bacteria incubator	Heraeus electronic, Hanau
balance Shinko Denshi	Vibra, Tokyo, Japan
balance, precision MC1 polyrange RC 210 P	Sartorius, Göttingen
centrifuge 5415 R, refrigerated, rotor F45-24-11	Eppendorf, Hamburg
centrifuge 5430 R, refrigerated, rotor F45-24-11 HS	Eppendorf, Hamburg
centrifuge 5810 R, refrigerated, rotor A-4-62	Eppendorf, Hamburg
centrifuge, mini MC 6	Sarstedt, Nümbrecht
cryostat CM1950	Leica, Wetzlar
developing machine Curix 60	AGFA, Düsseldorf
digital camera	Nikon, Melville, USA
dismembrator U	B. Braun, Melsungen
electron microscope EM902	Zeiss, Göttingen
electrophoresis, horizontal mini-sub cell GT	Biorad, Munich
electrophoresis, mini protean 3 cell	Biorad, Munich
electrophoresis, vertical system DCX-700	C.B.S. Scientific, Del Mar, USA
gel caster & comb	Biorad, Munich
gel documentation DeVision G	Decon Science Tec GmbH, Hohengandern
Hypercassette™	GE Healthcare, Buckinghamshire, UK
iCycler Thermal Cycler	Biorad, Munich

Table 2: Equipment

product	company, city
imaging system Chemi Doc™ XRS	Biorad, Munich
incubator (cell culture)	Heraeus electronic, Hanau
incubator (immunohistochemistry)	Memmert, Schwabach
magnetic stirrer with heating RCT basic IKAMAG®	IKA Werke GmbH&Co. KG, Staufen
microscope Axioskop40	Zeiss, Göttingen
microscope Eclipse TS 100	Nikon, Melville, USA
microtome SM2000R	Leica, Wetzlar
microwave Micromat	AEG, Frankfurt am Main
MyCylcer Thermal cycler (PCR)	Biorad, Munich
Neubauer counting chamber, 0.1mm	Assistent, Sondheim
paper cutting machine	Roth, Karlsruhe
pH meter CG 840	Shott, Mainz
photometer, biophotometer plus	Eppendorf, Hamburg
pipette boy	Integra Bioscience, Fernwald
pipette research fix 0.1-2.5 µl	Eppendorf, Hamburg
pipette research fix 100-1000 µl	Eppendorf, Hamburg
pipette research fix 10-100 µl	Eppendorf, Hamburg
pipette research fix 1-10 µl	Eppendorf, Hamburg
powersupply, easy volt	Stratagene, Waldbronn
powersupply, PowerPac basic	Biorad, Munich
printer P93D	Mitsubishi, Ratingen
shaker, overhead rotationbar	Hartenstein, Würzburg
shaker, platform shaker STR 6	Stuart Scientific, Essex, UK
spectrophotometer µQuant	Biotek, Bad Friedrichshall
sterile bench Thermo Electron Corpoation Herasafe	Heaeus electronic, Hanau
thermomixer compact	Eppendorf, Hamburg
ultracentrifuge L-60, rotor SW40 Ti	Beckman Coulter, Brea, USA
ultrasonograph Sonorex super RK103H	Bandelin electronic, Berlin
Ventana Benchmark XT	Ventana, Tuscon, Arizona, USA
vortex-genie 2	Scientific industries, New York, USA
waterbath	P-D Industriegesell. mbH, Dresden

3.2 Chemicals and Consumables

All chemicals and consumables used in this study were listed according to the applied method and in an alphabetical order in table 3-11. If not stated otherwise, salts, acids and bases were from Merck, Darmstadt, Sigma-Aldrich, Munich or Fluka, Neu Ulm.

3.2.1. RNA/ DNA Analysis

Table 3: Chemicals and consumables for RNA/ DNA analysis

product	company, city
1 Kb DNA Plus-ladder	Invitrogen, Darmstadt
2-bromo-2-chloro-1,1,1-trifluoroethane (Halothan)	Sigma, Munich
2-propanol	Riedel-de Haen, Seelze
3-(N-Morpholino)propane Sulfoneacid (MOPS)	Sigma, Munich
acetic acid	Roth, Karlsruhe
agarose	Invitrogen, Darmstadt
autoclaved aqua bidest	UKE, Hamburg
bromophenol blue	Merck, Darmstadt
desoxynucleoside Triphosphate Set (dNTPs)	Fermentas, St. Leon-Rot
diethylpyrocarbonate (DEPC)	Sigma, Munich
dream taq polymerase	Fermentas, St. Leon-Rot
ethanol, denature	UKE, Hamburg
ethidium bromide	Sigma, Munich
ethylendiaminetetraacetat (EDTA)	Sigma, Munich
formaldehyde 37 % (v/v)	Merck, Darmstadt
formamide	AppliChem, via Th. Geyer, Hamburg
Gene Jet PCR purification Kit	Fermentas, St. Leon-Rot
glycerol	Merck, Darmstadt
microseal adhesive sealer Biorad (MSB-1001)	Biorad, Munich
multiply PCR plate natural 96-well	Sarstedt, Nümbrecht
proteinase K	Qiagen, Hilden
restrictionenzyme Pst1	Roche, Munich
RevertAid H Minus First Strand cDNA Synthesis Kit	Fermentas, St. Leon-Rot
RNA Miniprep Kit	Stratagene, Waldbronn

Table 3: Chemicals and consumables for RNA/ DNA analysis

product	company, city
safeseal tips premium from Biozym	Biozym, Hessisch Ohlendorf
safeseal tips premium from Biozym	Sarstedt, Nümbrecht
SYBR Green/Fluorescein qPCR Master Mix	Fermentas, St. Leon-Rot
trizma base, minimum, 99.9 % titration	Sigma, Munich
UVette® for spectrophotometer	Eppendorf, Hamburg

3.2.1.1. Oligonucleotides

All oligonucleotides were purchased from Sigma-Aldrich. Generally, a synthesis scale of 0.025 µmol was chosen. The oligonucleotides were desalted and purified by HPLC, and solved in autoclaved distilled water to a final concentration of 100 µM (according to a datasheet supplied by Sigma-Aldrich). For PCR-analysis and DNA-sequencing a 1:10 dilution of the 100 µM stock solution was prepared and 1 µl of each oligonucleotide was added to 25 µl final reaction mix.

Table 4: Oligonucleotides applied in polymerase chain reactions

gene	sequence	primercode
XBP1[(a)]	5′- AAACAGAGTAGCAGCGCAGACTGC-3	10XBP1_FW
	5′-GGATCTCTAAAACTAGAGGCTTGGTG-3′	10XBP1_RV
ATF4	5’- AATGGATGACCTGGAAACCATGCC -3’	3ATF4_FW
	5’- TCACATGTGTCATCCAACGTGGTC -3’	3ATF4_RV
chop[(b)]	5'-ACAGAGGTCACACGCACATC-3'	Chop_S_FW
	5'-GGGCACTGACCACTCTGTTT-3'	Chop_AS_RV
actin	5'-GATTACTGCTCTGGCTCCTAG-3'	actb_2FW
	5'-GACTCATCGTACTCCTGCTTG-3'	actb_2RV
Neuroserpin[(c)]	5'-TCC CCA CCA CAG AAT CCA AGT CG - 3`	hNS- F
	5'-CAC CCA CTT ATT GAT GTA GTT GG - 3`	hNS- R
UBB^{+1} [(d)]	5'-GGTGAGTACTCCCTCTCAAAAGC-3'	UBB-FW
	5'-CTGCAGTTGGACCTGGGAGTGGA-3'	UBB-RV

Several oligonucleotides were synthesised according to published protocols: [(a)]Calfon et al. 2002; [(b)]Namba et al. 2009; [(c)] Galiciotti et al. 2007; [(d)]Fischer et al. 2009.

3.2.1.2. Plasmid

Table 5: Used plasmid

plasmid	insert	established from
pcDNA3.1	wt human Neuroserpin	Beata Szalay
pcDNA3.1	S49P human Neuroserpin	Beata Szalay

3.2.2. Protein analysis

Table 6: Chemicals and consumables used for protein analysis

product	company, city
2-mercaptoethanol	Merck, Darmstadt
2-propanol	Riedel-de Haen, Seelze
acrylamide/bisacrylamide (305), Mix 37,5:1	Roth, Karlsruhe
ammoniumperoxidesulfate (APS)	Roth, Karlsruhe
bovine serum albumin (BSA), protein standard	PAA, Pasching, Österreich
bradford	Biorad, Munich
bromophenol blue	Merck, Darmstadt
Complete Mini, EDTA-free, proteinase inhibitor mix	Roche, Munich
cumaric acid	Sigma, Munich
developer G153	AGFA, Düsseldorf
developing machine western blot	AGFA, Düsseldorf
di-Sodium hydrogen phosphate dihydrate	Roth, Karlsruhe
ECL Western Blotting Substrate	Thermo Scientific, Bremen
ethanol, denature	Walter CMP, Alte Weide
ethylendiaminetetraacetic acid (EDTA)	Sigma, Munich
fixer G354	AGFA, Düsseldorf
Fujifilm Super RX medical X-ray	Fujifilm, Düsseldorf
gel releaser	Biorad, Munich
glycerol	Merck, Darmstadt

Table 6: Chemicals and consumables used for protein analysis

product	company, city
glycine	Sigma, Munich
hydrogen peroxide 35 % (w/v)	Sigma, Munich
luminol	Sigma, Munich
methanol	J.T.Baker, Griesheim
N',N'-tetramethylethylenediamine (TEMED)	Sigma-Aldrich, Hamburg
Page Ruler^{TM} , Prestained Protein Ladder	Fermentas, St. Leon.Rot
ponceau S	Sigma-Aldrich, Hamburg
potassium chloride	Fluka Biochemika, Deisenhofen
potassium dihydrogen phosphate (KH_2PO_4)	Merck, Darmstadt
PVDF Membran Immunoblot^{TM} (0.2 µm)	Biorad, Munich
skimmed milk powder instant „Frema“	Granovita GmbH, Lüneburg
sodium azide	Fluka Biochemika, Deisenhofen
sodium chloride	Sigma, Munich
sodium hydroxide	Roth, Karlsruhe
sodiumdodecyl sulfate (SDS)	Sigma, Munich
SuperSignal West Femto	Thermo Scientific, Bremen
SuperSignal West Pico	Thermo Scientific, Bremen
tissue, precision wipes	Kimberly-Clark, Koblenz
tissue, Samtess Clou Prestige	Wepa, Arnsberg-Müschede
trizma base, minimum, 99.9 % titration	Sigma, Munich
Tween 20 (polyethylene-sorbitane monolaurate)	Roth, Karlsruhe
Whatman® Paper 3MM (blotting-paper)	Schleicher&Schuell, Dassel

3.2.2.1. Antibodies and sera

Table 7: Primary antibodies used for immunodetection

primary antibody	company, city	dilution [(a)]
ATF6 [(1)]	Imgenex, San Diego, USA	IB 1:1000
beta actin [(1)]	Sigma-Aldrich, Hamburg	IB 1:5000
beta actin [(2)]	Sigma-Aldrich, Hamburg	IB 1:5000

Table 7: Primary antibodies used for immunodetection

primary antibody	company, city	dilution [a]
beta tubulin [1]	Developmental Studies Hybridoma Bank, Iowa City, USA	IB 1:1000
Caspase3	R&D Bisosystems, Wiesbaden	IH 1:1000
eIF2 alpha [2]	Cell Signaling, Danvers, USA	IB 1:1000
Hsp70 [1]	BD Bioscience, Franklin Lakes, USA	IB 1:1000
Hsp90 [1]	BD Bioscience, Franklin Lakes, USA	IB 1:1000
LC3 [1]	Nano Tools, Teningen	IB 1:200
NeuN	Chemicon, Schwalbach	IH 1:50
Neuroserpin [1]	Santa Cruz Biotechnologie, USA	IH 1:200
Neuroserpin [3]	kind gift of Prof. Peter Sonderegger, Zurich, Switzerland	IB 1:200; IF 1:50
Neuroserpin [2]	abcam, Cambridge, UK	IB 1:250; EI 2µg/ml
Neuroserpin 1A10 [1]	kind gift of Prof. Lomas, Cambridge, UK	EI 333ng/ml EM 1:2000
Neuroserpin 10B8 [1]	kind gift of Prof. Lomas, Cambridge, UK	EI 333ng/ml
Neuroserpin 10G12 [1]	kind gift of Prof. Lomas, Cambridge, UK	EI 333ng/ml
Neuroserpin 706 [1]	kind gift of Prof. Lomas, Cambridge, UK	EI 1µg/ml
phospho-eIF2 alpha (Ser51) [2]	Cell Signaling, Danvers, USA	IB 1:500

[a] ELISA (EI), Immunblot (IB), Immunfluorescent (IF), Immunhistochemistry (IH), Electron Microscopy (EM)

[1] mouse anti-mouse; [2] rabbit anti-mouse; [3] goat anti-mouse

Table 8: Secondary antibodies used for immunodetection

secondary antibody	company, city	dilution [a]
donkey anti-goat IgG, HRP	Promega, Mannheim	IB 1:10000
goat anti-mouse IgG, HRP	Promega, Mannheim	IB 1:10000
goat anti-rabbit IgG, HRP	Promega, Mannheim	IB 1:10000
rabbit anti-mouse IgG, HRP	Sigma-Aldrich, Hamburg	EI 1:20000
donkey anti-goat IgG Alexa 555	Molecular Probes, Invitrogen, Darmstadt	IF 1:500

Table 8: Secondary antibodies used for immunodetection

goat anti-rabbit IgG, biotinylated	Vector laboratories, Burlingame, USA	EM 1:1000

[(a)] ELISA (EI), Immunblot (IB), Immunfluorescent (IF), Electron Microscopy (EM)

Table 9: Sera used for immunodetection

sera	**company, city**
donkey serum	Dianova, Hamburg
antibody diluent solution (Zymed)	Zymed, San Francisco, USA
horse serum	Dianova, Hamburg

3.2.3. Cell culture

Table 10: Chemicals and consumables used for cell culture

product	**company, city**
4'6-Diamidino-2'-phenylindole (DAPI)	Roche, Munich
plasmid DNA purification nucleo bond Xtra midi	Macherey-Nagel, Düren
invisorb spin plasmid mini two	Invitek, Berlin
Cryovial®-cryotubes, sterile	Roth, Karlsruhe
cover slip	Glaswarenfabrik K. Hecht, Sondheim
DMEM medium high-glucose(4.5 g/l) with L-glutamine	PAA, Pasching, Österreich
Dulbecco's PBS (1x)	PAA, Pasching, Österreich
Fetal Bovine Sera (FBS), standard quality	PAA, Pasching, Österreich
FuGENE® HD transfection reagent	Roche, Munich
G418 (Gentamycin) supliate solution (50 mg/ml)	PAA, Pasching, Österrreich
microscope slide 12 mm Ø	Glaswarenfabrik K. Hecht, Sondheim
Opti-MEM® reduced serum medium (1x)	Invitrogen, Darmstadt
glas pipette 230 mm AdvantageTM, sterile	BD Labware, Heidelberg
Penicillin/Streptomycin (100x)	PAA, Pasching, Österreich
pipettes Serol 2 ml, 5 ml, 10 ml, 25 ml	BD Labware, Heidelberg
Trypsin-EDTA (1x)	PAA, Pasching, Österreich
cell culture dish, 6 wells, sterile	Nunc, Langenselbold

Table 10: Chemicals and consumables used for cell culture

product	company, city
cell culture dish, 10 cm, sterile	Nunc, Langenselbold
DMSO (Dimethyl sulfoxide)	Sigma, Munich
chloroquine	Sigma, Munich
rapamycin	Sigma, Munich

3.2.4. Immunhistochemistry

Table 11: Chemicals and Consumables used for immunohistochemistry

product	company, city
coverslips	Glaswarenfabrik K. Hecht, Sondheim
eosin	Merck, Darmstadt
ethanol, absolute	Pharmacy UKE, Hamburg
eukitt	Kindler GmbH, Freiburg
Mayer's Hämalaun	Merck, Darmstadt
Harri's Hämatoxylin	ROTH, Karlsruhe
methanol	J.T.Baker, Griesheim
object slide Superfrost	Glaswarenfabrik K. Hecht, Sondheim
paraformaldehyd	Büfa Chemikalien, Hude
diaminiobenzidine (DAB)	Sigma, Munich
Tissue Tek	Sakura Finetek GmbH, Staufen
hydrogen peroxide	Sigma, Munich
Phloxin B	Fluka, Neu-Ulm
Xylol	Fischer, Wiesbaden
tragant	Sigma, Munich
mounting media GLC	Sakura Finetek GmbH, Staufen
Triton X 100	ROTH, Karlsruhe
antibody diluent solution	Zytomed, Berlin
goat serum	DAKO, Hamburg
anti-rabbit histofine simple stain Max po(R)	Nichirei Biosciences, Wedel
anti-goat histofine Simple Stain MAX PO	Nichirei Biosciences, Wedel

Table 11: Chemicals and Consumables used for immunohistochemistry

product	company, city
anti-mouse histofine stain kit	Nichirei Biosciences, Wedel

3.3 Mouse strains

Table 12: Mouse strains

mouse strain	location
transgene neuroserpin *Tg*(NS), line 682 [(a)]	animal facility UKE, Hamburg
transgene neuroserpin *Tg*(NS^{S49P}), line 680 [(a)]	animal facility UKE, Hamburg
transgene neuroserpin *Tg*(NS^{S52R}), line 794 [(a)]	animal facility UKE, Hamburg
transgene *Tg*(UBB^{+1}) [(b)]	animal facility UKE, Hamburg
transgene *Tg*(UBB^{+1}/NS^{S49P})	animal facility UKE, Hamburg
transgene neuroserpin-deficient ($Ns^{-/-}$)[(c)]	animal facility UKE, Hamburg

Mouse strains were generated and published by [(a)]Galiciotti et al. 2007; [(b)]Fischer et al. 2009; [(a)]Madani et al. 2003.

4. Methods

4.1 Housing and breeding of animals

4.1.1. Animal housing

Mice were maintained under pathogen-free conditions in the animal facility of the University Medical Centre Hamburg-Eppendorf on a 12-hrs light/dark cycle at around 21 °C with 50-60 % humidity. All mice were provided with water and standard food pellets *ad libitum*. Pups were separated from their mother 21 days after birth. Up to four animals were housed in a Makrolon Standard cage typ II. All males were kept separately after breeding.

4.1.2. Breeding of transgenic mice

All mice strains (see table 12) were kept heterozygous. Every 6 months two new mating pairs per mouse line, where a transgenic male was bred with two C57BL/6 females, were started. The offspring's were genotyped by PCR-analysis (see 4.1.5) with specific primers for the

transgene (see table 4). In general, around 50 % of the littermates were heterozygous for the transgene. *Tg*(UBB^{+1}/NS^{S49P}) mice were generated by crossing two *Tg*(UBB^{+1}) female with one *Tg*(NS^{S49P}) male.

4.1.3. Isolation of genomic DNA from tail biopsy

Tail biopsy from 7 days old animals were taken and digested over night at 56 °C with 650 rpm agitation in 500 µl lysis buffer supplemented with 0.1 mg/ml proteinase K. To separate DNA from debris a 5 min centrifugation with 13000 rpm at RT was performed. The supernatant was transferred to a fresh 1.5 ml microcentrifuge tube and DNA was precipitated by adding 500 µl of isopropanol. The precipitate was sedimented by centrifugation at 13000 rpm, for 10 mins at RT, washed twice with 70 % ethanol and air dried for 15 min under the hood. Afterwards DNA was resuspended in 50 µl pre-warmed (37 °C) sterile distilled water with an agitation of 800 rpm for 10 mins.

Proteinase K lysis buffer

Tris-HCl pH 8.5	100 mM
EDTA	5 mM
SDS	0.2 % (w/v)
NaCl	200 mM

4.1.4. Genotyping of transgenic mice by PCR

DNA from tail biopsy was checked for the presence of the transgene by PCR (see 4.3.4.2) with specific primer pairs (see 4.1.5). Each PCR reaction consists of the following mix and was added to 1 µl of genomic DNA:

gene-specific 5'- and 3'- primer (each 10 µM)	1 µl each
dNTPs (each nucleotide 10 mM)	4x 0.25 µl
10x reaction buffer	2.5 µl
distilled water	18.75 µl
taq-polymerase (5 U/µl)	0.25 µl

In heterozygous animals a 540 bp amplicon of neuroserpin as well as a 400 bp amplicon of ubiquitin could be detected, whereas in wild-type animals no product was seen.

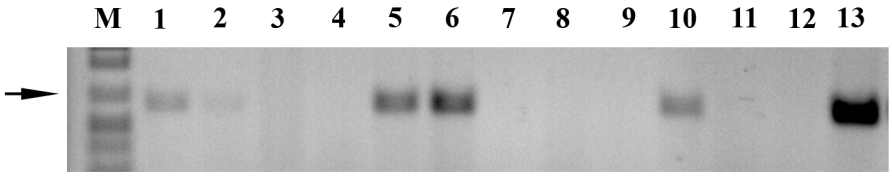

Figure 11: PCR analysis of genomic DNA to identify heterozygous transgenic mice

1 µl genomic DNA from tail biopsy of 7 days old animals was checked by PCR analysis with transgene specific primer pair hNS-F/hNS-R. The amplified 540 bp product was analysed on a 1 % agarose gel and stained with ethidiumbromide. The transgene was detected in the samples 1, 5, 6 and 10; 11-1kb DNA ladder; 12-negative control, PCR reaction without DNA; 13-positive control, PCR reaction with DNA carrying the transgene; arrow indicates the 600 bp band.

4.2 Animal experiments

4.2.1. Permission for animal experiments

All animal experiments were licensed from the city of Hamburg department for health and consumer protection (ID-nr. 419, ID-nr. 264).

4.2.2. Extraction of brain tissue

Transgenic animals were deeply anesthetized with Halothan and sacrificed by cervical dislocation. Skin and ears were removed and the skull was opened with scissor starting from the foramen magnum along the middle suture to the nose, as well as laterally above the maxilla. The brain was carefully isolated from the skull at which the optic nerves and the medulla oblongata were cut. The frontal part of the brain, including the olfactory bulbs, the frontal cortex and the striatum was immediately frozen down at dry ice and stored at -80 °C for subsequent biochemical analysis, whereas the residual part of the brain was fixed for at least 16 hours in formaldehyde for immunohistochemical analysis.

4.3 Molecular biological methods

4.3.1. Isolation of RNA

RNA from frozen brain tissue and N2a cells was purified using RNA Miniprep Kit (Stratagene) following usage instructions. Briefly, frozen samples (-80 °C) were fractured with a dismembrator (2000 rpm) for 1 min in pre-cooled lysis buffer, containing guanidine thiocyanate, one of the strongest protein denaturants which at the same time prevents RNA

degradation by ribonucleases (RNases). The sample was cleaned by a 5 mins centrifugation step at 4000 rpm, the supernatant was loaded on a column and centrifuged for 5 mins at maximum speed to remove particles and to reduce the amount of DNA. The filtrate was mixed with an equal volume of 70 % ethanol (with DEPC water), the mixture was transferred to a RNA-binding column and centrifuged several times for 2-3 mins with maximum speed to capture the RNA. To remove the remaining DNA, the column was treated with a low-salt wash buffer and RNase-free DNase I digestion buffer for 15 mins at 37 °C. A series of washes with high salt and low salt washing buffer eliminated the DNAse and other proteins. Afterwards, pure RNA was eluted from the spin cup matrix with 60 µl of pre-heated 60 °C warm autoclaved DEPC water and captured in a microcentrifuge tube. The RNA concentration was measured by optical density recording (see 4.3.2.) and RNA integrity and purity was assessed on an agarose gel (see 4.3.3.).

DEPC water

1 ml of DEPC was solved in 1 litre distilled water, incubated over night with constant stirring and autoclaved.

4.3.2. Nucleic acid concentration measurement

To determine the concentration of RNA and DNA, samples were diluted 1:100 in water. The absorbance of the diluted sample was measured at 260 and 280 nm in a cuvette with a spectrophotometer. Water was used as a blank. The reading at 260 nm allows for calculation of the concentration of nucleic acids in the sample. An optical density of 1 corresponds to approximately 40 µg/ml for RNA and 50 µg/ml for double-stranded DNA; as a result the concentration of nucleic was calculated as follows:

RNA concentration (µg/ml) = OD_{260} x 40 µg/ml x dilution factor

DNA concentration (µg/ml) = OD_{260} x 50 µg/ml x dilution factor

The ratio of OD_{260}/OD_{280} is an indicator for the purity of nucleic acid, as absorbance at 280 nm determines the amount of protein in a sample. For clean nucleic acid the values should be between 1.8 and 2.0. For example, a ratio of 1.8 means, there are 60 % of unwanted proteins and just 40 % nucleic acid in the sample, whereas a ratio of 2.0 stands for 100 % nucleic acid (after Sambrook and Russell “Molecular Cloning 1” Third Edition).

4.3.3. RNA-agarose gel

The electrophoretic separation of RNA was done in a 1.4 % agarose gel supplemented with formaldehyde, to destroy the secondary structure of RNA in order to see a migration with the true molecular weight. Therefore, 1.4 g of agarose and 88 ml of RNAse free water were boiled, cooled to 60 °C and 10 ml of 10x MOPS as well as 2.7 ml of 37 % formaldehyde were added. The gel mixture was casted in a sealed horizontal chamber with an inserted comb to form loading pockets. 1x MOPS was used as running buffer.

To control RNA preparation 1 µg of RNA was mixed with 10 µl RNA loading buffer and adjusted with DEPC water to a volume of 20 µl. The mixture was heated for 10 mins at 65 °C, chilled on ice for 2 mins, centrifuged with maximum speed to collect condensation and immediately loaded on the gel. Electrophoresis was performed with constant 80 V for 40 mins.

Intact total RNA migrated as a sharp 28S (5kb) and 18S (2kb) rRNA band on the gel, ideally the 28S rRNA band should be approximately twice as intense as the 18S rRNA band (see Fig. 15, lane 2). This 2:1 ratio (28S:18S) is a good indicator for intact RNA. Partially degraded RNA will not exhibit a 2:1 ratio or will lack the sharp rRNA bands; completely degraded RNA will appear as a smear with lower molecular weight.

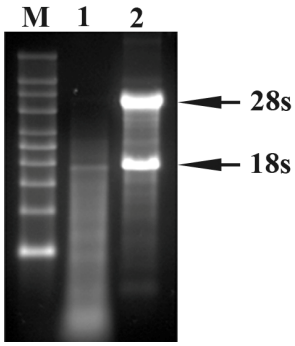

Figure 12: Intact versus degraded RNA

One µg of degraded total RNA and intact total RNA were run on a 1 % denaturing agarose gel. The 18S and 28S ribosomal RNA bands are clearly visible in the intact RNA sample. The degraded RNA appeared as a smear with lower molecular weight. (modified after Applied Biosystems 2011)

10x MOPS buffer

MOPS	200 mM
sodium acetate	50 mM
EDTA	10 mM

adjust to pH 7 with NaOH

RNA loading buffer (100µl freshly prepared)

10x MOPS buffer	10 µl
RNAse free distilledwater	11.5 µl
deionized formamide	50 µl
37 % formaldehyde	17.5 µl
10x loading dye	10 µl

10x loading dye

sterile glycerol	50 %
EDTA	1 mM
bromophenol blue	0.25 %

4.3.4. Reverse transcriptase polymerase chain reaction (rt-PCR)

4.3.4.1. Reverse transcription

To synthesize cDNA from total RNA the RevertAid^{TM} kit (Fermentas) was used according to operating instructions. Thereby, isolated RNA (see 4.3.1.) was transcribed to first strand cDNA by H-Minus-Reverse-Transcriptase. To hybridize mRNA from total RNA, oligo(dT) primers selectively annealed to the poly(A)- region at the 3' terminus of mRNA. To protect RNA from degradation recombinant RNase-Inhibitor was added.

For each rt-PCR reaction, 500 ng RNA was mixed with 1 µl oligo(dT) primer (100 µM), adjusted to a volume of 11 µl with DEPC treated water and pre-incubated for 10 mins at 65 °C to denature the RNA with subsequent cooling at 4 °C. Afterwards, 8 µl of a mixture containing

5x reaction buffer	4 µl
dNTP mix (dATP, dCTP, dGTP, dTTP) (each 10 mM)	2 µl
RNase inhibitor (20 U/µl)	1 µl
MULV reverse transcriptase (200 U/µl)	1 µl

was added. The reaction mix was shortly centrifuged and incubated for 8 mins at 25 °C. Afterwards, the sample was heated to 42 °C for 70 mins for the reverse transcription. To stop the reaction the temperature was increased to 70 °C for 5 mins, to denature the enzyme. 4 µl of synthesised cDNA was needed as template for the following PCR reaction.

4.3.4.2. Polymerase chain reaction (PCR)

The polymerase chain reaction was used to exponentially amplify specific segments of synthesised cDNA (see 4.3.4.1.) or of genomic DNA isolated from tail biopsies (see 4.1.5.).

PCR amplification of DNA occurred by repeated cycles of three temperature dependent steps: (1) the double-stranded DNA template was denatured by heating to 94 °C; (2) oligonucleotide primers were annealed to single-stranded DNA template (typically about 45-55 °C); and (3) DNA fragments were elongated by DNA polymerase (normally at approximately 72 °C) in 5' to 3' direction starting from each primer. With each cycle of denaturation, annealing, and elongation the specific DNA fragment was amplified exponentially.

The specific primers were designed to match the 5'- and 3'-terminus, of the cDNA fragment which needs to be amplified, respectively. To insure adequate specificity, the primers must be 20-30 nucleotides long and should span intron boundaries. The melting temperature (Tm) of the primer pairs defines the annealing temperature of the PCR, whereas annealing is usually done 5 °C below the Tm. As a rule of thumb, the Tm of a primer was estimated by adding 2 °C for each adenine or thymine and 4 °C for each guanine or cytosine. The rate of primer extension by thermostable *Taq* polymerase is about 50-100 nucleotides/second. Thus, the time required for primer elongation depends on the length of the sequence to be amplified.

Each PCR reaction consisted of the following mix and was added to 4 µl (~5 ng) of synthesised cDNA:

genspecific 5'- and 3'- primer (each 10 µM)	1 µl each
dNTPs (each nucleotide (10 mM)	4x 0.25 µl
10x reaction buffer	2.5 µl
distilled water	15.375 µl
taq-polymerase (5 U/µl)	0.125µl

To amplify DNA fragments of interest a PCR thermal cycler was used. In our example, the amplification of XBP1 was done with the following programme:

initial denaturation	94 °C	5 min
denaturation	94 °C	30 sec
annealing	55 °C	30 sec

elongation	72 °C	1 min
final elongation	72 °C	10 min
cooling	4 °C	hold

Each cycle of denaturation, annealing, and elongation was repeated 30 times. A 600 bp amplicon could be detected on an 1 % agarose gel.

All other genes analysed via PCR in this study are registered with their respective elongation time, annealing temperature and cycling number in table 13.

Table 13: Annealing temperatures, elongation times and number of cycles for primer taken in PCR reactions to amplify specific cDNA sequences

Gen	annealing temperature	elongation time	number of cycles
ß-actin*	58 °C	30 sec	40
ATF4*	64 °C	30 sec	40
Chop*	64 °C	30 sec	40
neuroserpin	58 °C	45 sec	40
UBB+1	60 °C	30 sec	35
XBP1	55 °C	30 sec	30

* primers used for quantitative real-time-PCR

4.3.5. Quantitative real-time polymerase chain reaction (qrt-PCR) with iCycler (Biorad)

To measure mRNA expression of a particular gene in brains of transgenic and wild-type mice quantitative real time PCR was performed.

A relative quantification approach based on the relative expression of a target gene versus a reference gene after Pfaffl (Pfaffl, 2001) was chosen. The amplified DNA was detected by a fluorescent signal as the polymerase chain reaction progressed. As fluorogenic dye served SYBR Green which binds double-stranded DNA, and upon excitation (LED with 470 nm) starts emitting light with the characteristic wavelength of 530 nm.

For the mathematical model of Pfaffl it is necessary to detect the efficiency (E) of each PCR assay and to determine crossing points (CP) for each transcript. CP was defined as the point at which the fluorescence rises above the background fluorescence (threshold

fluorescence). E was calculated by $E=10^{(-1/slope)}$ using the slope of a standard curve where CP values were blotted against the concentration of cDNA. For each primer pair efficiencies were assessed by three independent experiments. Typical efficiencies range from 1.7 to 2. Based on PCR efficiency (E) and crossing point (CP) deviation of an unknown sample versus a control, the relative expression ratio (R) of a target gene is calculated with respect to a reference gene:

$$\text{Ratio} = (E_{target})^{\Delta CP \text{ target (control - sample)}} / (E_{ref})^{\Delta CP \text{ ref (control – sample)}}$$

E_{target} -efficiency of target gene transcript;
E_{ref} -efficiency of a reference gene transcript;
ΔCP_{target} -CP deviation of control – sample of the target gene transcript;
ΔCP_{ref} -CP deviation of control – sample of reference gene transcript.

As reference gene served ß-actin since it is a stable and secure unregulated transcript in the brain. Moreover, it compensates variations between runs. Furthermore, to proof specificity and purity of RT-PCR products a melting curve analysis, where the melting temperature was blotted against the change of fluorescence over time (dF/dT) was performed. A single melting peak in the diagram reflects a pure sample without any contamination.

Quantitative real-time PCR was performed with an iCycler from Biorad and a ready to use SYBR Green/Fluorescein qPCR Master Mix kit. Samples were assessed in triplicates. Each reaction was done with 6.25 µl 2x Master Mix in a total volume of 12.5 µl, where 0.5 µl (0.25 ng) cDNA were used as a template. The final primer concentrations were 0.3 µM. The following thermal cycling programme was used:

	temperature	time	number of cycles
initial denaturation	95 °C	10 sec	1
denaturation	95 °C	15 sec	40
annealing	60 °C	30 sec	
elongation	72 °C	30 sec	

After each cycle a single fluorescence measurement was done and the CP values were calculated by iCycler software (settings: PCR Base Line Subtracted Data). Finally, the reaction was heated to 95 °C with 0.1 °C per second with continuous fluorescence measurement (melting curve programme) and cooled down to 4 °C.

4.3.6. DNA-agarose gel electrophoresis

To separate PCR products according to their size, a horizontal electrophoresis with 1 % agarose in 1x TAE buffer was performed. Therefore, agarose was melted in 1x TAE, cooled to 60 °C and casted in a sealed chamber with an inserted comb to form loading wells. Each PCR reaction (25 µl) was mixed with 5 µl of 6x DNA sample buffer and loaded to the gel. A 1kb DNA ladder served as size standard. Electrophoresis was performed with 10 V per cm. After electrophoresis the gel was incubated for 5 mins in a bath containing ethidiumbromide which binds strongly to DNA by intercalating between the bases. Visualization of DNA fragments was done under invisible UV light which stimulated ethidiumbromide to transmit visible orange light. Pictures were taken for documentation via a digital camera.

1x TAE

Tris base	40 mM
acetic acid	40 mM
EDTA	1 mM
pH 8	

6x DNA sample buffer

Tris HCl pH 7.6	10 mM
EDTA	60 mM
glycerol	60 %
bromophenol blue	0.03 %

4.3.7. Purification of PCR products

To purify DNA fragments from a solution a GeneJet PCR kit (Fermentas) was used following instructor's guidelines. The purification is based on the immanent binding capacity of DNA to silica gel surfaces in the presence of high chaotropic salt concentrations; whereas low-ionic-strength solutions loosen that particular bonding.

Therefore, 30 µl binding buffer where mixed with 25 µl PCR reaction, 20 µl of isopropanol were added, the total was loaded on a purification column and centrifuged at 16000 rpm for 1 min. The flow through was discarded and the column was washed with 300 µl buffer containing ethanol. To completely remove the washing buffer, the column was centrifuged again at 16000 rpm for 1 min. The DNA was eluted in 20 µl of sterile distilled

water pre-warmed to 37 °C. The concentration of the DNA fragment was determined by their absorbance at 260 nm (see 4.3.2.).

4.3.8. Restriction digestion with endonucleases

For further biochemical analysis with a restriction enzyme 20 µl purified PCR reaction mix with purified DNA (see 4.3.7) were digested with 0.5 µl Pst1 restriction enzyme in 2.3 µl reaction buffer H, for one hour at 37 °C (water bath). The whole reaction was mixed with 5 µl 6x DNA sample buffer and analysed on a 1 % agarose gel (see 4.3.6.).

4.3.9. Preparation of plasmid DNA for transient transfection

The pcDNA3.1 plasmid construct was purchased from Invitrogen and the genes for human wild-type and S49P neuroserpin were cloned into the multiple cloning-site between EcoRI and XhoI restriction sites. The gene encoding the sequence for each individual protein was linked to their original mammalian secretion peptide. The sequence used for cloning strategies for neuroserpin is identified under BC018043.1 (NCBI). Mutation of neuroserpin gene was done by site directed mutagenesis with a kit from Stratagene using oligonucleotide primers containing the desired mutation. All pcDNA3.1 constructs were generated in Prof. Glatzels lab by Beata Szalay and Dr. Markus Geissen.

4.3.10. Transformation of competent cells

Previous prepared DNA (from midi purification of plasmid DNA see 4.3.12.) was used for transformation of XL10-Gold competent cells (Stratagene, 200315). Therefore, 50 µl ultracompetent cells were quickly thawed on ice and 1 µl (100 ng) of DNA was added carefully and gently mixed by flicking. The mixture was incubated for 30 mins before being heat-shocked at 42 °C for 30 secs and then replaced on ice for 2 mins. Afterwards, 450 µl of sterile antibiotic-free Lysogeny Broth media (LB) was added and incubated for 1 hour at 37 °C with agitation at 300 rpm. This incubation step, allowed the selection antibiotic resistance gene to be expressed. Approximately, 200 µl of each transformation was plated on ampicillin containing selecting LB agar plates under sterile conditions and incubated for 16 hours over night at 37 °C. Transformation efficiency was estimated from the number of colonies found on each plate against control transformation.

Lysogeny Broth media (LB)

Bacto Tryptone	10g
Bacto yeast extract	5 g
NaCl	10
distilled water	1 l
ampicillin	100 µg/ml

Adjust pH to 7 and autoclave to sterilize. For plating add 15 g/l agar-agar.

4.3.11. Mini purification of plasmid DNA

Colonies were selected from LB agar plates with a sterile toothpick and grown for 16 hours with shaking at 300 rpm at 37 °C in 2 ml LB medium containing 100 µg/ml ampicillin. The plasmid was purified using Plasmid DNA purification kit (Invitek) following suppliers manual. Cells were pelleted by centrifugation at 12000 x g for 1 min at 4 °C. The supernatant was discarded and the tube was dabbed on tissue to remove excess of media. Cells were resuspended in 250 µl solution A supplemented with RNase A, then 250 µl lysis solution B was added and mixed gently by inverting 6 times. Before a 5 mins incubation time, 250 µl of solution C was added and mixed by inverting 6 times. The whole homogenate was centrifuged at 16000 x g for 5 mins. The clarified supernatant was transferred onto a spin filter, incubated for 1 min and centrifuged at 10000 x g for 1 min. After the flow-through was discarded, 750 µl wash buffer was added followed by centrifugation twice at 16000 x g for 2 and 3 mins, respectively. The column was then placed into a sterile 1.5 ml microcentrifuge tube and DNA was eluted by addition of 50 µl sterile distilled water, incubation at room temperature for 5 mins and centrifugation at 16000 x g for 1 min.

4.3.12. Midi purification of plasmid DNA

Large quantities of plasmid DNA (up to 500 µg) were purified using Plasmid DNA purification kit from Macherey-Nagel, a silica-based anion-exchange kit. 20 µl cells from a 2 ml starter culture were grown for 16 hours with shaking at 300 rpm at 37 °C in 100 ml (high- copy plasmid) LB medium supplemented with 100 µg/µl ampicillin. The cultured bacterial cells were pelleted by centrifugation at 6000 x g for 10 min at 4 °C and the supernatant was discarded. Cells were resuspended in 8 ml of resuspension buffer containing RNase A by vortexing until no clumping was observed any more, then 8 ml of lysis buffer containing sodium hydroxide/SDS was added and mixed gently by inverting the tube 5 times.

During 5 mins of incubation, proteins as well as DNA are denatured and RNA is degraded. Then, 8 ml of neutralization buffer, containing potassium acetate, were added and mixed by inverting the tube 15 times. NucleoBond columns with an integrated filter were equilibrated by applying 12 ml of equilibration buffer. The whole lysate (24 ml) was loaded on the column with an integrated filter where it was simultaneously cleared from cell debris and precipitate by gravity flow. Two washing steps, one with 8 ml equilibration buffer and one with 8 ml washing buffer, were followed by elution of the plasmid DNA into a 15 ml tube by applying 5 ml elution buffer to the column. DNA was precipitated by adding 3.5 ml room temperature isopropanol for 2 mins, before being pelleted at 15000 x g for 30 mins at 4 °C. Pelleted DNA was washed with 2 ml 70 % ethanol, centrifuged at 15000 x g for 5 min, air dried for at least 10 min under a hood and eluted in 500 µl sterile distilled water pre-warmed at 37 °C.

4.3.13. DNA sequencing

DNA samples at 1 µg concentration were processed and determined by sequencing service of the UKE using DNA Analyzer. 1 µl sequencing primers at a concentration of 10 pmol/µl were provided per reaction.

4.4 Methods in protein biochemistry

4.4.1. Brain tissue homogenates

A 10 % (w/v) brain homogenate of frozen samples (see 4.2.2) in lysis buffer supplemented with proteases and phosphates inhibitors was prepared. Therefore, 55 mg brain tissue was lysed in 500 µl of buffer using a dismembrator at 2000 rpm for 90 seconds. The mixture was incubated for 5 mins at 4 °C and centrifuged at 4000 x g for 10 min at 4 °C. The supernatant was transferred into a new microcentrifuge tube and the protein concentration was determined (see 4.4.2.).

brain lysis buffer (RIPA)

NaCl	150 mM
NP-40	1 %
DOC	0.5 %
SDS	0.1%
Tris base pH 8	50 mM

EDTA 1 mM

4.4.2. Quantification of Protein Concentration by Bradford

A standard curve with concentrations of 0.25, 0.5, 1, 1.5, 2 mg/ml of BSA in sterile distilled water was generated. Protein samples were pre-diluted according to expected protein content (mouse brain 1:20 dilution). To end up with ready-to-use protein concentrations in [µg/µl], 5 µl of each standard dilution were premixed with 5 µl of water, as well as 1 µl pre-diluted protein sample with 9 µl of water. The samples were done at least in duplicates. As blank were taken water and homogenisation buffer for standard and samples, respectively. Afterwards, the protein samples were prepared by adding 200 µl of Bradford reagent to 10 µl of each sample and standard. The final protein concentration was measured at an absorbance of 595 nm with a spectrophotometer (Biotek). For the standard curve, protein concentrations of BSA were blotted against their absorbance values and protein concentration of unknown samples were calculated taking into account their dilution factor. Table 14 shows the chosen standard dilutions:

Table 14: Preparation of protein standards by Bradford

standard dilution	**1**	**2**	**3**	**4**	**5**
BSA standard concentration [mg/ml]	2	1.5	1	0.5	0.25
Volume of 2 mg/ml BSA [µl]	70	52.5	70	70µl from 1µg/µl BSA	70µl from 0.5µg/µl BSA
sterile distilled water [µl]		17.5	70	70	70

The BSA protein standards were prepared by using a 2 mg/ml stock solution. Final protein concentrations were measured at an optical density (OD) of 595 nm. Protein concentrations of brain homogenates were determined according to a standard curve, where protein concentrations of BSA at 595 nm were plotted against their absorbance values. MS excel version 1997 was used for further calculations.

4.4.3. SDS- polyacrylamide gel electrophoresis after Laemmli (SDS-PAGE)

To analyse homogenates as well as cell lysates a discontinuous (tank and gel buffers are different from each other) gel electrophoresis under denaturating conditions after Laemmli (Laemmli, 1970) was performed to separate proteins according to their molecular weight. For

SDS-PAGE, 1 mm gels were prepared using DCX-700 Dual Cool Vertical Gel System from CBS Scientific. An acrylamide concentration of 10 % (v/v) or 16 % (v/v) was required to analyse proteins.

Percentage of the separating gel	**10 %**	**16 %**
Acrylamid/Bisacrylamid (37, 5:1)	2.5 ml	3.75 ml
sterile distilled water	3 ml	1.75 ml
1.5 M Tris HCl pH 8.8	1.9 ml	1.9 ml
10 % SDS	75 µl	75 µl
10 % APS	75 µl	75 µl
TEMED	3 µl	3 µl

The separating gel with a volume of 7.5 ml was overlaid with 50 % (v/v) isopropanol/water to obtain a plane surface. After polymerisation was completed, the mixture was washed away with water and 2 ml of a 5 % (v/v) stacking gel were added.

Percentage of the stacking gel	**5 %**
Acrylamid/Bisacrylamid (37, 5:1)	650 µl
sterile distilled water	2.75 ml
0.5 M Tris HCl pH 6.8	500 µl
10 % SDS	40 µl
10 % APS	40 µl
TEMED	4 µl

A 15 or 10 well comb to form loading pockets for the samples with an average loading capacity of 20 µl or 40 µl, respectively, was pouched into the stacking gel. Samples were mixed with 4x SDS loading buffer, cooked at 95 °C in a heating block for 10 mins to denature the proteins. Ten µl of each sample with 2 µg/µl protein concentration was loaded next to a pre-stained SDS-PAGE standard (10000-170000 Dalton). Electrophoresis took place in 1x running buffer at constant 80 V until the samples passed the separation gel; afterwards the proteins were separated at constant 100 V until the bromophenol blue front reached the lower edge of the gel.

4x SDS loading buffer

bromphenol blue	0.4 % (w/v)
DTT	400 mM
glycerol	40 % (v/v)
Tris Base pH 6.8	250 mM
SDS	8% (w/v)

10x SDS running buffer

Tris Base	250 mM
glycin	1,92 M
SDS	1 %

4.4.4. Non-denaturating PAGE

For non-denaturating PAGE, the Mini-Protean 3 system from Biorad with 1.5 mm spacer and 10 well-combs were used. The gels were prepared as described above but with a concentration of 7.5 % (v/v) acrylamide and no SDS.

Percentage of the separating gel	**7.5 %**
Acrylamid/Bisacrylamid (37, 5:1)	2.5 ml
sterile distilled water	3 ml
1.5 M Tris HCl pH 8.8	1.9 ml
10 % APS	75 µl
TEMED	3 µl

Sample preparation was the same as for SDS-PAGE except a 2x loading buffer without SDS was used. A total volume of 30 µl was loaded to the native gel. Electrophoresis was performed in buffer, been composed of a cathode and anode one, at constant 80 V until the samples entered the separation gel voltage was increased to 100 V. Before the bromophenol blue front reached the bottom of the gel, electrophoresis was stopped.

2x native loading buffer

bromophenol blue	0.02 % (w/v)
glycerol	20 % (v/v)
Tris base pH 6.8	125 mM?

10x native running buffer	**cathode**	**anode**
Tris base	0.53 M	0.1 M
Glycin	0.68 M	0.68 M
pH	8.9	7.8

4.4.5. Western Transfer

To transfer the separated proteins from the gel on a PVDF membrane for immunodetection, tank-blotting after (Towbin et al., 1979) was performed.

A stock solution of 10x transfer buffer was prepared and diluted according to the gel type (SDS-PAGE: 10 % (v/v) 10x transfer buffer, 20 % (v/v) methanol, 70 % (v/v) water; non-denaturating PAGE: 10 % (v/v) 10x transfer buffer, 90 % (v/v) water) for transfer. The added methanol prevents the gel from swelling during transfer and improves the absorption of proteins on the membrane. Before transferring, the PVDF membrane and 3MM Whatman paper was cut to the size of the gel and equilibrated in transfer buffer for 5 mins at RT. The PVDF membrane was activated for 1 min in methanol and equilibrated in transfer buffer. Since the proteins in the acrylamide gel are negatively charged as they are encircled by SDS, they will run towards the anode. The sandwich for transfer was assembled in a cassette as followed: (cathode-side) sponge pad, 2x Whatman paper, acrylamide gel, PVDF membrane, 2x Whatman paper (anode-side). The sandwich was inserted together with two ice blocks into the transfer chamber which was filled with the corresponding buffer. The protein transfer was carried out at constant 100 V for 90 mins with continuous stirring to maintain a homogenous ion concentration and cool temperature.

To proof the efficiency of protein transfer the PVDF membrane was stained for 1 min with Ponceau S-solution, which as a negative stain binds positively charged amino groups of proteins. Rinse the blot in distilled water until background is reduced and red protein bands appeared, and highlighted Protein standards with a ball pen. Wash blot 2 times in distilled water to remove Ponceau S-solution.

10x transfer buffer

Tris base	250 mM
glycine	1,92 M
pH 8.3	

Ponceau S-solution

Ponceau S	0.5 % (w/v)
acetic acid	1 % (v/v)

4.4.6. Immunoblotting

To saturate unspecific binding sites the PVDF membrane was blocked over night at 4 °C or 1 hour at room temperature in 5 % PBST-milk with constant agitation. The membrane was probed with primary antibody (Table 7) diluted in 5 % PBST-milk over night or over the weekend at 4 °C with constant agitation. Thereafter, the membrane was washed 3 to 6 times for 5 mins in PBST. The secondary HRP coupled antibody (Table 8) was diluted in 5 % PBST-milk and put on the membrane for 1 hour at room temperature with constant shaking. Afterwards the membrane was washed for 30 mins in PBST, changing it every 5 mins.

To detect specific proteins an enhanced-chemiluminescence-reagent (ECL) was used. Luminol from the reagent is oxidized by the peroxidase coupled to the secondary antibody, thereby emitting light which can be detected by an X-ray film or a camera. Phenol from the reagent is enhancing the light emission by 1000 times. The membrane was incubated for 5 mins in the respective detection kit corresponding to the sensitivity of the signal, with femto kit being most sensitive. The blot was placed bubble free between plastic foil and positioned in X-ray cassette or at the bottom of Chemidoc XRS machine. The X-ray film was processed by an automatic film developer after a total exposure time of 5 mins. Digital images which could be further analysed by µQuant software were taken with the Chemidoc XRS machine after an exposure time of 30 secs and 5 mins.

Blots for further analysis were stripped with stripping buffer. The membrane was washed quickly with PBST and incubated in stripping buffer twice for 30 mins at room temperature with agitation. Afterwards, the membrane was washed twice in PBST for 10 mins, blocked for 1 hour in PBST-milk and re-probed over night at 4 °C with a different antibody.

10x PBS

NaCl	1.37 M
KCl	26.8 mM
$Na_2HPO_4*2H_2O$	64.6 mM
KH_2PO_4	14.7 mM
pH 7.2	

PBST

10x PBS	10 %
Tween 20	1 %
distilled water	90 %

5 % PBST-milk

skim milk powder	5 % (w/v)

The skim milk powder was solved in PBST.

stripping buffer

glycine	0.2 M
SDS	1 %
pH 2	adjust with HCl

4.4.7. ELISA

To measure the concentration of polymeric and total neuroserpin in mouse brain homogenates an enzyme-linked-immuno-absorbance-assay (ELISA) according to published protocol (Miranda et al., 2008; Miranda et al., 2004) was performed.

Therefore, 96 well plates with a high binding capacity were coated over night with neuroserpin antibody (2 µg/ml, see Table 7) in PBS. After 3 washes with washing buffer, the plates were incubated for 2 hours with blocking buffer at room temperature. The samples and standards were diluted in blocking buffer and incubated over night at 4 °C. The work was done at least in duplicates, with several sample dilutions. Antibodies for detection were left on for 2 h, they were either a blend of three monoclonal neuroserpin antibodies (final concentration 1 µg/ml), or a polymer specific monoclonal antibody 7C6 (used at 1 µg/ml)

(Table 7). The secondary rabbit anti-mouse IgG HRP-coupled antibody (Table 8) was incubated for 1 hour. To develop the reaction TMB liquid substrate was added. After 10 mins in the dark, the reaction was stopped with 1M H_2SO_4 and absorbance was read at 450 nm using a spectrophotometer.

Washing buffer		**Blocking buffer**	
PBS	pH 7.4	PBS	pH 7.4
NaCl	0.9 % (w/v)	BSA	0.25 % (w/v)
Tween 20	0.05 % (v/v)	Tween 20	0.05 % (v/v9

4.5 Immunohistochemistry

To detect the presence of specific proteins in cells or tissue, immunohistochemistry was performed. The method is based on specific antibody-antigen binding and contains the following steps: 1) binding of primary antibody to antigen; 2) recognition of the antibody-antigen complex by secondary, enzyme conjugated, antibody; 3) forming of coloured precipitate at the sites of antibody-antigen binding, after addition of substrate and chromogen. Preservation and fixation of the sample is critical for tissue architecture, cell morphology and antigen retrieval of target epitopes.

4.5.1. Formalin fixed tissue

Brains were fixed in 3.5 % formaldehyde solution for at least 16 hours followed by dehydration in ethanol of ascending concentrations, then put into xylol solutions, and finally transferred into paraffin solution using an ASP 300S dehydration machine. Afterwards, tissue was embedded in liquid paraffin (60 °C). After cooling to 4 °C to set paraffin, the blocks were released of their embedding cassettes and stored at room temperature for further processing.

4.5.2. Sectioning

Coronal sections were taken starting from the olfactory bulbs to the cerebellum. Paraffin blocks were cut into 4 µm thick sections with a microtome. The sections were collected and flattened in a water bath, transferred to a 65 °C water bath when taken up onto Superfrost slides. To drain off remaining paraffin and to dry the sections incubation at 60 °C over night was performed.

4.5.3. Haematoxylin/ Eosin staining

Haematoxylin and eosin staining is a standard laboratory procedure in histology. Thereby, basophilic nuclei were stained blue by haematoxylin, whereas eosinophilc structures like cytoplamsa, collagen and muscles were stained red by eosin.

Therefore, paraffin sections were incubated for 15 mins in Xylol and hydrated in descending series of alcohol rinsed in water and incubated for 5 min in haemalaun (after Mayer). The staining was stopped by rinsing the slides for 5 mins in distilled water. Differentiation was performed in HCl-water for 20 seconds, followed by a 5 mins rinse under running water, to reach a clear blue staining of the nuclei. Afterwards, the slides were incubated for 2-3 mins in 70 % ethanol. Counterstaining with hydrophobic eosin solution up to 3 mins was performed. To remove unbound dye, several washing steps in 100 % ethanol were done. The sections were dehydrated in ascending series of ethanol (each 2 times for 1 mins in 90 %, 96 % and 100 % ethanol), put into xylol (2 times for 2 mins) embedded in Sakura GLC mounting media and dried at 60 °C in an incubator.

HCl- water

distilled water	500 ml
HCl	2.5 ml of 37 % (v/v)

Eosin

Eosin	3 g
distilled water	300 ml

Phloxin B

Phloxin B	0.5 g
distilled water	50 ml

Eosin solution

Eosin	50 ml
Phloxin B	5 ml
ethanol	390 ml
acetic acid	2 ml

4.5.4. Immunohistochemical staining and analysis

Paraffinsections were stained using the Ventana Benchmark XT machine. Deparaffinated sections (see 4.5.3.) were boiled for 30–60 min in 10 mM citrate buffer, pH 6.0, for antigen

retrieval. To block endogenous peroxidase, the sections were incubated for 5 min with 3 % H_2O_2 in methanol and washed in distilled water as well as in TBS 2 times for 10 mins. Sections were incubated for 90 mins with primary antibodies diluted in antibody diluting agent (NeuN, activated Caspase3, Neuroserpin; Table 7); simultaneously unspecific binding sites were blocked. Slides were washed 3 times in TBS and incubated for 1 hour with appropriate immunoperoxidase-polymer coupled secondary antibodies diluted in Histofine. Visualisation was achieved by a 10-90 mins incubation step in the dark with DAB-H_2O_2 solution. Subsequently, several washes in distilled water and TBS were performed. Nuclei were counterstained using haemalaun (principle see 4.5.3). Sections were dehydrated according to the standard settings of the machine, cover-slipped using mounting media and dried in an incubator at 60 °C.

Pictures were taken using an axioscope40 bright field microscope from Zeiss equipped with a digital camera. At least three mice were analyzed per experimental group and time point. Immunosignals for Neuroserpin, NeuN and activated Caspase3 were quantified in the entire CA1 and CA2 hippocampal region at three anatomically matched levels.

antibody diluting agent

goat serum	20 %
antibody diluent	80 %

4.5.5. Fixed cell immunocytochemistry

CCL-136$^{GFP\text{-}LC3}$ cells transfected with pcDNA3.1 harbouring wild-type and mutant neuroserpin grown on glass cover slips, were washed in PBS, fixed in ice-cold acetone and blocked for 15 mins in PBS containing 1.2 mg/ml donkey serum. After incubation with goat anti-neuroserpin antibody (Table 7) for 20 mins, cells were washed, and Alexa555-labelled secondary antibody (Table 8) was applied for 20 mins. Nuclei were counterstained by 0.4 µg/ml 4’6-Diamidino-2’-phenylindole (DAPI) in PBS for 5 mins and slides were mounted in Fluoromount G. Images were taken on a fluorescence light microscope (Nikon###) equipped with digital camera. The percentage of neuroserpin expressing cells with autophagosomes and the percentage of autophagosomes containing neuroserpin was evaluated (at least three independent experiments; >100 cells/genotype).

4.5.6. Electron microscopy

For electron microscopy, animals were deeply anaesthetized by a mixture of Ketamin/Xylazine and perfused through the heart with perfusion solution.

For preembedding DAB-immunohistochemistry 150 µm thick sagittal vibratome sections of the brain were cut. After rinsing in PBS, endogenous peroxidase activity was blocked by applying peroxidase blocker for 30 min. Following additional washes in PBS, unspecific binding sites were saturated with blocker for 15 mins and sections were incubated over night with in carrier diluted neuroserpin antibody (Table 7). Slides were washed in PBS, incubated for 90 min with in carrier diluted biotinylated secondary antibody (Table 8) and incubated for additional period of 90 mins with Vectastain-ABC-kit (1:1000 in PBS). Afterwards, sections were rinsed in PBS and reacted with diaminobenzidine (DAB)-H_20_2 solution for 10 min. Thereafter, sections were postfixed with 1% (w/v) osmiumtetroxide, dehydrated in an ascending series of ethanol and embedded in Epon.

For postembedding immunogold labelling small pieces of cryoprotected cortices were mounted on specimen holders and immersed in liquid nitrogen. Ultrathin sections were cut, labelled according to (Slot and Geuze, 2007), and examined with a Zeiss EM 902. Electron microscopy was kindly done by Michaela Schweitzer from the morphological service unit of the ZMNH Hamburg.

perfusion solution		**peroxidase blocker**	
paraformaldehyde	4 % (w/v)	hydrogen peroxide (H_2O_2)	0.3 %
glutaraldehyde	0.1 % (w/w)	sodium borhydride ($NaBH_4$)	1 %
PBS pH 7.2		PBS pH 7.2	

blocker		**carrier**	
horse serum	10 %	horse serum	1 %
bovine serum albumin (BSA)	0.2 %	BSA	0.2 %

4.6 Cell culture

The cell culture work was done in collaboration with Markus Geissen.

4.6.1. Cell line

CCL-136$^{GFP-LC3}$ cells were a kind gift of Jan Lünemann (Lunemann et al., 2007b). These cells are human muscle cells stably expressing a GFP-Atg/LC3 fusion construct.

4.6.2. Thawing of frozen cell lines and cell culturing

A frozen aliquot of CCL-136$^{GFP-LC3}$ cells (stored in a cryovial at -80 °C) were collected on dry ice. The frozen aliquot was thawed for 1 min at 37 °C using a water bath until a small amount of ice remained. One ml of thawed cells were transferred into a 10 cm dish prepared with 10 ml of pre-warmed DMEM supplemented with 10 % (v/v) FBS and 1x Penicillin/Streptomycin (further considered as DMEM+). Cells were maintained at 37 °C and 5 % (v/v) in a humidified incubator. On the next day the media was replaced by fresh one, and the cells were culture for one to two days more. The cells were split at least twice before use in experiments.

Confluent cells were split (every 3-4 days) by washing with 10 ml 1x PBS, adding of 200 µl trypsin/EDTA and incubation for 5 mins at 37 °C; trypsin digestion was stopped by adding 10 ml of DMEM+. Cells were diluted into a new 10 cm dish at a ratio of 1:10 in a total volume of 20 ml.

4.6.3. Cryopreservation of cell lines

The cultured cells were assessed under a light microscope to evaluate the cell density and to confirm absence of bacterial and fungal contaminants. Cells from a confluent 10 cm dish were washed once with 1x PBS, trypsinised and resuspended in 10 ml culture media. After centrifugation at 500 x g for 10 mins, cell pellet was resuspended in 1 ml freezing media and transferred in a cryovial for storage at -80 °C.

Freezing media

40 % DMEM media

50 % FBS

10 % DMSO

4.6.4. Transient transfection of adherent cells and treatment with pharmacological agent

The day before transfection, cells were plated into a six well-dish to reach a confluency of 90% at the next day, as this is necessary for transfection with FUGeneHD. 4 µg of total DNA

(wt or S49P) was diluted with 100 µl of DMEM+, 10 µl of FUGeneHD was added and incubated at room temperature for 15 mins. The plated cells were washed with PBS, followed by adding approximately 1.9 ml fresh pre-warmed DMEM+ into each well. 100 µl of FUGeneHD-DNA mix were added into the appropriate wells and incubated for 3 days at 37 °C and 5 % CO_2 for protein expression. The cells were treated for 6h with Chloroquine with concentrations of 50 µM, or left untreated.

5. Results

5.1 Progressive accumulation of polymeric neuroserpin in the ER of neurons

To study polymeric neuroserpin deposition in neurons in detail, we used transgenic mice over-expressing wild-type and S49P human neuroserpin under the control of the neuronal Thy-1 promoter (Galliciotti et al., 2007). Firstly, we monitored the accumulation of neuroserpin aggregates over time. Therefore, coronal brain sections of *Tg*(NS^{S49P}) and *Tg*(NS) mice aged 8, 12, 20, 34, 45, 64, and >80weeks (each n=3) were stained with a neuroserpin antibody (Fig. 13A). In the entire CA1 and CA2 hippocampal region at three anatomically matched levels neuroserpin inclusion bodies were quantified (Fig. 13B). Mutant neuroserpin mice showed progressive accumulation of polymeric neuroserpin in neurons (Fig. 13B; t-Test $p<0.05$). At eight weeks of age the first inclusions emerged, increasing moderately up to week 20 (0.16 % area of neuroserpin immunoreactivity (area NSR) +/-0.02 at 8 weeks; 1.43 % area NSR +/- 0.39 at 12 weeks, 3.09 % area NSR +/- 0.82 at 20 weeks for *Tg*(NS^{S49P})). Neuroserpin aggregation rose, reaching a plateau between 34 and 45 weeks of age (5.87 % area NSR +/-0.63 at 34 weeks; 6.77 % area NSR +/- 1.1 at 45 weeks, for *Tg*(NS^{S49P})). From week 45 onwards inclusions rose exponentially, reaching a second plateau around 64 weeks (17.79 % area NSR +/- 0.81 at 64 weeks; 20.03 % area NSR +/- 2.94 at 80 weeks, for *Tg*(NS^{S49P})). In control mice expressing wild-type neuroserpin, no aggregates could be detected at any investigated time point (Fig. 13).

Next, we were interested to define the intracellular localization of polymeric neuroserpin. For this, we performed standard and immuno electron microscopy. Perinuclear inclusion bodies, differing in size and shape, were detected in hippocampal neurons of 70 weeks old *Tg*(NS^{S49P}) mice (Fig. 14A; left panel). Using immunogold labelled primary neuroserpin antibody, we could identify these structures as neuroserpin (Fig. 14A; middle panel). Detailed analyses using diaminobenzidin (DAB) labelled neuroserpin revealed that inclusions were engulfed by membranes in close proximity to ribosomes, suggesting that inclusions are retained within the rough ER (Fig. 14A; right panel). To further characterize these inclusions, non-denaturating gel electrophoresis from cerebrum of 8 weeks old transgenic mice was performed. Here, the polymeric nature of these aggregates became apparent. Higher molecular weight material could only be detected in *Tg*(NS^{S49P}) mice,

whereas in *Tg*(NS) mice neuroserpin migrated as a single band at the predicted mass of monomeric neuroserpin (Fig. 14B).

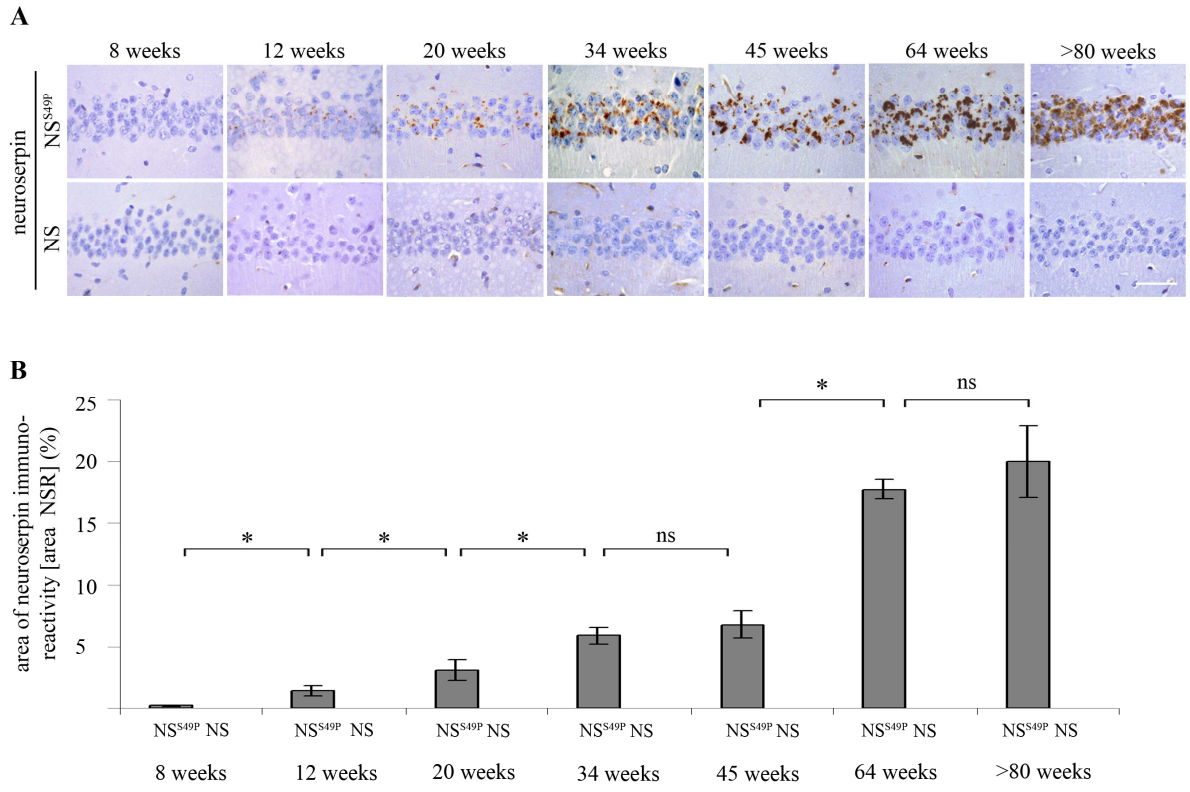

Figure 13: Progressive accumulation of mutant neuroserpin in FENIB mice

(A) Formalin-fixed, paraffin-embedded sections of CA1 and CA2 hippocampal region of aged (8, 12, 20, 34, 45, 64, and >80 weeks) *Tg*(NS^{S49P}) and *Tg*(NS) mice were stained with an antibody against neuroserpin to visualize inclusion bodies. Neuroserpin accumulates progressively in *Tg*(NS^{S49P}) but not in *Tg*(NS) mice (scale bar: 50 µm). (B) Quantification of neuroserpin inclusions from sections depicted in (A). Neuroserpin accumulation plateaued between 34 and 45 weeks, rising exponentially to week 64 where a second plateau is reached. The area of inclusions was quantified and presented as the percentage of the hippocampus (CA1 and CA2) [area NSR] (mean; ±STD; *: $p \leq 0.05$, ns: $p \geq 0.05$ in student's T-test).

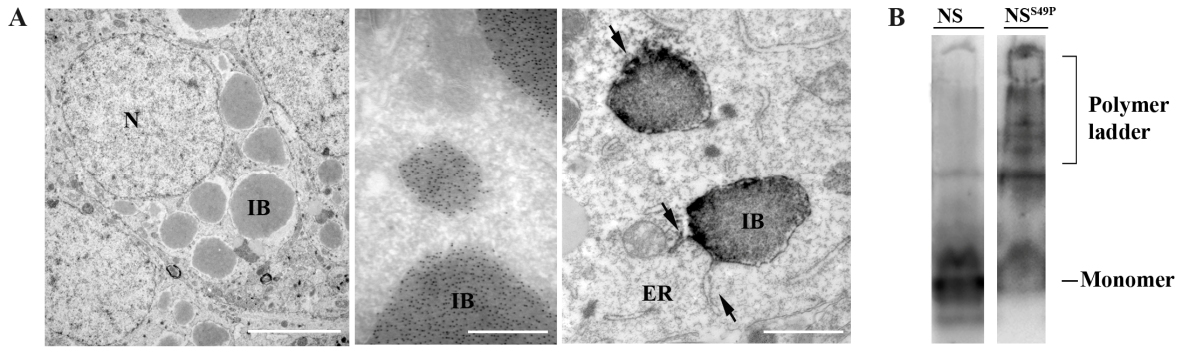

Figure 14: Ultrastructural analysis of mutant neuroserpin mice

(A) Electron micrographs from cortical neurons of >70 weeks old *Tg*(NS^{S49P}) mice (left panel). Numerous inclusion bodies (IB) are found in the cytoplasm (N, Nucleus). Immunogold labelling with an antibody specific for neuroserpin identifies these structures as neuroserpin (IB, middle panel). Analysis using DAB labelled neuroserpin revealed ER- localisation of aggregated neuroserpin (arrows right panel) (scale bar left to right: 5 µm, 500 nm, 1 µm; from Michaela Schweitzer). (B) Brain homogenates of 45 weeks old *Tg*(NS^{S49P}) and *Tg*(NS) neuroserpin mice, analysed by non-denaturating PAGE showed mutant neuroserpin as a polymer ladder, whereas wild-type neuroserpin separated as monomers.

5.2 Neurodegeneration in *Tg*(NS^{S49P}) mice

Since it has been suggested that accumulation of polymeric neuroserpin correlates with neurodegeneration (Davis et al., 1999a; Davis et al., 2002; Lomas, 2002), we assessed neuronal loss and apoptotic cell death morphologically. For this, immunohistochemical analysis of hippocampal brain sections of *Tg*(NS^{S49P}) and *Tg*(NS) mice (12, 45 and >80 weeks; each n=3) was performed. Mature neurons (NeuN positive) and apoptotic cells (activated caspase3 positive) were immunolabelled and quantified in the entire CA1 and CA2 hippocampal region at three anatomically matched levels (Fig. 15). *Tg*(NS) mice showed constant quantities of neurons over time (Fig. 15B; 5620 neurons/mm^2, +/- 139 at 12 weeks; 5610 neurons/mm^2, +/- 124 at 45 weeks; 5896 neurons/mm^2, +/- 202 at >80 weeks for *Tg*(NS)). In contrast, *Tg*(NS^{S49P}) mice exhibit a mild decline of neurons from 12 to 45 weeks of age (Fig. 15B; 5912 neurons/mm^2, +/- 99 at 12 weeks; 5324 neurons/mm^2, +/- 96 at 45 weeks for *Tg*(NS^{S49P})). This loss in neurons is more prominent at >80 weeks of age (Fig. 15B; 4027 neurons/mm^2, +/- 285 for *Tg*(NS^{S49P}) p=0.01). This neurodegeneration was accompanied by the occurrence of apoptotic cells (Fig. 15C). Apoptosis was only significant at 12 weeks of age in *Tg*(NS^{S49P}) (Fig. 15D; 3 Casp3+neurons/area, +/- 0.22 for *Tg*(NS^{S49P}) and 1 Casp3+neurons/area, +/- 0.67 for *Tg*(NS) p=0.04; at 45 weeks 2 Casp3+neurons/area,

+/- 0.59 for *Tg*(NS^{S49P}) and 1 Casp3+neurons/area, +/- 0.36 for *Tg*(NS); at 80 weeks 3 Casp3+neurons/area, +/- 1.09 for *Tg*(NS^{S49P}) and 2 Casp3+neurons/area, +/- 0.5 for *Tg*(NS)).

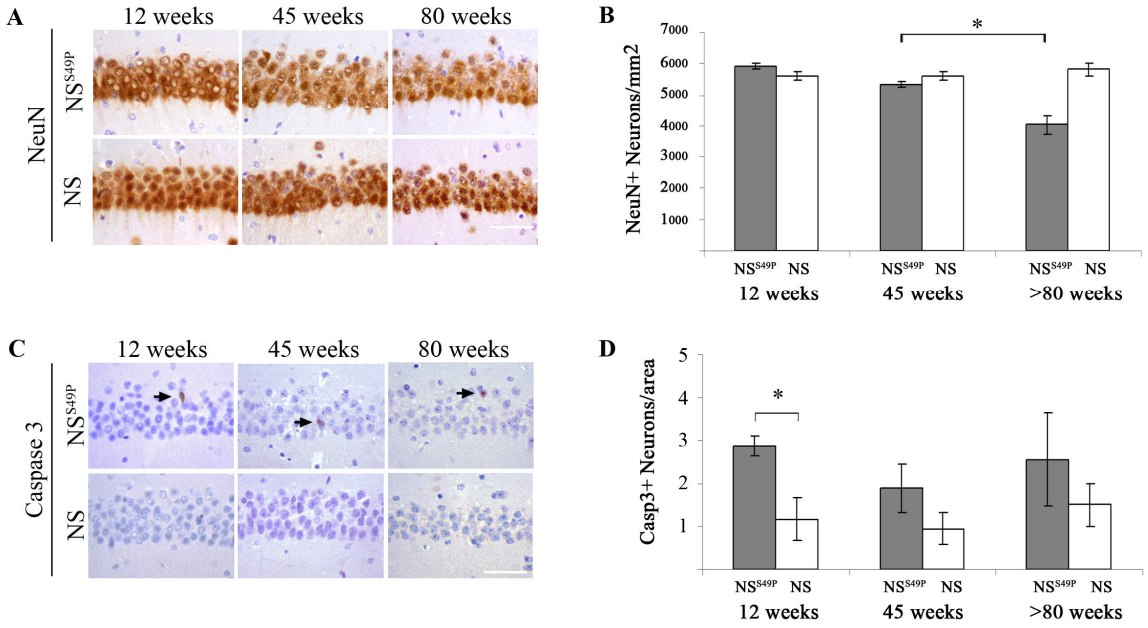

Figure 15: Neurodegeneration in FENIB mouse model

(A and B) Substantial loss of NeuN positive neurons in CA1 and CA2 hippocampal region only in aged (45 and 80 weeks) *Tg*(NS^{S49P}) but not in *Tg*(NS) mice when compared to younger littermates (12 weeks). (C and D) Caspase-3 positive neurons in brain revealed significant induction of apoptosis only at 12 weeks of age in *Tg*(NS^{S49P}) when compared to *Tg*(NS) (scale bars: 50 µm; mean; ±STD; *: p≤ 0.05 in student's T-test).

5.3 Degradation of mutant neuroserpin

5.3.1. Mild and unspecific induction of autophagy in FENIB mice

Recently, it was shown that in conformational diseases, such as mutant α1-antitrypsin deficiency (Kamimoto et al., 2006; Kruse et al., 2006), and in dementias, such as Alzheimer's disease (Nixon et al., 2000) or Huntington's disease (Ravikumar et al., 2002; Ravikumar et al., 2004); protein aggregates are processed by autophagy. Additionally, mice with defects in autophagic pathways show neurodegeneration (Komatsu et al., 2006; Mizushima et al., 2008). Therefore, we investigated the role of autophagy in degradation of mutant and wild-type neuroserpin.

5.3.1.1. Autophagic degradation of mutant and wild-type neuroserpin in a cell culture model

Microtubule-associated protein 1 light chain 3 (LC3), the mammalian homologue of Atg8, is a unique marker of the autophagic pathway (Klionsky et al., 2007), as the lipidated form (phosphatidylethanolamine conjugated LC3 II) is associated with the autophagosomal membrane (Fig. 10) (Kabeya et al., 2000). To investigate if neuroserpin itself is subject to degradation by autophagy, we made use of the muscle cell line CCL-136 stably transfected with a GFP-conjugated LC3 II construct (CCL-136$^{GFP-LC3}$). In CCL-136$^{GFP-LC3}$ cells, induction of autophagy leads to the appearance of fluorescent dots visualizing autophagosome formation which can be monitored by microscopy (Lunemann et al., 2007a).

Firstly, we were interested if neuroserpin expression in CCL-136$^{GFP-LC3}$ cells induces autophagy. For this, chloroquine treated CCL-136$^{GFP-LC3}$ cells transfected with neuroserpin were used as positive control. Cloroquine is an inhibitor of lysosomal acidification and therefore blocks the fusion of autophagosomes with lysosomes resulting in an increase of GFP-LC3 II positive vesicles (Fig. 16A). We transfected CCL-136$^{GFP-LC3}$ cells with wild-type (wtNS) or S49P mutant (S49P NS) neuroserpin, respectively, counted the total number of neuroserpin expressing cells and calculated the percentage of GFP-LC3 II positive cells expressing neuroserpin. In Fig. 16B ~64 % of CCL-136$^{GFP-LC3}$ cells expressing S49P NS showed GFP-LC3 II positive vesicles, whereas only ~43 % of cells transfected with wtNS showed positive autophagic vesicles. This result suggested that the expression of S49P NS induces autophagy.

Secondly, we analyzed if mutant or wild-type neuroserpin itself is a target for autophagy. Therefore we counted the total number of GFP-LC3 II positive autophagosomes per cell and determined the percentage of neuroserpin positive compartments colocalizing with GFP-LC3 II positive autophagic vesicles (Fig. 16C). Only 1.6 % S49P NS and just 1.5 % wtNS autophagosomes showed colocalisation of LC3 with neuroserpin. Thus, we concluded that presence of S49P NS induces autophagy, yet it is not a substrate for autophagy itself.

Then, we inhibited or induced autophagy in CCL-136$^{GFP-LC3}$ cells transfected with S49P NS and wtNS by applying chloroquine or rapamycin, respectively (Fig. 16C). Rapamycin induces autophagy by inhibiting TOR kinase (Jung et al., 2010; Kamada et al., 2000). We determined the percentage of neuroserpin positive cells harbouring GFP-LC3 II positive vesicles. Interestingly, a block in autophagy leads only to a slight increase of autophagic cells harbouring S49P NS compared to cells carrying wtNS (Fig. 16C;

chloroquine treated). Induction of autophagy does not lead to decreased numbers of autophagosomes in cells expressing S49P NS when compared to cells expressing wtNS (Fig. 16C; rapamycin treated). These data confirmed our initial conclusion that S49P-caused induction of autophagy is a secondary effect and that S49P NS is not a substrate for autophagy.

Figure 16: Mild induction of autophagy in a cell culture model of FENIB

(A) CCL-136$^{GFP-LC3}$ cells were transfected with wild-type (wtNS) or mutant (S49P) neuroserpin. Cells were treated with chloroquine (+Chlorquine, 5h) or left untreated. Neuroserpin is red, LC3 II green, merge is yellow representing autophagosomes containing Neuroserpin (scale bar: 20µm). (B) Combined data from three independent repeats of (A). Non-transfected CCL-136$^{GFP-LC3}$ (control) display baseline levels of autophagy. Chloroquine treated cells served as positive control, thus representing 100 % induction of autophagy. Cells expressing mutant neuroserpin show more activation of autophagy, demonstrated as increased percentage of cells with LC3-GFP positive vesicles within the subsets of cells harbouring neuroserpin. (C) Combined data from three independent repeats of (A). The percentage of autophagic vesicles positive for LC3 II and neuroserpin was determined with or without CQ treatment. Only a minor fraction of autophagic vesicles contain neuroserpin, irrespective of expression of wild-type or mutant neuroserpin (mean; ±STD; *: $p \leq 0.05$ in student's T-test).

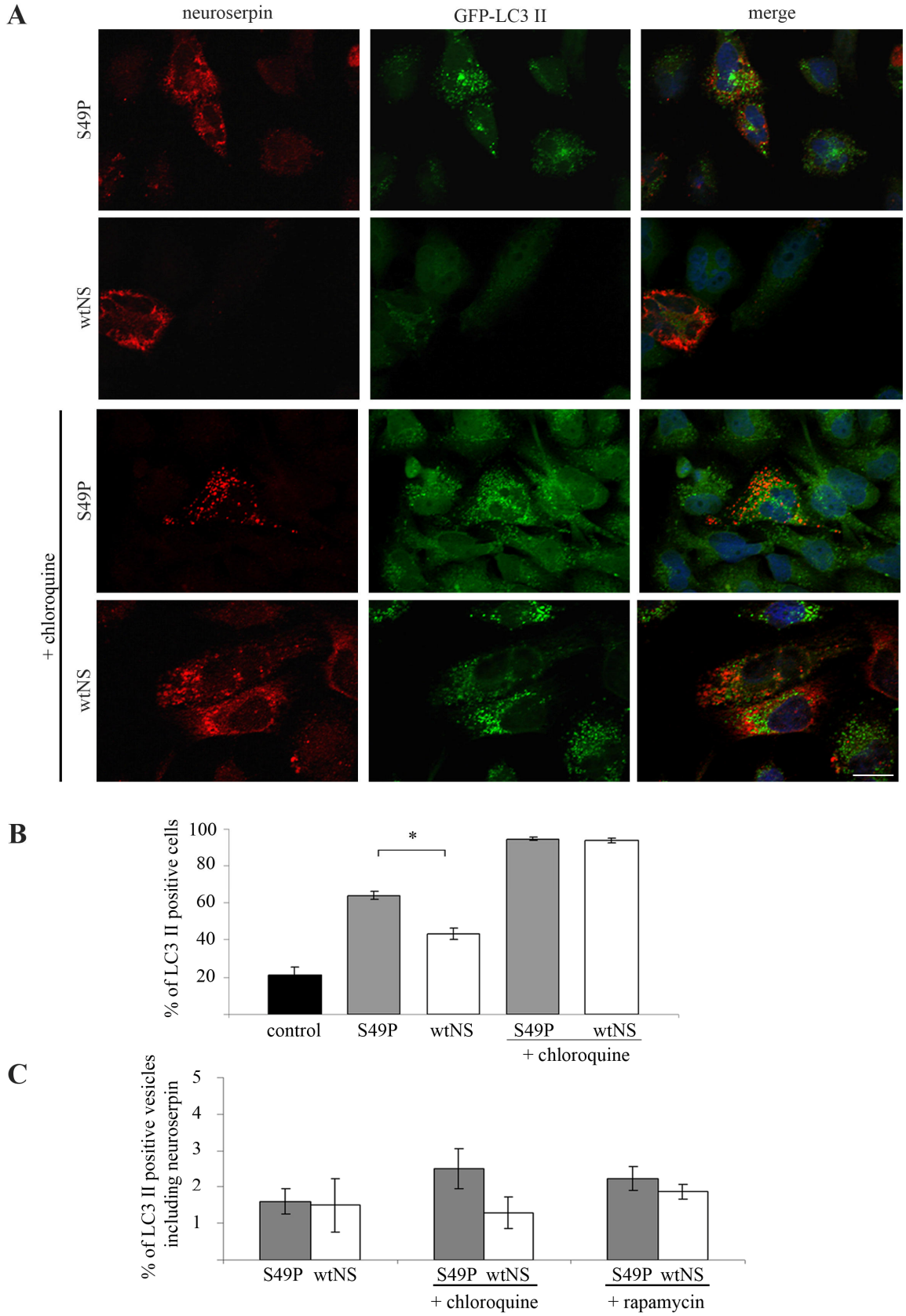

Figure 16: Mild induction of autophagy in a cell culture model of FENIB

5.3.1.2. Minor role of autophagy in degradation of mutant neuroserpin in *Tg*(NS^{S49P}) mice

In order to assess the contribution of autophagy in degradation of mutant S49P neuroserpin we measured the cytosolic (LC3 I) and the lipidated (LC3 II) form of LC3 by immunoblot, using LC3 II as a surrogate for autophagy (Klionsky et al., 2007; McLeland et al., 2011; Mizushima and Klionsky, 2007), in *Tg*(NS^{S49P}) and *Tg*(NS) mice. Soluble cytosolic LC3 I migrated at 16 kD on SDS-PAGE, whereas lipidated LC3 II, despite a higher molecular weight, migrated at 18 kD on SDS-PAGE due to its hydrophobicity (Mizushima and Klionsky, 2007).

We performed western blot analyses with subsequent densitometric quantification from *Tg*(NS^{S49P}) and *Tg*(NS) mice (n=3) aged 12, 20, 34, and 45weeks. As positive control we used cathepsin D-deficient mice (Koike et al., 2005), which showed impaired autophagosome formation leading to the abundant presence of the 16 kD LC3 II band (Fig. 17A; lane CD-/-). Wild-type mice showed a basal processing of LC3 (Fig. 17A; lane CD). There were no prominent differences in LC3 II expression over time comparing *Tg*(NS^{S49P}) and *Tg*(NS) mice (Fig. 17), suggesting no prominent induction of autophagy in neuroserpin degradation.

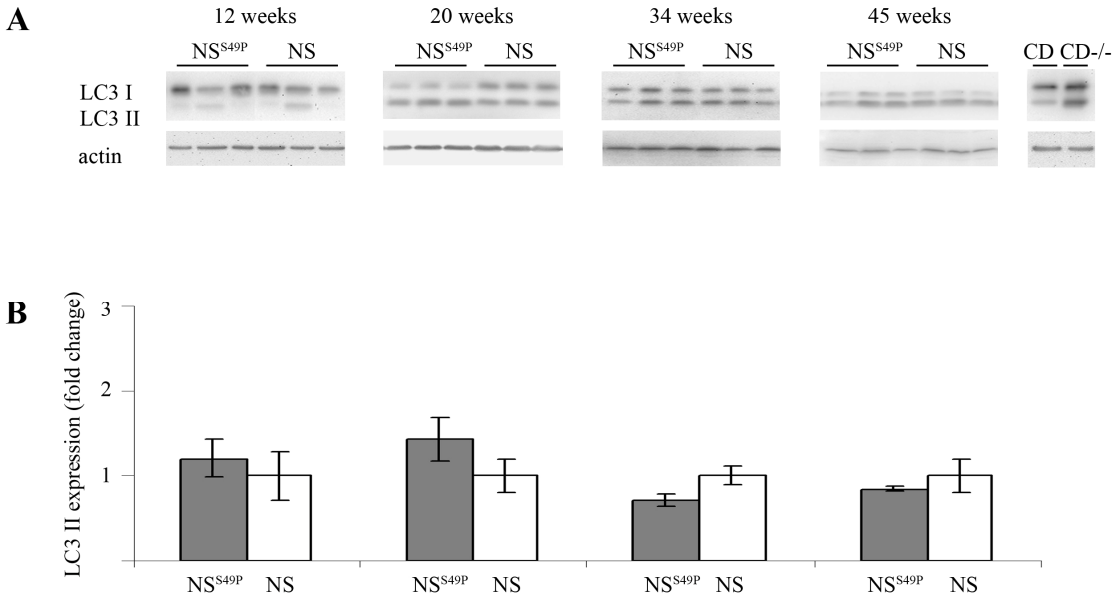

Figure 17: Absence of autophagic activity in FENIB mice

(A) *Tg*(NS^{S49P}) and *Tg*(NS) neuroserpin mice (each n= 3) aged 12, 20, 34, and 45 weeks were analysed by western blot for the expression of lipidated LC3 (LC3 II), a marker for autophagy. Cathepsin

D-deficient mouse (CD-/-) served as a positive control showing presence of LC3 II. (B) Densitometric quantifications of three independent experiments from (A) are shown graphically (mean; ±STD). Both transgenic mice exhibited basal levels of autophagy, with just minor changes in mutant neuroserpin mice.

Furthermore, we analyzed autophagy morphologically by transmission electron microscopy to validate the biochemical outcome. For this, cortical neurons of 20 and 45 weeks old *Tg*(NS^{S49P}) and *Tg*(NS) mice were assessed. We could not observe significant differences in the abundance of autophagic vacuoles between *Tg*(NS^{S49P}) and *Tg*(NS) mice (Fig. 18).

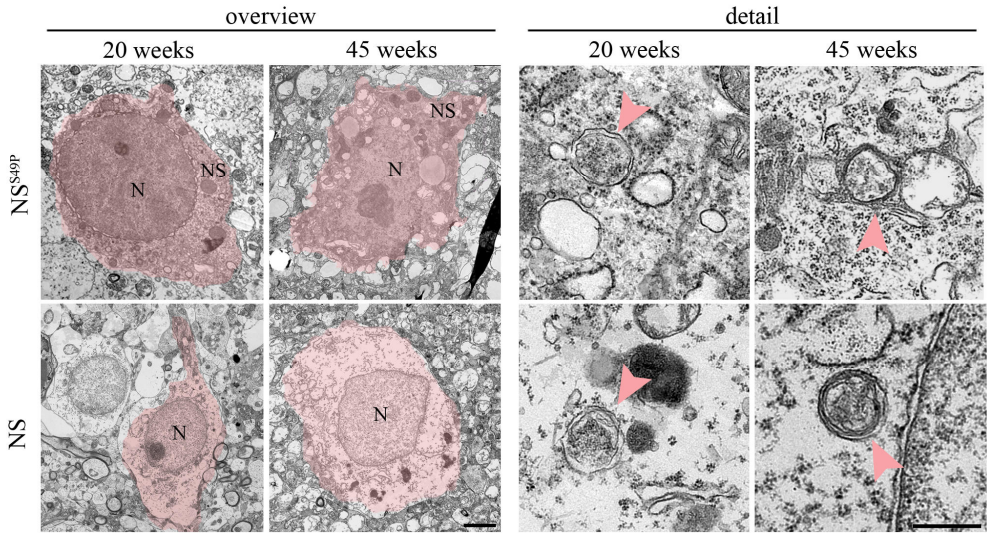

Figure 18: Ultrastructural assessment for autophagosomes in FENIB mice

Electron micrographs from cortical neurons of 20 and 45 weeks old *Tg*(NS^{S49P}) and *Tg*(NS) mice. Numerous inclusion bodies (NS) are found in the cytoplasm (N, Nucleus) of *Tg*(NS^{S49P}) aged mice. Autophagosomes (red arrow head) are present both in *Tg*(NS^{S49P}) and *Tg*(NS) mice at 20 and 45 weeks (scale bar left to right: 1 µm, 500 nm).

5.3.2. Mutant neuroserpin is predominantly degraded by the proteasome

We investigated the role of ERAD in the degradation of mutant neuroserpin. Therefore we crossed mice impaired in proteasomal degradation (*Tg*(UBB^{+1}), (Fischer et al., 2009)) with *Tg*(NS^{S49P}) neuroserpin mice. *Tg*(UBB^{+1}) mice express an aberrant ubiquitin B (UBB^{+1}) which was shown to accumulate in dementia such as Alzheimer's disease (van Leeuwen et al., 1998). UBB^{+1} has lost the ability to ubiquitinate proteins (De Vrij et al., 2001), but is ubiquitinated itself and is thereby both a substrate (Lindsten et al., 2002), and an inhibitor of the UPS (Lam et al., 2000).

We quantified neuroserpin inclusion bodies in the CA1 and CA2 hippocampal region of *Tg*(UBB^{+1}/NS^{S49P}) and *Tg*(NS^{S49P}) mice at 12, 21, 29, 36, and 45 weeks of age (each n=4). At 12 weeks of age *Tg*(UBB^{+1}/NS^{S49P}) and *Tg*(NS^{S49P}) mice showed comparable amounts of neuroserpin inclusions (Fig. 19B; 0.46 % area of neuroserpin immunoreactivity (area NSR) +/- 0.06 for *Tg*(UBB^{+1}/NS^{S49P}) and 0.36 % area NSR +/- 0.05 for *Tg*(NS^{S49P})). Neuroserpin accumulation markedly increased in *Tg*(UBB^{+1}/NS^{S49P}) mice at 21 and 29 weeks, reaching a plateau between week 36 and 45, when compared to *Tg*(NS^{S49P}) mice (Fig. 19B; 1.27 % area NSR +/- 0.26 at 21 weeks; 3.08 % area NSR +/- 0.21 at 29 weeks; 6.85 % area NSR +/- 0.29 at 36 weeks; 6.30 % area NSR +/- 0.52 at 45 weeks for *Tg*(UBB^{+1}/NS^{S49P}) and 0.39 % area NSR +/- 0.13 at 21 weeks; 1.36 % area NSR +/- 0.23 at 29 weeks; 3.74 % area NSR +/- 0.55 at 36 weeks; 3.60 % area NSR +/- 1.08 at 45 weeks for *Tg*(NS^{S49P})). As *Tg*(UBB^{+1}/NS^{S49P}) mice harbour twice as much neuroserpin inclusions when compared to *Tg*(NS^{S49P}) mice, we concluded that mutant neuroserpin is substrate for ERAD and is degraded by the ubiquitin proteasome system (UPS).

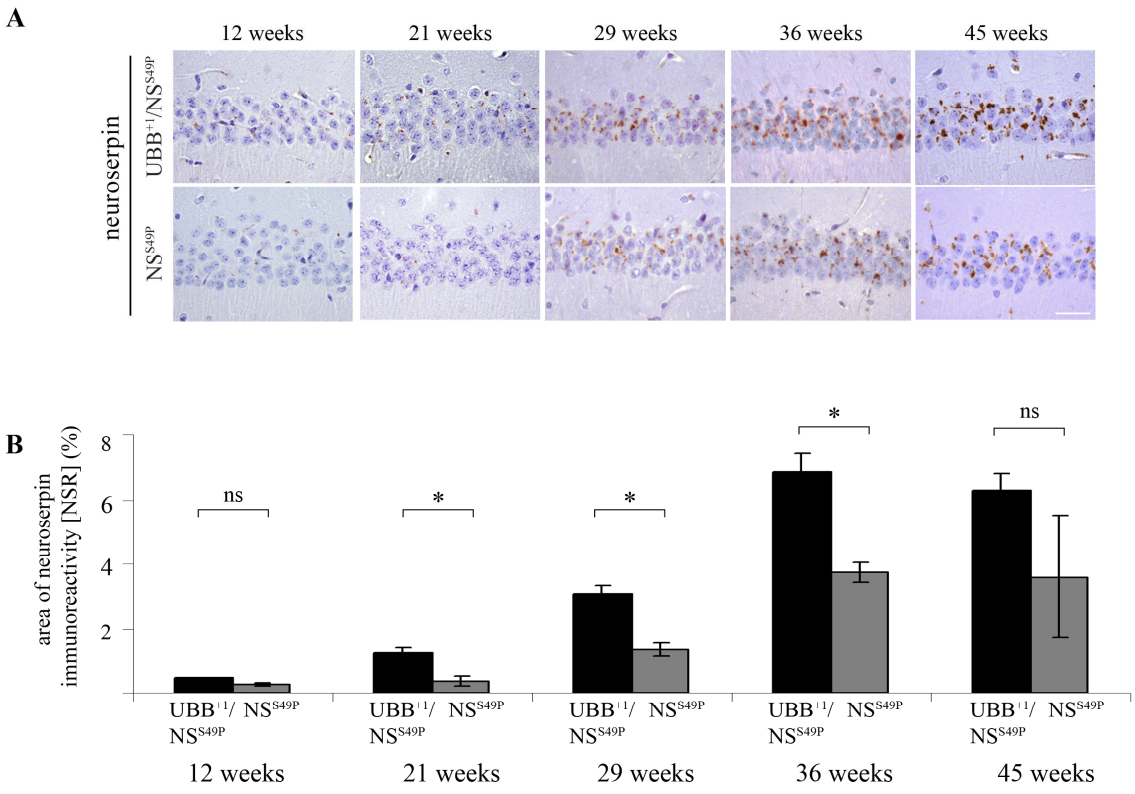

Figure 19: Proteasomal inhibition accelerates accumulation of mutant neuroserpin

(A) The hippocampus (CA1 and CA2) of *Tg*(UBB^{+1}/NS^{S49P}) and *Tg*(NS^{S49P}) mice aged 12, 21, 29, 36, and 45 weeks of age (each n=4) were stained with anti-neuroserpin antibody. *Tg*(UBB^{+1}/NS^{S49P}) showed elevated neuroserpin loads compared to *Tg*(NS^{S49P}) mice for each time point, demonstrating

that mutant neuroserpin is cleared by the UPS (scale bar: 50 µm). (B) The area of inclusions was quantified and presented as the percentage of the hippocampus (CA1 and CA2) [area NSR] (mean; ±STD; *: p≤ 0.05, ns: p≥ 0.05 in student's T-test).

5.3.3. Proteasomal inhibition leads to induction of autophagy in FENIB mice

Several reports describe an up-regulation of autophagy resulting from ER dysfunction (Ogata et al., 2006; Yorimitsu and Klionsky, 2007). Recently, Kroeger and colleagues described in an *in vitro* model of FENIB that inhibition of the proteasome leads to induction of autophagy (Kroeger et al., 2009). Therefore, we evaluated autophagy in *Tg*(UBB^{+1}/NS^{S49P}) and *Tg*(NS^{S49P}) mice at 12, 20, 36 and 45 (each n=3) weeks of age by western blot analyses followed by densitometric quantification for lipidated LC3 II. This analysis revealed an enhanced induction of autophagy at 36 and 45 weeks in *Tg*(UBB^{+1}/NS^{S49P}) mice when compared to *Tg*(NS^{S49P}) mice which were set to one (Fig. 20B; 1.59 fold increase +/- 0.19 at 36 weeks; 1.88 fold increase +/- 0.20 at 45 weeks for *Tg*(UBB^{+1}/NS^{S49P})). These findings suggest that *in vivo* autophagy is induced only when the proteasomal degradation capacity is overwhelmed.

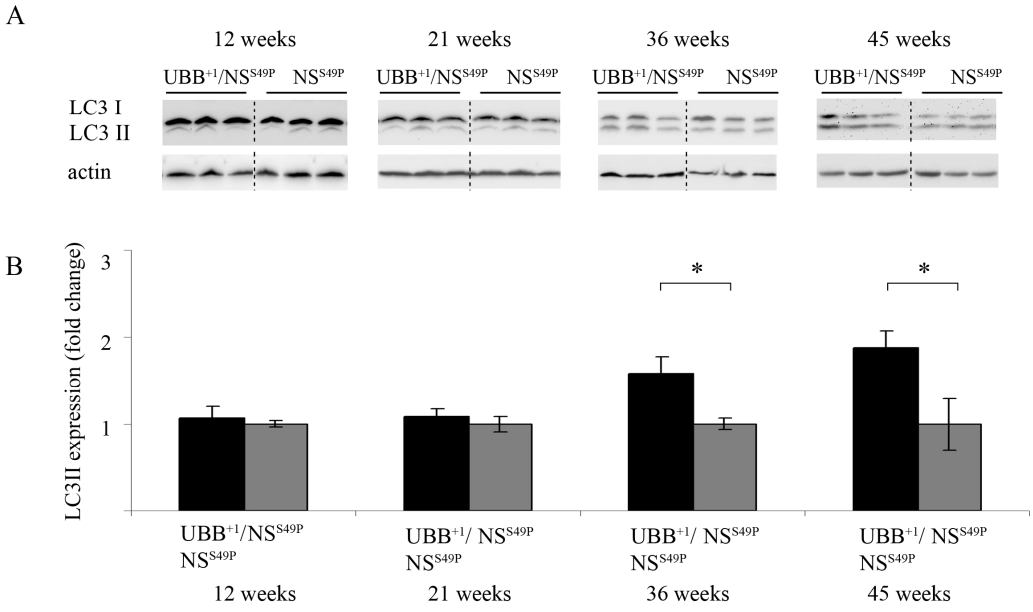

Figure 20: Proteasomal impairment FENIB mice showed induction of autophagy

(A) *Tg*(UBB^{+1}/NS^{S49P}) and *Tg*(NS^{S49P}) mice at 12, 20, 36 and 45 (each n=3) were accessed by western blot analysis for LC3 II. β–actin served as a loading control. (B) Densitometric quantification as a repetition of three independent experiments is shown graphically (mean, ±STD; p<0.05, student's

T-test). *Tg*(UBB^{+1}/NS^{S49P}) showed an enhanced induction of autophagy compared to *Tg*(NS^{S49P}) (mean; ±STD; *: p≤ 0.05 in student's T-test).

5.4 Specific degradation of polymeric mutant neuroserpin

5.4.1. Selective activation of heat shock chaperone Hsp90 in FENIB mice

In conformational diseases where protein aggregation occurs such as Alzheimer's disease (Di Domenico et al., 2010; Magrane et al., 2004), Parkinson's disease (Auluck et al., 2002; Klucken et al., 2004), Huntington disease (Sakahira and Nagata, 2002; Sittler et al., 2001), and trinucleotide repeat diseases (Fujikake et al., 2008; Muchowski et al., 2000; Warrick et al., 1999), the rapid and transient programme of the heat shock response is triggered. The molecular basis of neuro-protection of heat shock response in these models of neurodegeneration still remains to be elucidated (Muchowski and Wacker, 2005; Richter et al., 2010). It has been proposed that release of chaperone Hsp90 from transcription factor hsf-1 (heat shock factor-1) in response to the accumulation of unfolded proteins, induces the production of Hsp70 and Hsp40, as well as other chaperons, to promote protein degradation, disaggregation, and refolding (Fig. 21) (Luo et al., 2010; Richter et al., 2010).

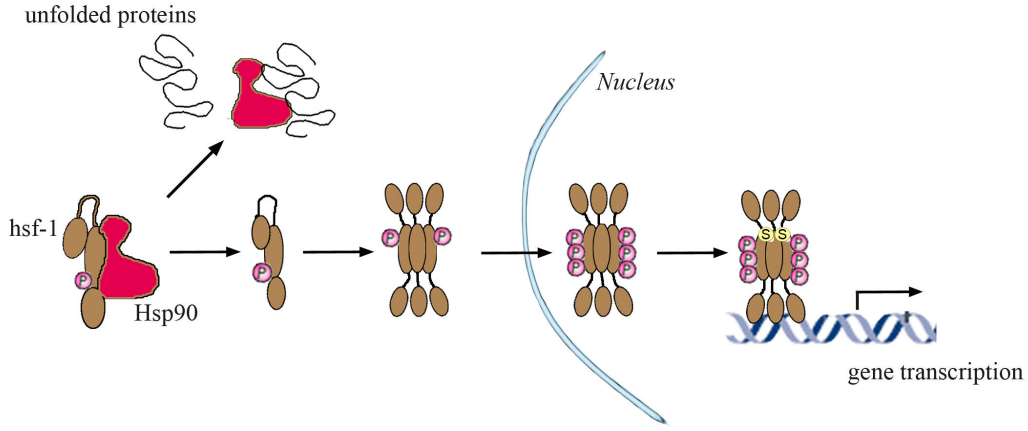

Figure 21: Regulation of heat shock response

Heat shock specific transcription factor hsf-1 is maintained in an inactive monomeric form in a complex with chaperone Hsp90. Upon accumulation of aberrant proteins, Hsp90 dissociates from hsf-1 binding native-like misfolded proteins (Jakob et al., 1995) to prevent their aggregation. Monomeric released hsf-1 homotrimerizes, translocates into the nucleus where it is hyperphosphorylated (Holmberg et al., 2001) and sumoylated (Hietakangas et al., 2003) to induce transcription of heat shock genes, predominantly chaperones Hsp70 and hsp40 that promote protein disaggregation and refolding.

Therefore we assessed protein levels of the chaperones Hsp90 and Hsp70 by western blot analysis in *Tg*(NS^{S49P}) and *Tg*(NS) neuroserpin mice over time at 12, 20, 34, 45, 64, and >80 weeks (each n=3). Interestingly, densitometric analyses revealed an induction of Hsp90 expression at 45 weeks of age in *Tg*(NS^{S49P}) mice when compared to *Tg*(NS) (1.83 fold increase +/- 0.06 for *Tg*(NS^{S49P})). Hsp90 expression levels in *Tg*(NS^{S49P}) mice at earlier (12, 20 and 34 weeks) as well as at later time points (64 and >80 weeks) are unchanged when compared to *Tg*(NS) mice (Fig. 22).

To track the specific activation of the chaperone response, we analyzed expression levels of Hsp70, which as a consequence should be elevated (see Fig. 21). Astonishingly, we could not detect any changes in Hsp70 protein levels over time in *Tg*(NS^{S49P}) mice when compared to *Tg*(NS) mice (Fig. 23). Additionally, immunohistochemical staining with anti-hsp70 antibody of hippocampal sections from transgenic mice aged 20 and 45 weeks of age was performed. This analysis confirmed comparable expression levels of Hsp70 protein in *Tg*(NS^{S49P}) and *Tg*(NS) mice over time (Fig. 23C). Taken together, these findings indicate that neuroserpin accumulation selectively induces a unique activation of heat shock chaperone Hsp90 after a particular time span.

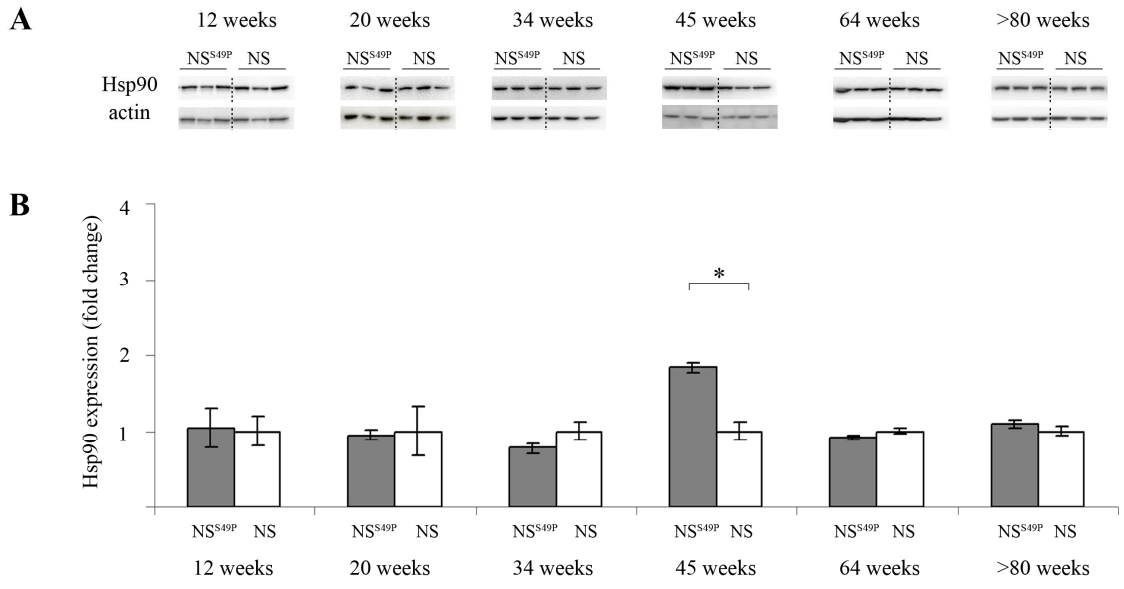

Figure 22: Selective induction of heat shock chaperone Hsp90 in FENIB mice

(A) In *Tg*(NS^{S49P}) and *Tg*(NS) neuroserpin mice (each n= 3) at 12, 20, 34, 45, 64, and >80 weeks of age the expression of Hsp90 was measured by western blot analysis. Actin expression levels served as a loading control. (B) Densitometric quantifications of three independent experiments are shown graphically (mean; ±STD; *: p≤ 0.05 in student's T-test). *Tg*(NS^{S49P}) mice showed an activation of Hsp90 at 45 weeks of age when compared to *Tg*(NS) mice.

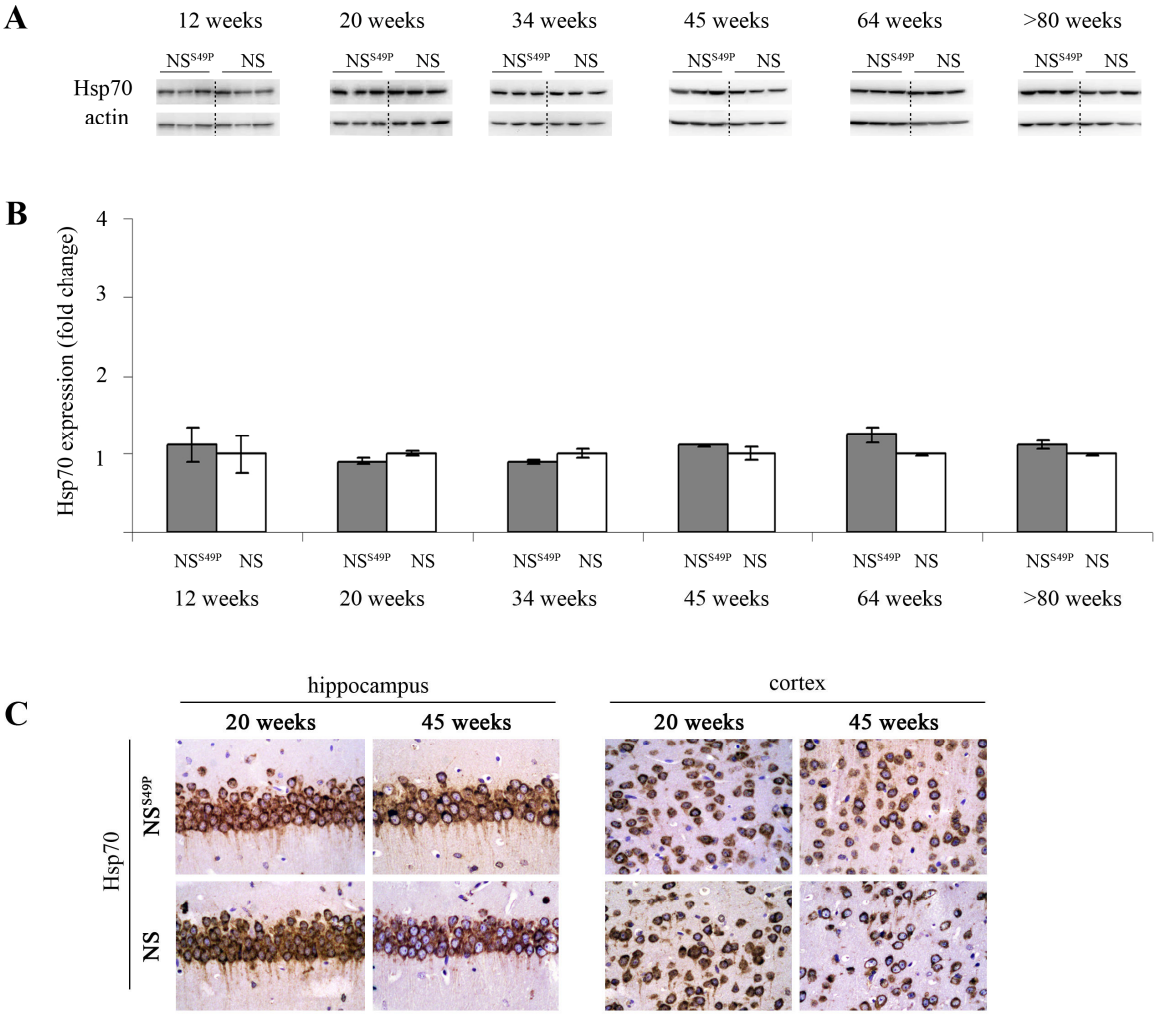

Figure 23: No induction of heat shock chaperone Hsp70 in FENIB mice

(A) Protein expression levels of Hsp70 were assessed by western blot analysis in *Tg*(NS^{S49P}) and *Tg*(NS) mice aged 12, 20, 34, 45, 64, and >80 weeks (each n= 3). Actin expression levels served as a loading control. (B) Densitometric quantifications form the depicted western blots in (A) do not show altered expression of Hsp70 proteins in *Tg*(NS^{S49P}) and *Tg*(NS) mice (mean; ±STD). (C) Hippocampal regions (CA1 and CA2) of *Tg*(NS^{S49P}) and *Tg*(NS) neuroserpin mice aged 20 and 45 weeks were stained with anti-hsp70 antibody. No changes in Hsp70 immunoreactivity could be detected, confirming western blot data.

5.4.2. Transient and exhaustible induction of UPR in *Tg*(NS^{S49P}) mice

As FENIB mice show progressive accumulation of neuroserpin in the ER (Fig. 14) we investigated involvement of the unfolded protein response (UPR) over time (see 2.4). Firstly, we looked at IRE1 cleavage of XBP1 mRNA. Generally, XBP1 is found in an unprocessed state and is processed by IRE1 mediated splicing of a small intron upon ER stress, giving rise

to bands of different sizes upon Pst1 restriction enzyme digestion (Calfon et al., 2002). Therefore, RNA from *Tg*(NS) and *Tg*(NS^{S49P}) neuroserpin mice (n=3) aged 12, 20 and 34 weeks was isolated, reverse transcribed to cDNA and digested with Pst1. N2a cells treated with Tunicamycin, which inhibit N-glycosylation and thereby elicite ER stress, served as positive control. We could not detect processed forms of XBP1 in *Tg*(NS^{S49P}) or *Tg*(NS) mice at any of the assessed time points, arguing against a dramatic induction of this arm of the UPR in FENIB mice (Fig. 24).

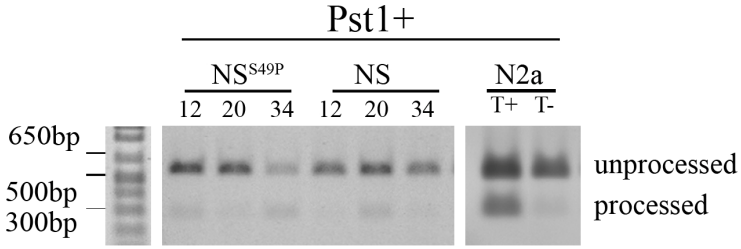

Figure 24: No induction of the IRE1-arm of UPR in FENIB mice

Reverse transcriptase-PCR from mice, *Tg*(NS^{S49P}) and *Tg*(NS) aged 12, 20, 34 weeks, and cells, untreated (T-) or treated with Tunicamycin (T+), was performed to evaluate levels of XBP1. A representative agarose gel out of three independent experiments is shown. Pst1 restriction cut distinguishes between processed (300bp) and unprocessed (600bp) XBP1.

Secondly, we measured expression of the phosphorylated form of eukaryotic initiation factor 2α (eIF2αP) in order to monitor the PERK-arm of UPR. For this we sacrificed *Tg*(NS^{S49P}) and *Tg*(NS) mice at the ages of 12, 20, 34, 45, 64, and >80weeks (n=3 each) and performed western blot analysis for phosphorylated and non-phosphorylated forms of eIF2α followed by densitometric quantification (Fig. 25). Interestingly, expression level of eIF2αP was increased by a factor of three in *Tg*(NS^{S49P}) mice when compared to *Tg*(NS) mice at 20 weeks of age (Fig. 25B; 3.19 fold increase +/- 0.29 for *Tg*(NS^{S49P})). A comparable increase in expression of eIFαP was not detected at any other investigated time point (12, 34 and 45 weeks), neither for *Tg*(NS) nor for *Tg*(NS^{S49P}) mice. At later time points, 64 and >80 weeks, *Tg*(NS^{S49P}) mice showed a reduced expression of eIF2αP when compared to *Tg*(NS) mice (Fig. 25B; 0.28 fold decrease +/- 0.07 at 64 weeks; 0.59 fold decrease +/- 0.17 at >80 weeks for *Tg*(NS^{S49P})) (Fig. 25).

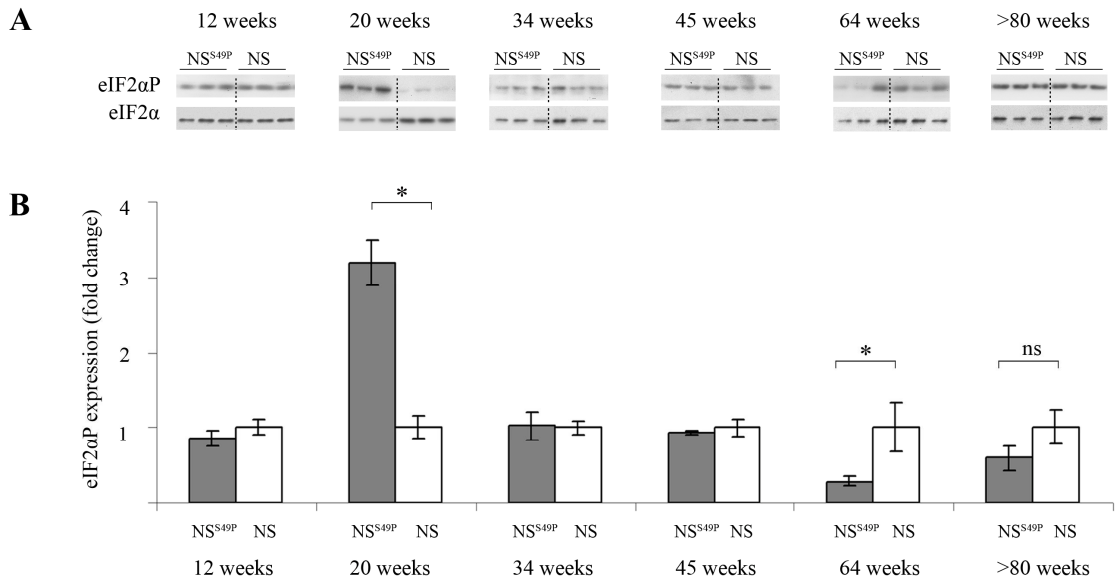

Figure 25: Selective activation of the PERK-arm of UPR in FENIB mice

(A) Western blot analysis for expression of phosphorylated eIF2α in *Tg*(NS^{S49P}) and *Tg*(NS) neuroserpin mice (n= 3) aged 12, 20, 34, 45, 64, and >80 weeks. Expression levels of eIF2α served as a loading control. (B) Densitometric quantification (three independent experiments) of (A), revealed high expression of phosphorylated eIF2α in *Tg*(NS^{S49P}) mice at 20 weeks of age in comparison to *Tg*(NS) mice (mean; ±STD; *: $p \leq 0.05$, ns: $p \geq 0.05$ in student's T-test).

Phosphorylation of eIF2α leads to a selective increase in translation of ATF4 transcripts and simultaneously to a general block of protein translation (Ron and Walter, 2007; Scheuner et al., 2001). Therefore, we evaluated protein expression levels of ATF4 by western blot analysis followed by a densitometric quantification in *Tg*(NS^{S49P}) and *Tg*(NS) mice aged 12, 20 and 34 weeks. Interestingly, we could not observe alterations in ATF4 protein translation comparing *Tg*(NS^{S49P}) and *Tg*(NS) mice (Fig. 26).

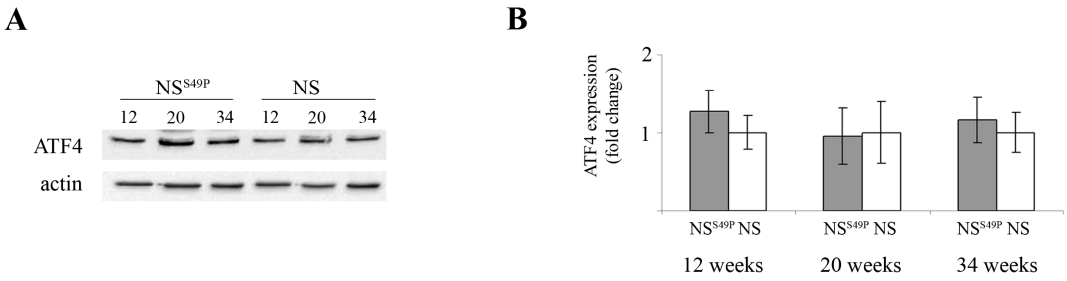

Figure 26: No induction of ATF4 specific translation in FENIB mice

(A) Expression levels of ATF4 were assessed by western blot analysis in *Tg*(NS^{S49P}) and *Tg*(NS) mice at 12, 20 and 34 weeks of age. Actin expression levels served as loading control. (B) Densitometric quantification (three independent experiments) from (A) showed equal expression for ATF4 in mutant and wild-type neuroserpin mice at any investigated time point (mean, ±STD).

To rule out any alterations in ATF4 transcripts, we performed quantitative rt-PCR analysis. Therefore RNA from *Tg*(NS^{S49P}) and *Tg*(NS) mice (n=3) aged 12, 20 and 34 weeks was isolated and reverse transcribed to cDNA to determine quantities of ATF4 RNA by quantitative PCR. This analysis revealed comparable ATF4 transcript levels over time in *Tg*(NS^{S49P}) and *Tg*(NS) mice (Fig. 27). Gene expression analysis for Chop, a downstream target of ATF4, did not show transcriptional alterations over time (12, 20, 34 weeks) in *Tg*(NS^{S49P}) and *Tg*(NS) mice (Fig. 27). These data suggested that aggregated mutant neuroserpin selectively induces the PERK-arm of UPR by phosphorylation of eIF2α in a time-dependent manner in FENIB mice.

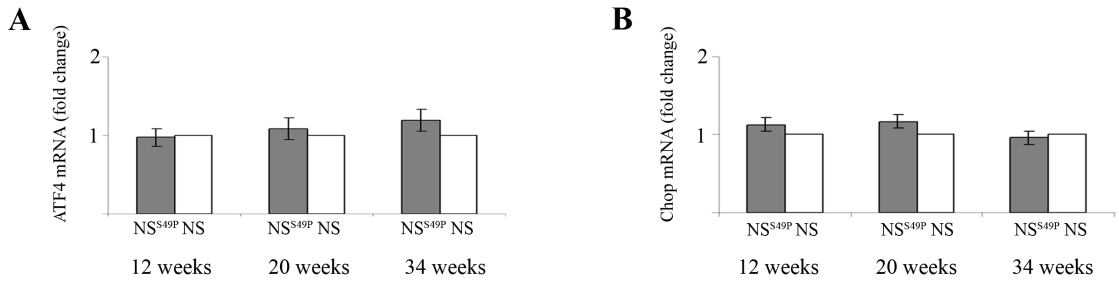

Figure 27: Neither ATF4 nor Chop transcripts show alterations in FENIB mice

RNA from *Tg*(NS^{S49P}) and *Tg*(NS) mice aged 12, 20 and 34 weeks was isolated. mRNA expression was analyzed by quantitative rt-PCR and normalized for ß-actin. Relative mRNA amounts (three independent experiments) for ATF4 (A) and Chop (B) are shown graphically (mean, ±STD).

Thirdly, we assessed the expression of cleaved ATF6 to define the involvement of the third arm of UPR. Therefore, *Tg*(NS^{S49P}) and *Tg*(NS) mice aged 12, 20, 34, 45, 64, and >80 weeks were analyzed by western blot for cleaved ATF6 with densitometric quantification. Expression of cleaved ATF6 peaked in *Tg*(NS^{S49P}) mice between 34 and 45 weeks of age when compared to *Tg*(NS) mice (3.25 fold increase +/- 0.62 at 34 weeks; 3.54 fold increase +/- 0.19 at 45 weeks for *Tg*(NS^{S49P})). With disease progression (64 and >80 weeks) expression of cleaved ATF6 initially drastically dropped down to below *Tg*(NS) mice levels (0.41 fold decrease +/- 0.13 at 64 weeks; 1.17 fold increase +/- 0.49 at >80 weeks for *Tg*(NS^{S49P})) (Fig. 28). This dynamic and exhaustible time course of ATF6 activation in *Tg*(NS^{S49P}) mice suggested a selective involvement of this arm of UPR in FENIB.

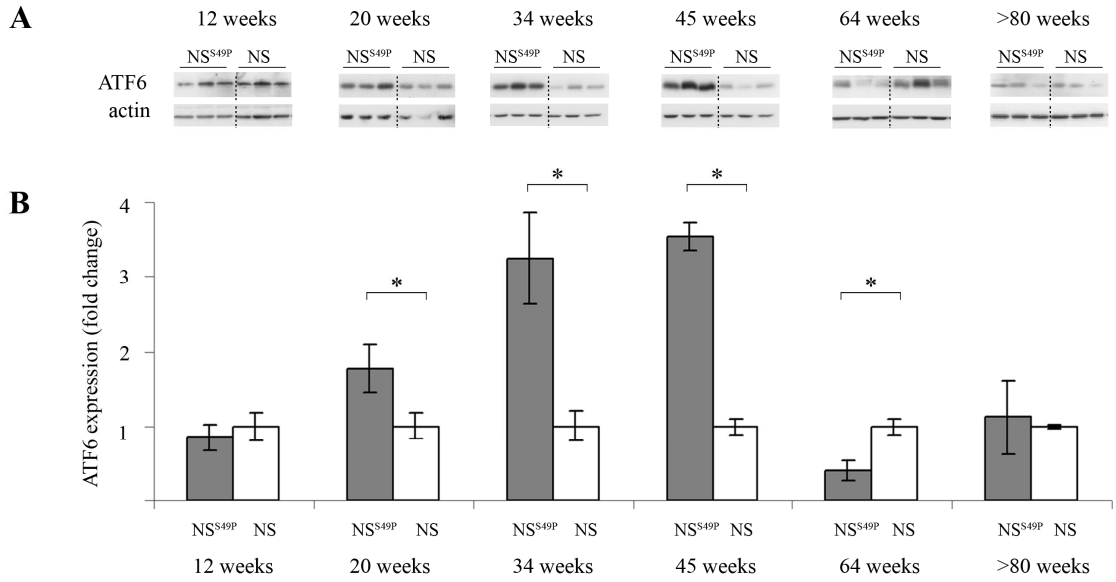

Figure 28: Temporary and exhaustible induction of the ATF6-arm of UPR in FENIB mice

(A) Mutant *Tg*(NS^{S49P}) and *Tg*(NS) neuroserpin mice (n= 3) were analyzed at 12, 20, 34, 45, 64, and >80 weeks of age by western blot for expression of cleaved ATF6; actin served as loading control. (B) Densitometric analysis out of three independent experiments of western blot assessments from (A) showed an increase of cleaved ATF6 reaching a maximum between 34 and 45 weeks (3.25 and 3.54 fold-increase compared to wild-type expression levels at 34 and 45 weeks) of age in *Tg*(NS^{S49P}) mice when compared to *Tg*(NS). This response is exhausted with disease progression (64 and >80 weeks) (mean; ±STD; *: $p \leq 0.05$, ns: $p \geq 0.05$ in student's T-test).

5.4.3. Polymeric neuroserpin formation is temporarily silenced by induction of UPR

Intraneuronal inclusions present in *Tg*(NS^{S49P}) and *Tg*(NS) mice consist mainly of mutant neuroserpin (Fig. 14) (Davis et al., 1999a; Galliciotti et al., 2007). Biochemical analysis of cerebrum from 8 week old *Tg*(NS^{S49P}) mice using non denaturing gels showed presence of

polymeric neuroserpin whereas *Tg*(NS) mice only contained monomeric conformers of neuroserpin (Fig. 14B).

The availability of an ELISA specific for polymeric neuroserpin (Miranda et al., 2008; Miranda et al., 2004) allowed us to investigate the temporal distribution of polymeric neuroserpin in *Tg*(NS^{S49P}) and *Tg*(NS) mice. This analysis revealed a temporary decline of polymeric neuroserpin between weeks 20 and 45 (1376 ng/ml, +/- 71 at 8 weeks; 1996 ng/ml, +/- 402 at 12 weeks; 959 ng/ml, +/- 270 at 20 weeks; 585 ng/ml, +/- 59 at 34 weeks; 873 ng/ml, +/- 56 at 45 weeks) and an exponential increase from week 64 onwards (1982 ng/ml, +/- 317 at 64 weeks, 3915 ng/ml, +/- 628 at >80 weeks) in *Tg*(NS^{S49P}), whereas polymeric neuroserpin could not be detected in *Tg*(NS) at any investigated time point (Fig. 29A). This is partially paralleled by a slight decrease of total mutant neuroserpin from week 12 to week 34 (2129 ng/ml, +/-698 at 12 weeks, 1752 ng/ml, +/-258 at 20 weeks, 1754 ng/ml, +/-241 at 34 weeks) followed by an exponential increase from week 45 onwards (3424 ng/ml, +/-443 at 45 weeks, 9016 ng/ml, +/-2507 at 64 weeks, 9923 ng/ml, +/-3674 at >80 weeks) (Fig. 29B). Total wild-type neuroserpin was constant at low levels (e.g. 462 ng/ml, +/- 90 at 20 weeks) (Fig. 29B). The temporary decline of polymeric neuroserpin formation seems to be silenced by the induction of UPR.

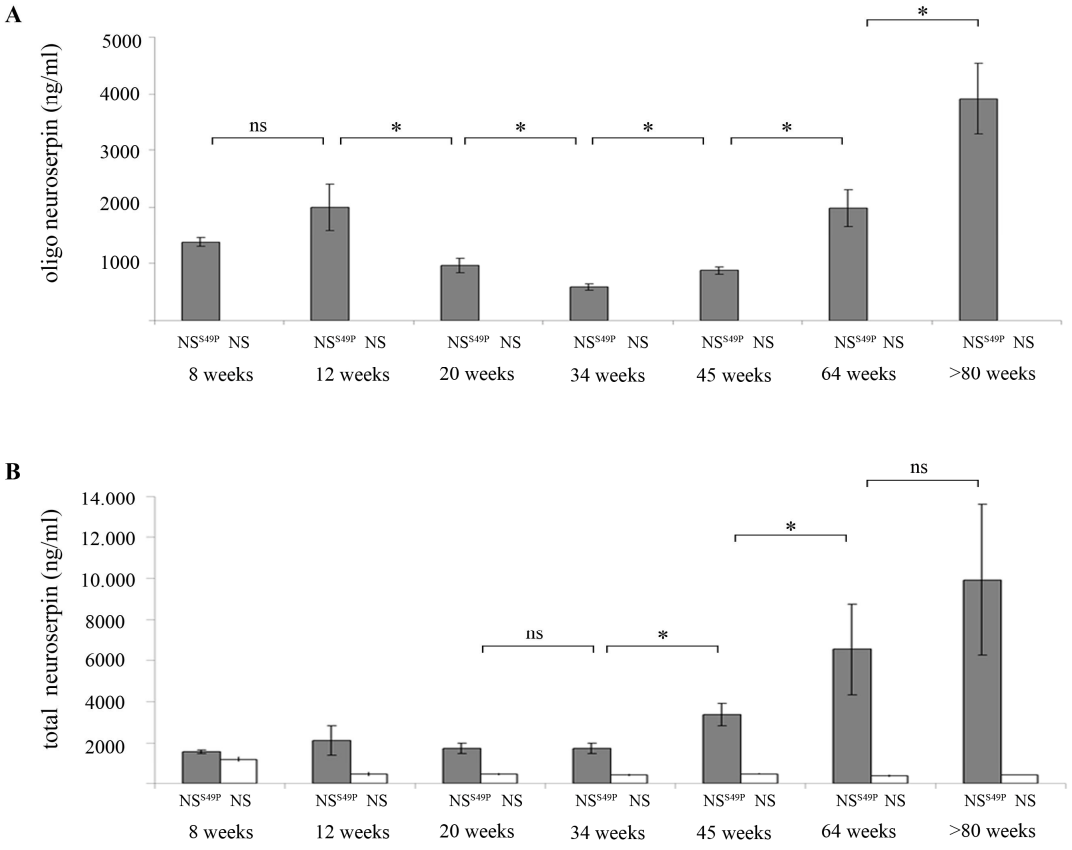

Figure 29: Quantification of polymeric neuroserpin over time follows a parabolic distribution

Brain homogenates of *Tg*(NS^{S49P}) and *Tg*(NS) neuroserpin mice (each n= 3) aged 8, 12, 20, 34, 45, 64, and >80 weeks were assessed for polymeric (A) and total (B) neuroserpin by sandwich ELISA. (A) Polymeric neuroserpin was assessed by ELISA with 7C6 monoclonal antibody, which shows high affinity for polymerized S49P neuroserpin (Miranda et al., 2008). *Tg*(NS) mice showed no polymeric neuroserpin at any of the investigated time points. Polymeric neuroserpin was readily detectable in *Tg*(NS^{S49P}) at 8 weeks of age. Surprisingly, levels of polymeric neuroserpin dropped, at 34 weeks of age reaching a minimum. With disease progression, levels of polymeric neuroserpin increased exponentially. (B) Assessment of total neuroserpin in *Tg*(NS) mice revealed constant low levels of neuroserpin whereas in *Tg*(NS^{S49P}) neuroserpin plateaus between week 12 and 34. With disease progression levels of total neuroserpin increased exponentially (mean; ±STD; *: $p \leq 0.05$, ns: $p \geq 0.05$ in student's T-test).

6. Discussion

Dementias are neurodegenerative diseases, most of them characterized by accumulation of aggregated proteins. The most common cause for protein aggregation is misfolding by aberrant intermolecular linkage resulting in intracellular or extracellular deposition of protein. FENIB is an autosomal dominant inherited dementia. Mutations in the gene encoding for neuroserpin, a neuron specific serine protease inhibitor, lead to intraneuronal accumulation of neuroserpin-polymers resulting in neurodegeneration. Typically, long before the first clinical symptoms arise, protein aggregation takes place and deposits challenge the fidelity of protein homeostasis, or proteostasis, of the cell. The proteostasis network ensures the integrity of intracellular protein components by regulating biological processes that influence protein synthesis and folding, trafficking as well as disaggregation and degradation of misfolded proteins (Balch et al., 2008). The maintenance of protein homeostasis in the cytosol is supported by the UPS and the autophagy-lysosomal pathway. The UPS degrades cytosolic or ER resident proteins which are transported to the UPS via ERAD and autophagy degrades bulk cytoplasmic proteins or organelles (Rubinsztein et al., 2005; Schwartz and Ciechanover, 2009). Similarly, proteostasis in the ER is assisted by the UPR (Schroder and Kaufman, 2005), by ERAD (Tsai et al., 2002) and by autophagy (Cuervo, 2004b; Kruse et al., 2006). The role of ER overload response (EOR), in which ER-retained folded proteins lead to the activation of NF-kappaB (Davies and Lomas, 2008; Pahl and Baeuerle, 1995, 1997), is unclear in this context. In dementias, where intracellular protein aggregation is thought to be causally involved in disease pathology, the implications of the proteostasis network remain to be elucidated. Little is known about the interplay between proteostasis maintaining mechanisms and disease causing protein aggregation. This prompted us to investigate this aspect in a murine model of the conformational dementia FENIB.

FENIB – a suitable model to study conformational diseases

Genetically modified animal models, resembling aspects of the corresponding human disease, are used to investigate neurodegenerative disorders (Jucker, 2010). Many murine models for dementias have been generated and helped to dissect pathogenic processes (Dawson et al., 2010; Jucker, 2010; Kokjohn and Roher, 2009). Still, these models do not represent the full spectrum of disease, as many of them lack progressive loss of neurons (Duyckaerts et al., 2008). Moreover, they do not show a correlation between protein deposition and

neurodegeneration (Duyckaerts et al., 2008). In this study we used a murine model of the FENIB dementia where aberrantly folded neuroserpin accumulates within neurons leading to neurodegeneration (Galliciotti et al., 2007). We advanced the descriptions of the FENIB model of Galliciotti and colleagues by performing an extended time-course analysis of mutant neuroserpin aggregation (Galliciotti et al., 2007). Thereby, we demonstrated ER localization of mutant neuroserpin inclusions (Fig. 14A). We also found mutant neuroserpin inclusions solely surrounded by membranes of unknown origin. A similar observation was reported for inclusion bodies of serpin Z α1-antitrypsin, a member of the serpin superfamily (Granell and Baldini, 2008; Granell et al., 2008). Furthermore, we observed prominent neurodegeneration with the involvement of apoptotic pathways (Fig. 15). Substantial neuronal loss occurs at advanced disease stages (45 weeks or later) correlating with an increased amount of inclusion body deposition (Fig. 13). Accordingly, FENIB mice display a strong genotype-phenotype correlation, fully mimicking pathophysiology of human disease. Therefore, FENIB is ideally suited as a model disease to investigate the linkage between proteostasis and protein aggregation.

Mutant neuroserpin is degraded by ERAD with the assistance of autophagy

Activation of autophagy has been reported to play a crucial role in cell protection during neurodegenerative diseases (Cuervo, 2004a). In Parkinson disease (PD) (Webb et al., 2003) and in trinucleotid repeat diseases (Kegel et al., 2000; Ravikumar et al., 2002; Ravikumar et al., 2004), autophagy-mediated isolation and degradation of aggregated proteins was shown to be prominently induced. We used a cell culture model of FENIB to investigate the role of autophagy in mutant neuroserpin degradation. Interestingly, the presence of mutant S49P neuroserpin per se induces autophagy; nevertheless it is not a substrate for autophagy itself (Fig. 16). These data were validated through pharmacological stimulation of autophagy by treatment with rapamycin which does not lead to enhanced clearance of mutant neuroserpin (Fig. 16A and C). Assessment of autophagy in *Tg*(NS^{S49P}) and *Tg*(NS) mice equally confirmed degradation of mutant and wild-type neuroserpin as no prominent induction of autophagy was detected (Fig. 17 and 18).

Conceivably, the occurrence of neuroserpin inclusion bodies surrounded by membranes of unknown origin in *Tg*(NS^{S49P}) mice might explain the discordance in autophagic activity with other model systems studying conformational diseases. Granell and colleagues showed that serpin inclusion bodies of mutant Z α1-antitrypsin neither carry

classical autophagosomal (LC3 II) nor lysosomal markers (LAMP-1), but contain several ER components (Granell and Baldini, 2008). The authors used Hepa 1-6 cells to demonstrate the concentration of Z α1-antitrypsin aggregates in special subdomains of the ER before budding off to form separated inclusion bodies (Granell and Baldini, 2008). Similarly, Zuber and colleagues reported for another polymeric member of the serpin superfamily, the null Hong Kong (NHK) variant of α1-antitrypsin that inclusion bodies originate by shedding off the ER (Zuber et al., 2007 5236). Possibly, mutant neuroserpin aggregation and sequestration into inclusion bodies occurs in a comparable manner. This remains to be determined by additional experiments. Furthermore, serpins were proposed to be sufficiently conserved and studying one member might offer insights to the behaviour of others. Obviously this is not the case as aggregates of Z α1-antitrypsin in hepatocytes specifically activated autophagy (Kamimoto et al., 2006; Kruse et al., 2006; Teckman and Perlmutter, 2000). This indicates that degradation of aggregated proteins display cell type-selectivity with respect to the cells and tissues which undergo degeneration (Gidalevitz et al., 2010).

As recently revealed by *in vitro* studies by Kroeger and colleagues, autophagy degrades mutant neuroserpin only when the proteasomal activity is blocked (Kroeger et al., 2009). Within our research we demonstrated for the first time *in vivo* that mutant neuroserpin is selectively degraded by autophagy when the proteasomal activity is impaired, as *Tg*(UBB^{+1}/NS^{S49P}) mice showed increased levels of autophagic activity when compared to *Tg*(NS^{S49P}) mice suffering from FENIB only (Fig. 20). These findings are of clinical significance, as enhancement of autophagy by treatment with rapamycin, which has been shown to work *in vitro*, might represent an option for *in vivo* application (Kroeger et al., 2009).

Proteasomal degradation of wild-type and mutant neuroserpin has been shown in a cell culture model of FENIB using PC12 cells as well as COS7 cells (Kroeger et al., 2009; Miranda et al., 2004). In those cases a block of proteasomal degradation with pharmacological agents, such as lactacystein or MG132, leads to increased accumulation of mutant neuroserpin. In that scenario, misfolded mutant neuroserpin is a substrate for ERAD being retranslocated to the cytosol where it is degraded by the UPS. In our case we demonstrated - for the first time in an *in vivo* mode - mutant neuroserpin to be predominantly degraded by the proteasome, as *Tg*(UBB^{+1}/NS^{S49P}) mice accumulate twice as much neuroserpin inclusions as *Tg*(NS^{S49P}) mice (Fig. 19). Presumably, it is the soluble fraction of mutant neuroserpin which is a substrate for ERAD (Kroeger et al., 2009). A possible route to deliver misfolded mutant neuroserpin to ERAD is by lectins containing mannose-6-phosphate receptor-like

domains, such as OS9 and XTP3-B (Christianson et al., 2008; Hosokawa et al., 2010; Hosokawa et al., 2008). Recently, Christianson and colleagues were able to show *in vitro* an association of mutant serpin Z α1-antitrypsin with OS9 and XTP3-B, which interacts with an ubiquitin ligase being a part of the translocon (Christianson et al., 2008).

To summarize, we observed mutant neuroserpin to be specifically degraded by the proteasome via ERAD and nonspecifically by autophagy. Therefore, one might assume that separate pathways exist for degrading soluble mutant neuroserpin and larger aggregates. This approach is further supported by studies from yeast in which soluble and aggregated mutant α1-antitrypsin is target for degradation via different routes (Kruse et al., 2006). Nevertheless, only when the proteasomal degradation capacity is overwhelmed does autophagy gain importance and possibly helps the cell to eliminate toxic aggregates.

Hsp90 promotes mutant neuroserpin degradation

Molecular chaperones of the conserved heat shock response are induced upon protein deposition in a variety of conformational diseases (Muchowski and Wacker, 2005; Yenari, 2002). Chaperones as components of the proteostasis network promote disaggregation, degradation or refolding (Gidalevitz et al., 2010). In a *Drosophila* as well as in a murine model for PD overexpression of Hsp70 was reported to mitigate α-synuclein toxicity and thereby prevented neuronal loss associated with α-synuclein (Auluck et al., 2002; Klucken et al., 2004). The authors attributed the protective effect of Hsp70 to its destabilising impact to toxic, misfolded α-synuclein monomers and/ or small polymeric micro-aggregates (Auluck et al., 2002). Recently, Hsp70 was discovered to solubilizes α-synuclein and promote the degradation of its insoluble forms via chaperone-mediated autophagy and the proteasome (Witt, 2010). In another study, Dou and colleagues showed an interaction between hyperphosphorylated tau, Hsp70 and Hsp90 in brains of Alzheimer's disease (AD) patients (Dou et al., 2003). Quantification of Hsp90 in FENIB mice revealed a selective induction of this chaperone after advanced disease pathogenesis at 45 weeks (Fig. 22). At the same time, accumulation of mutant neuroserpin seized (Fig. 13), suggesting that Hsp90 activity promotes mutant neuroserpin degradation. Since we could not observe activation of Hsp70 chaperone in FENIB mice (Fig. 23), this response seems to be specific. The molecular basis of neuroprotection in neurodegeneration still remains to be elucidated (Muchowski and Wacker, 2005; Richter et al., 2010). Cell culture experiments with an AD model using RNAi and drug-induced chaperone overexpression indicate Hsp70 and Hsp90 chaperones to maintain tau in a

soluble, functional conformation and concomitantly prevent tau aggregation (Dou et al., 2003). Accordingly to this assumption, interaction of mutant neuroserpin polymers with Hsp90 could prevent their aggregation, keeping it soluble for potential proteasomal degradation.

The involvement of heat shock proteins in serpinopathies is not new. It has been shown that Hsp70 and Hsp90 synthesis was increased in individuals suffering from α1-antitrypsin deficiency and liver disease (Perlmutter et al., 1989). Nevertheless, this is the first report linking cytosolic chaperones of the heat shock response with the pathophysiology of FENIB.

Transient induction of UPR leads to transient depression of polymeric mutant neuroserpin

The involvement of UPR in aggregated protein deposition in dementia has been discussed controversially (Davies et al., 2009a; Hoozemans et al., 2009; Yang and Paschen, 2009). Since mutant neuroserpin deposits in the ER, we investigated the induction of UPR in FENIB. In mammals, UPR is conveyed through three signalling arms IRE1, PERK and ATF6, which act in a concerted manner to restore ER homeostasis (Bernales et al., 2006; Ron and Walter, 2007; Schroder and Kaufman, 2005).

We do not see activity of IRE1 signalling, as we could not detect spliced XBP1 mRNA (Fig. 24). The lack of XBP1 signalling in FENIB may help to explain the fact that autophagy is not induced (Ogata et al., 2006). Further on, we detected PERK-mediated phosphorylation of eIF2α at 20 weeks of age in FENIB mice (Fig. 25). The fact that we did not find significant up-regulation of eIF2αP in very young or aged mice speaks in favour of a specific induction upon mutant neuroserpin accumulation. Hence, eIF2αP conceivably limits protein synthesis to a level the existing ER machinery can cope with. We could not detect induced expression levels of downstream factors of eIF2αP, such as ATF4 or Chop (Fig. 26 and 27). The absent induction of ATF4 expression indicates missing activity of the integrated stress response (Harding et al., 2003). This correlation again points towards a specific impact of mutant neuroserpin accumulation regarding phosphorylation of eIF2α. The missing induction of Chop, a transcription factor promoting cell death, suggests successful limitation of protein synthesis by eIF2α phosphorylation. Moreover, we detected a specific induction of ATF6 over an extended time span. A maximum of ATF6 activity was shown between 34 and 45 weeks of age in FENIB mice (Fig. 28). At identical time points we detected an arrest of

neuroserpin inclusion accumulation (Fig. 13). With disease progression, ATF6 activity is exhausted (Fig. 28; 64 and >80 weeks), concomitantly neuroserpin inclusions rise exponentially (Fig. 13). On the one hand, our data are in agreement with previous studies showing induction of UPR in serpinopathies (Carroll et al., 2010; Lawless et al., 2004; Lawless et al., 2007). On the other hand, our data contradict other studies proposing UPR independent activation of neurodegenerative mechanism in serpinopathies and dementias (Dadakhujaev et al., 2010; Davies et al., 2009b; Hidvegi et al., 2005; Pahl and Baeuerle, 1995). Besides serpinopathies, UPR has been shown to be prominently involved in the pathophysiology of other dementias with intracellular protein accumulation (Hoozemans et al., 2009; Salminen and Kaarniranta, 2010). Active ATF6 acts as a transcription factor in regulating ER quality control proteins (Adachi et al., 2008; Wu et al., 2007), probably supporting enhanced delivery of soluble mutant neuroserpin to ERAD and thereby helping to recover ER homeostasis.

Recently, it was proposed that PERK signalling is implicated in the activation of EOR (Deng et al., 2004; Jiang et al., 2003; Pahl and Baeuerle, 1995, 1996). PERK signalling functions by translational attenuation preferentially lowering levels of inhibitory I-kappaB subunits, releasing NF-kappaB to execute its prosurvival signal (Deng et al., 2004; Jiang et al., 2003). The activation of EOR has been reported for serpinopathies, such as α1-antitrypsin deficiency (Hidvegi et al., 2007; Hidvegi et al., 2005; Lawless et al., 2004). An elevated level of NF-kappaB signalling was also found in patients with FENIB (Gill and Windebank, 2000; Graham and Gibson, 2005; Tergaonkar, 2006). In addition, Davies and colleagues proposed an activation of EOR by a reduced ER efficiency and/or perturbance in Ca^{2+} homeostasis due to accumulation of neuroserpin polymers in the ER (Davies et al., 2009b). Induction of EOR by reactive oxygen species due to perturbations in ER homeostasis has been also reported for serpinopathies (Teckman et al., 2004). Since the majority of studies on EOR in mutant serpin degradation were performed in cell culture, further investigations in FENIB mice will provide insights into the impact of EOR signalling on mutant neuroserpin accumulation *in vivo* (Davies et al., 2009a; Hidvegi et al., 2005; Lawless et al., 2004).

Using an ELISA specific for polymeric mutant neuroserpin (Miranda et al., 2008; Miranda et al., 2004) we discovered a transient decrease in polymeric neuroserpin reaching minimal concentrations at 34 weeks, rising exponentially up to 80 weeks of age (Fig 29). This parabolic distribution of polymeric mutant neuroserpin coincides with transient and exhausted induction of ATF6-arm of UPR (Fig. 30), underlining a crucial time window between 34 and 45 weeks. We hypothesized that activation of UPR is able to keep ER protein homeostasis

only balanced during young age. With increasing age these mechanisms cease, resulting in an exponential increase of polymers leading to neurodegeneration. Why the ability to mount efficient UPR responses decreases with age is currently unknown, but recent data show that this might be correlated to a general reduction in metabolic activity (Naidoo, 2009; Terman and Brunk, 2004). The fact that dementias show age specific distribution and exponential incidence rise with age argues in favour of age specific phenomena perturbing neuronal protein homeostasis (Rubinsztein, 2006; Salminen and Kaarniranta, 2010).

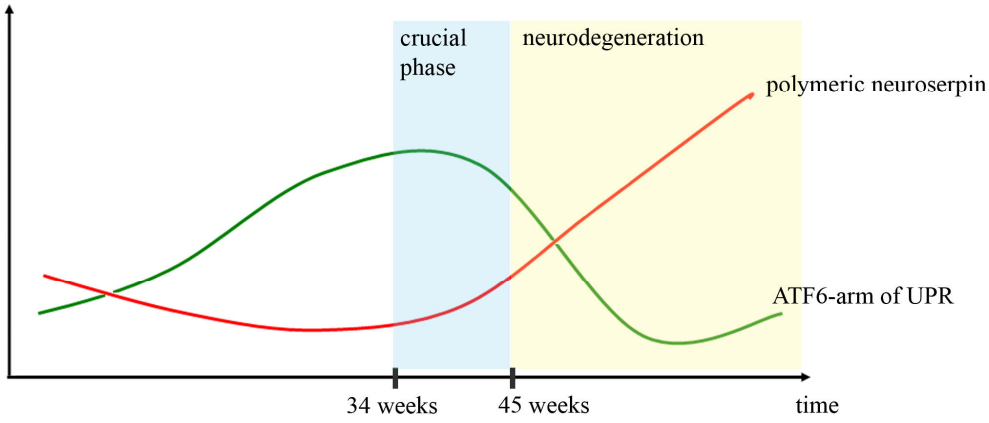

Figure 30: ATF6-arm of UPR promotes polymeric mutant neuroserpin degradation

Transient induction of the ATF6-arm of UPR (green curve) promotes transient decrease in polymeric mutant neuroserpin (red curve). A maximum of ATF6 activity was shown between 34 and 45 weeks, a time frame when polymeric mutant neuroserpin reached minimal concentrations (blue area). With increasing age and disease progression these mechanism cease resulting in an exponential increase of polymers leading to neurodegeneration (yellow area).

In summary, we have systematically investigated involvement of cellular mechanism of protein degradation in a murine model of FENIB. We showed mutant neuroserpin to be specifically degraded by the proteasome and non-specifically by autophagy. Augmentation of proteasomal capacity demonstrated importance of autophagic protein turnover in mutant protein degradation, revealing a close interplay among degradation routes. Further on, our data suggested that the tightly regulated balance between formation of protein polymers and cell encoded protective mechanism such as UPR as well as ERAD are in a delicate equilibrium which may be shifted by additional stressors such as old age. Future studies will have to address if our conclusions are specific for dementias with intracellular protein depositions, such as FENIB, or can be generalized to other dementia with extracellular protein

deposits. The ameliorating impact of UPR on polymeric neuroserpin indicated that targeting of UPR-pathways may hold therapeutic potential.

7. References

Adachi, Y., Yamamoto, K., Okada, T., Yoshida, H., Harada, A., and Mori, K. (2008). ATF6 is a transcription factor specializing in the regulation of quality control proteins in the endoplasmic reticulum. Cell Struct Funct *33*, 75-89.

Ahlberg, J., Marzella, L., and Glaumann, H. (1982). Uptake and degradation of proteins by isolated rat liver lysosomes. Suggestion of a microautophagic pathway of proteolysis. Lab Invest *47*, 523-532.

Arstila, A.U., and Trump, B.F. (1968). Studies on cellular autophagocytosis. The formation of autophagic vacuoles in the liver after glucagon administration. Am J Pathol *53*, 687-733.

Auluck, P.K., Chan, H.Y., Trojanowski, J.Q., Lee, V.M., and Bonini, N.M. (2002). Chaperone suppression of alpha-synuclein toxicity in a Drosophila model for Parkinson's disease. Science *295*, 865-868.

Balch, W.E., Morimoto, R.I., Dillin, A., and Kelly, J.W. (2008). Adapting proteostasis for disease intervention. Science *319*, 916-919.

Belorgey, D., Crowther, D.C., Mahadeva, R., and Lomas, D.A. (2002). Mutant Neuroserpin (S49P) that causes familial encephalopathy with neuroserpin inclusion bodies is a poor proteinase inhibitor and readily forms polymers in vitro. J Biol Chem *277*, 17367-17373.

Belorgey, D., Sharp, L.K., Crowther, D.C., Onda, M., Johansson, J., and Lomas, D.A. (2004). Neuroserpin Portland (Ser52Arg) is trapped as an inactive intermediate that rapidly forms polymers: implications for the epilepsy seen in the dementia FENIB. Eur J Biochem *271*, 3360-3367.

Berger, P., Kozlov, S.V., Krueger, S.R., and Sonderegger, P. (1998). Structure of the mouse gene for the serine protease inhibitor neuroserpin (PI12). Gene *214*, 25-33.

Bernales, S., Papa, F.R., and Walter, P. (2006). Intracellular signaling by the unfolded protein response. Annual review of cell and developmental biology *22*, 487-508.

Bertolotti, A., Zhang, Y., Hendershot, L.M., Harding, H.P., and Ron, D. (2000). Dynamic interaction of BiP and ER stress transducers in the unfolded-protein response. Nature cell biology *2*, 326-332.

Bonifacino, J.S., and Weissman, A.M. (1998). Ubiquitin and the control of protein fate in the secretory and endocytic pathways. Annual review of cell and developmental biology *14*, 19-57.

Bradshaw, C.B., Davis, R.L., Shrimpton, A.E., Holohan, P.D., Rea, C.B., Fieglin, D., Kent, P., and Collins, G.H. (2001). Cognitive deficits associated with a recently reported familial neurodegenerative disease: familial encephalopathy with neuroserpin inclusion bodies. Arch Neurol *58*, 1429-1434.

Briand, C., Kozlov, S.V., Sonderegger, P., and Grutter, M.G. (2001). Crystal structure of neuroserpin: a neuronal serpin involved in a conformational disease. FEBS Lett *505*, 18-22.

Calfon, M., Zeng, H., Urano, F., Till, J.H., Hubbard, S.R., Harding, H.P., Clark, S.G., and Ron, D. (2002). IRE1 couples endoplasmic reticulum load to secretory capacity by processing the XBP-1 mRNA. Nature *415*, 92-96.

Carrell, R.W., and Lomas, D.A. (1997). Conformational disease. Lancet *350*, 134-138.

Carrell, R.W., and Lomas, D.A. (2002). Alpha1-antitrypsin deficiency--a model for conformational diseases. N Engl J Med *346*, 45-53.

Carroll, T.P., Greene, C.M., O'Connor, C.A., Nolan, A.M., O'Neill, S.J., and McElvaney, N.G. (2010). Evidence for unfolded protein response activation in monocytes from individuals with alpha-1 antitrypsin deficiency. J Immunol *184*, 4538-4546.

Carvalho, P., Goder, V., and Rapoport, T.A. (2006). Distinct ubiquitin-ligase complexes define convergent pathways for the degradation of ER proteins. Cell *126*, 361-373.

Chan, E.Y., Longatti, A., McKnight, N.C., and Tooze, S.A. (2009). Kinase-inactivated ULK proteins inhibit autophagy via their conserved C-terminal domains using an Atg13-independent mechanism. Molecular and cellular biology *29*, 157-171.

Christianson, J.C., Shaler, T.A., Tyler, R.E., and Kopito, R.R. (2008). OS-9 and GRP94 deliver mutant alpha1-antitrypsin to the Hrd1-SEL1L ubiquitin ligase complex for ERAD. Nature cell biology *10*, 272-282.

Ciechanover, A., and Brundin, P. (2003). The ubiquitin proteasome system in neurodegenerative diseases: sometimes the chicken, sometimes the egg. Neuron *40*, 427-446.

Coutelier, M., Andries, S., Ghariani, S., Dan, B., Duyckaerts, C., van Rijckevorsel, K., Raftopoulos, C., Deconinck, N., Sonderegger, P., Scaravilli, F., *et al.* (2008). Neuroserpin mutation causes electrical status epilepticus of slow-wave sleep. Neurology *71*, 64-66.

Cox, J.S., Shamu, C.E., and Walter, P. (1993). Transcriptional induction of genes encoding endoplasmic reticulum resident proteins requires a transmembrane protein kinase. Cell *73*, 1197-1206.

Cox, J.S., and Walter, P. (1996). A novel mechanism for regulating activity of a transcription factor that controls the unfolded protein response. Cell *87*, 391-404.

Cuervo, A.M. (2004a). Autophagy: in sickness and in health. Trends Cell Biol *14*, 70-77.

Cuervo, A.M. (2004b). Autophagy: many paths to the same end. Mol Cell Biochem *263*, 55-72.

Cuervo, A.M., and Dice, J.F. (1996). A receptor for the selective uptake and degradation of proteins by lysosomes. Science *273*, 501-503.

Dadakhujaev, S., Noh, H.S., Jung, E.J., Cha, J.Y., Baek, S.M., Ha, J.H., and Kim, D.R. (2010). Autophagy protects the rotenone-induced cell death in alpha-synuclein overexpressing SH-SY5Y cells. Neuroscience letters *472*, 47-52.

Dafforn, T.R., Mahadeva, R., Elliott, P.R., Sivasothy, P., and Lomas, D.A. (1999). A kinetic mechanism for the polymerization of alpha1-antitrypsin. J Biol Chem *274*, 9548-9555.

Davies, M.J., and Lomas, D.A. (2008). The molecular aetiology of the serpinopathies. The international journal of biochemistry & cell biology.

Davies, M.J., Miranda, E., Roussel, B.D., Kaufman, R.J., Marciniak, S.J., and Lomas, D.A. (2009a). Neuroserpin polymers activate NF-kappaB by a calcium signaling pathway that is independent of the unfolded protein response. J Biol Chem *284*, 18202-18209.

Davies, M.J., Miranda, E., Roussel, B.D., Kaufman, R.J., Marciniak, S.J., and Lomas, D.A. (2009b). Neuroserpin polymers activate NF-kappaB by a calcium signalling pathway that is independent of the unfolded protein response. J Biol Chem.

Davis, R.L., Holohan, P.D., Shrimpton, A.E., Tatum, A.H., Daucher, J., Collins, G.H., Todd, R., Bradshaw, C., Kent, P., Feiglin, D., *et al.* (1999a). Familial encephalopathy with neuroserpin inclusion bodies. Am J Pathol *155*, 1901-1913.

Davis, R.L., Shrimpton, A.E., Carrell, R.W., Lomas, D.A., Gerhard, L., Baumann, B., Lawrence, D.A., Yepes, M., Kim, T.S., Ghetti, B., *et al.* (2002). Association between conformational mutations in neuroserpin and onset and severity of dementia. Lancet *359*, 2242-2247.

Davis, R.L., Shrimpton, A.E., Holohan, P.D., Bradshaw, C., Feiglin, D., Collins, G.H., Sonderegger, P., Kinter, J., Becker, L.M., Lacbawan, F., *et al.* (1999b). Familial dementia caused by polymerization of mutant neuroserpin. Nature *401*, 376-379.

Dawson, T.M., Ko, H.S., and Dawson, V.L. (2010). Genetic animal models of Parkinson's disease. Neuron *66*, 646-661.

De Vrij, F.M., Sluijs, J.A., Gregori, L., Fischer, D.F., Hermens, W.T., Goldgaber, D., Verhaagen, J., Van Leeuwen, F.W., and Hol, E.M. (2001). Mutant ubiquitin expressed in Alzheimer's disease causes neuronal death. Faseb J *15*, 2680-2688.

Declerck, P.J., De Mol, M., Alessi, M.C., Baudner, S., Paques, E.P., Preissner, K.T., Muller-Berghaus, G., and Collen, D. (1988). Purification and characterization of a plasminogen activator inhibitor 1 binding protein from human plasma. Identification as a multimeric form of S protein (vitronectin). J Biol Chem *263*, 15454-15461.

Deng, J., Lu, P.D., Zhang, Y., Scheuner, D., Kaufman, R.J., Sonenberg, N., Harding, H.P., and Ron, D. (2004). Translational repression mediates activation of nuclear factor kappa B by phosphorylated translation initiation factor 2. Molecular and cellular biology *24*, 10161-10168.

Di Domenico, F., Sultana, R., Tiu, G.F., Scheff, N.N., Perluigi, M., Cini, C., and Butterfield, D.A. (2010). Protein levels of heat shock proteins 27, 32, 60, 70, 90 and thioredoxin-1 in amnestic mild cognitive impairment: an investigation on the role of cellular stress response in the progression of Alzheimer disease. Brain Res *1333*, 72-81.

Dou, F., Netzer, W.J., Tanemura, K., Li, F., Hartl, F.U., Takashima, A., Gouras, G.K., Greengard, P., and Xu, H. (2003). Chaperones increase association of tau protein with microtubules. Proc Natl Acad Sci U S A *100*, 721-726.

Dunn, W.A., Jr. (1994). Autophagy and related mechanisms of lysosome-mediated protein degradation. Trends Cell Biol *4*, 139-143.

Duyckaerts, C., Potier, M.C., and Delatour, B. (2008). Alzheimer disease models and human neuropathology: similarities and differences. Acta Neuropathol *115*, 5-38.

Ekeowa, U.I., Freeke, J., Miranda, E., Gooptu, B., Bush, M.F., Perez, J., Teckman, J., Robinson, C.V., and Lomas, D.A. (2010). Defining the mechanism of polymerization in the serpinopathies. Proc Natl Acad Sci U S A *107*, 17146-17151.

Ellgaard, L., and Helenius, A. (2003). Quality control in the endoplasmic reticulum. Nat Rev Mol Cell Biol *4*, 181-191.

Elliott, P.R., Abrahams, J.P., and Lomas, D.A. (1998). Wild-type alpha 1-antitrypsin is in the canonical inhibitory conformation. J Mol Biol *275*, 419-425.

Elliott, P.R., Lomas, D.A., Carrell, R.W., and Abrahams, J.P. (1996). Inhibitory conformation of the reactive loop of alpha 1-antitrypsin. Nat Struct Biol *3*, 676-681.

Eskelinen, E.L. (2005). Maturation of autophagic vacuoles in Mammalian cells. Autophagy *1*, 1-10.

Eskelinen, E.L., Tanaka, Y., and Saftig, P. (2003). At the acidic edge: emerging functions for lysosomal membrane proteins. Trends Cell Biol *13*, 137-145.

Fengsrud, M., Roos, N., Berg, T., Liou, W., Slot, J.W., and Seglen, P.O. (1995). Ultrastructural and immunocytochemical characterization of autophagic vacuoles in isolated hepatocytes: effects of vinblastine and asparagine on vacuole distributions. Experimental cell research *221*, 504-519.

Fischer, D.F., van Dijk, R., van Tijn, P., Hobo, B., Verhage, M.C., van der Schors, R.C., Li, K.W., van Minnen, J., Hol, E.M., and van Leeuwen, F.W. (2009). Long-term proteasome dysfunction in the mouse brain by expression of aberrant ubiquitin. Neurobiol Aging *30*, 847-863.

Flynn, G.C., Pohl, J., Flocco, M.T., and Rothman, J.E. (1991). Peptide-binding specificity of the molecular chaperone BiP. Nature *353*, 726-730.

Fujikake, N., Nagai, Y., Popiel, H.A., Okamoto, Y., Yamaguchi, M., and Toda, T. (2008). Heat shock transcription factor 1-activating compounds suppress polyglutamine-induced neurodegeneration through induction of multiple molecular chaperones. J Biol Chem *283*, 26188-26197.

Galliciotti, G., Glatzel, M., Kinter, J., Kozlov, S.V., Cinelli, P., Rulicke, T., and Sonderegger, P. (2007). Accumulation of mutant neuroserpin precedes development of clinical symptoms in familial encephalopathy with neuroserpin inclusion bodies. Am J Pathol *170*, 1305-1313.

Gardner, R.G., Shearer, A.G., and Hampton, R.Y. (2001). In vivo action of the HRD ubiquitin ligase complex: mechanisms of endoplasmic reticulum quality control and sterol regulation. Molecular and cellular biology *21*, 4276-4291.

Gardner, R.G., Swarbrick, G.M., Bays, N.W., Cronin, S.R., Wilhovsky, S., Seelig, L., Kim, C., and Hampton, R.Y. (2000). Endoplasmic reticulum degradation requires lumen to cytosol signaling. Transmembrane control of Hrd1p by Hrd3p. The Journal of cell biology *151*, 69-82.

Gauss, R., Jarosch, E., Sommer, T., and Hirsch, C. (2006). A complex of Yos9p and the HRD ligase integrates endoplasmic reticulum quality control into the degradation machinery. Nature cell biology *8*, 849-854.

Gething, M.J., and Sambrook, J. (1992). Protein folding in the cell. Nature *355*, 33-45.

Gettins, P.G. (2002). Serpin structure, mechanism, and function. Chem Rev *102*, 4751-4804.

Gidalevitz, T., Kikis, E.A., and Morimoto, R.I. (2010). A cellular perspective on conformational disease: the role of genetic background and proteostasis networks. Current opinion in structural biology *20*, 23-32.

Gill, J.S., and Windebank, A.J. (2000). Ceramide initiates NFkappaB-mediated caspase activation in neuronal apoptosis. Neurobiol Dis *7*, 448-461.

Gooptu, B., Hazes, B., Chang, W.S., Dafforn, T.R., Carrell, R.W., Read, R.J., and Lomas, D.A. (2000). Inactive conformation of the serpin alpha(1)-antichymotrypsin indicates two-stage insertion of the reactive loop: implications for inhibitory function and conformational disease. Proc Natl Acad Sci U S A *97*, 67-72.

Gooptu, B., and Lomas, D.A. (2008). Polymers and inflammation: disease mechanisms of the serpinopathies. The Journal of experimental medicine *205*, 1529-1534.

Gooptu, B., and Lomas, D.A. (2009). Conformational Pathology of the Serpins: Themes, Variations, and Therapeutic Strategies. Annual review of biochemistry.

Graham, B., and Gibson, S.B. (2005). The two faces of NFkappaB in cell survival responses. Cell Cycle *4*, 1342-1345.

Granell, S., and Baldini, G. (2008). Inclusion bodies and autophagosomes: are ER-derived protective organelles different than classical autophagosomes? Autophagy *4*, 375-377.

Granell, S., Baldini, G., Mohammad, S., Nicolin, V., Narducci, P., and Storrie, B. (2008). Sequestration of mutated alpha1-antitrypsin into inclusion bodies is a cell-protective mechanism to maintain endoplasmic reticulum function. Molecular biology of the cell *19*, 572-586.

Haas, I.G., and Wabl, M. (1983). Immunoglobulin heavy chain binding protein. Nature *306*, 387-389.

Hammond, C., Braakman, I., and Helenius, A. (1994). Role of N-linked oligosaccharide recognition, glucose trimming, and calnexin in glycoprotein folding and quality control. Proc Natl Acad Sci U S A *91*, 913-917.

Harding, H.P., Zhang, Y., Bertolotti, A., Zeng, H., and Ron, D. (2000). Perk is essential for translational regulation and cell survival during the unfolded protein response. Molecular cell *5*, 897-904.

Harding, H.P., Zhang, Y., and Ron, D. (1999). Protein translation and folding are coupled by an endoplasmic-reticulum-resident kinase. Nature *397*, 271-274.

Harding, H.P., Zhang, Y., Zeng, H., Novoa, I., Lu, P.D., Calfon, M., Sadri, N., Yun, C., Popko, B., Paules, R., *et al.* (2003). An integrated stress response regulates amino acid metabolism and resistance to oxidative stress. Molecular cell *11*, 619-633.

Hastings, G.A., Coleman, T.A., Haudenschild, C.C., Stefansson, S., Smith, E.P., Barthlow, R., Cherry, S., Sandkvist, M., and Lawrence, D.A. (1997). Neuroserpin, a brain-associated inhibitor of tissue plasminogen activator is localized primarily in neurons. Implications for the regulation of motor learning and neuronal survival. J Biol Chem *272*, 33062-33067.

Haze, K., Yoshida, H., Yanagi, H., Yura, T., and Mori, K. (1999). Mammalian transcription factor ATF6 is synthesized as a transmembrane protein and activated by proteolysis in response to endoplasmic reticulum stress. Molecular biology of the cell *10*, 3787-3799.

Hebert, D.N., and Molinari, M. (2007). In and out of the ER: protein folding, quality control, degradation, and related human diseases. Physiological reviews *87*, 1377-1408.

Hegde, R.S., and Ploegh, H.L. (2010). Quality and quantity control at the endoplasmic reticulum. Curr Opin Cell Biol *22*, 437-446.

Helenius, A., and Aebi, M. (2001). Intracellular functions of N-linked glycans. Science *291*, 2364-2369.

Helenius, A., and Aebi, M. (2004). Roles of N-linked glycans in the endoplasmic reticulum. Annual review of biochemistry *73*, 1019-1049.

Hidvegi, T., Mirnics, K., Hale, P., Ewing, M., Beckett, C., and Perlmutter, D.H. (2007). Regulator of G Signaling 16 is a marker for the distinct endoplasmic reticulum stress state associated with aggregated mutant alpha1-antitrypsin Z in the classical form of alpha1-antitrypsin deficiency. J Biol Chem *282*, 27769-27780.

Hidvegi, T., Schmidt, B.Z., Hale, P., and Perlmutter, D.H. (2005). Accumulation of mutant alpha1-antitrypsin Z in the endoplasmic reticulum activates caspases-4 and -12, NFkappaB, and BAP31 but not the unfolded protein response. J Biol Chem *280*, 39002-39015.

Hietakangas, V., Ahlskog, J.K., Jakobsson, A.M., Hellesuo, M., Sahlberg, N.M., Holmberg, C.I., Mikhailov, A., Palvimo, J.J., Pirkkala, L., and Sistonen, L. (2003). Phosphorylation of serine 303 is a prerequisite for the stress-inducible SUMO modification of heat shock factor 1. Molecular and cellular biology *23*, 2953-2968.

Hill, R.M., Parmar, P.K., Coates, L.C., Mezey, E., Pearson, J.F., and Birch, N.P. (2000). Neuroserpin is expressed in the pituitary and adrenal glands and induces the extension of neurite-like processes in AtT-20 cells. Biochem J *345 Pt 3*, 595-601.

Hinnebusch, A.G., and Natarajan, K. (2002). Gcn4p, a master regulator of gene expression, is controlled at multiple levels by diverse signals of starvation and stress. Eukaryot Cell *1*, 22-32.

Hollien, J., Lin, J.H., Li, H., Stevens, N., Walter, P., and Weissman, J.S. (2009). Regulated Ire1-dependent decay of messenger RNAs in mammalian cells. The Journal of cell biology *186*, 323-331.

Hollien, J., and Weissman, J.S. (2006). Decay of endoplasmic reticulum-localized mRNAs during the unfolded protein response. Science *313*, 104-107.

Holmberg, C.I., Hietakangas, V., Mikhailov, A., Rantanen, J.O., Kallio, M., Meinander, A., Hellman, J., Morrice, N., MacKintosh, C., Morimoto, R.I., *et al.* (2001). Phosphorylation of serine 230 promotes inducible transcriptional activity of heat shock factor 1. The EMBO journal *20*, 3800-3810.

Hoozemans, J.J., van Haastert, E.S., Nijholt, D.A., Rozemuller, A.J., Eikelenboom, P., and Scheper, W. (2009). The unfolded protein response is activated in pretangle neurons in Alzheimer's disease hippocampus. Am J Pathol *174*, 1241-1251.

Hosokawa, N., Kato, K., and Kamiya, Y. (2010). Mannose 6-phosphate receptor homology domain-containing lectins in mammalian endoplasmic reticulum-associated degradation. Methods in enzymology *480*, 181-197.

Hosokawa, N., Wada, I., Hasegawa, K., Yorihuzi, T., Tremblay, L.O., Herscovics, A., and Nagata, K. (2001). A novel ER alpha-mannosidase-like protein accelerates ER-associated degradation. EMBO reports *2*, 415-422.

Hosokawa, N., Wada, I., Nagasawa, K., Moriyama, T., Okawa, K., and Nagata, K. (2008). Human XTP3-B forms an endoplasmic reticulum quality control scaffold with the HRD1-SEL1L ubiquitin ligase complex and BiP. J Biol Chem *283*, 20914-20924.

Huntington, J.A., Read, R.J., and Carrell, R.W. (2000). Structure of a serpin-protease complex shows inhibition by deformation. Nature *407*, 923-926.

Ichimura, Y., Kirisako, T., Takao, T., Satomi, Y., Shimonishi, Y., Ishihara, N., Mizushima, N., Tanida, I., Kominami, E., Ohsumi, M., *et al.* (2000). A ubiquitin-like system mediates protein lipidation. Nature *408*, 488-492.

Irving, J.A., Pike, R.N., Lesk, A.M., and Whisstock, J.C. (2000). Phylogeny of the serpin superfamily: implications of patterns of amino acid conservation for structure and function. Genome research *10*, 1845-1864.

Iwawaki, T., Hosoda, A., Okuda, T., Kamigori, Y., Nomura-Furuwatari, C., Kimata, Y., Tsuru, A., and Kohno, K. (2001). Translational control by the ER transmembrane kinase/ribonuclease IRE1 under ER stress. Nature cell biology *3*, 158-164.

Jakob, U., Lilie, H., Meyer, I., and Buchner, J. (1995). Transient interaction of Hsp90 with early unfolding intermediates of citrate synthase. Implications for heat shock in vivo. J Biol Chem *270*, 7288-7294.

Jiang, H.Y., Wek, S.A., McGrath, B.C., Scheuner, D., Kaufman, R.J., Cavener, D.R., and Wek, R.C. (2003). Phosphorylation of the alpha subunit of eukaryotic initiation factor 2 is required for activation of NF-kappaB in response to diverse cellular stresses. Molecular and cellular biology *23*, 5651-5663.

Jousse, C., Oyadomari, S., Novoa, I., Lu, P., Zhang, Y., Harding, H.P., and Ron, D. (2003). Inhibition of a constitutive translation initiation factor 2alpha phosphatase, CReP, promotes survival of stressed cells. The Journal of cell biology *163*, 767-775.

Jucker, M. (2010). The benefits and limitations of animal models for translational research in neurodegenerative diseases. Nat Med *16*, 1210-1214.

Jung, C.H., Ro, S.H., Cao, J., Otto, N.M., and Kim, D.H. (2010). mTOR regulation of autophagy. FEBS Lett *584*, 1287-1295.

Kabeya, Y., Mizushima, N., Ueno, T., Yamamoto, A., Kirisako, T., Noda, T., Kominami, E., Ohsumi, Y., and Yoshimori, T. (2000). LC3, a mammalian homologue of yeast Apg8p, is localized in autophagosome membranes after processing. The EMBO journal *19*, 5720-5728.

Kamada, Y., Funakoshi, T., Shintani, T., Nagano, K., Ohsumi, M., and Ohsumi, Y. (2000). Tor-mediated induction of autophagy via an Apg1 protein kinase complex. The Journal of cell biology *150*, 1507-1513.

Kamimoto, T., Shoji, S., Hidvegi, T., Mizushima, N., Umebayashi, K., Perlmutter, D.H., and Yoshimori, T. (2006). Intracellular inclusions containing mutant alpha1-antitrypsin Z are propagated in the absence of autophagic activity. J Biol Chem *281*, 4467-4476.

Kanehara, K., Xie, W., and Ng, D.T. (2010). Modularity of the Hrd1 ERAD complex underlies its diverse client range. The Journal of cell biology *188*, 707-716.

Kaslik, G., Kardos, J., Szabo, E., Szilagyi, L., Zavodszky, P., Westler, W.M., Markley, J.L., and Graf, L. (1997). Effects of serpin binding on the target proteinase: global stabilization, localized increased structural flexibility, and conserved hydrogen bonding at the active site. Biochemistry *36*, 5455-5464.

Kato, K., and Kamiya, Y. (2007). Structural views of glycoprotein-fate determination in cells. Glycobiology *17*, 1031-1044.

Kaufman, R.J. (1999). Stress signaling from the lumen of the endoplasmic reticulum: coordination of gene transcriptional and translational controls. Genes & development *13*, 1211-1233.

Kaufman, R.J. (2002). Orchestrating the unfolded protein response in health and disease. The Journal of clinical investigation *110*, 1389-1398.

Kegel, K.B., Kim, M., Sapp, E., McIntyre, C., Castano, J.G., Aronin, N., and DiFiglia, M. (2000). Huntingtin expression stimulates endosomal-lysosomal activity, endosome tubulation, and autophagy. J Neurosci *20*, 7268-7278.

Kerscher, O., Felberbaum, R., and Hochstrasser, M. (2006). Modification of proteins by ubiquitin and ubiquitin-like proteins. Annual review of cell and developmental biology *22*, 159-180.

Kim, J., and Klionsky, D.J. (2000). Autophagy, cytoplasm-to-vacuole targeting pathway, and pexophagy in yeast and mammalian cells. Annual review of biochemistry *69*, 303-342.

Kim, S., Woo, J., Seo, E.J., Yu, M., and Ryu, S. (2001). A 2.1 A resolution structure of an uncleaved alpha(1)-antitrypsin shows variability of the reactive center and other loops. J Mol Biol *306*, 109-119.

Kirisako, T., Baba, M., Ishihara, N., Miyazawa, K., Ohsumi, M., Yoshimori, T., Noda, T., and Ohsumi, Y. (1999). Formation process of autophagosome is traced with Apg8/Aut7p in yeast. The Journal of cell biology *147*, 435-446.

Klionsky, D.J. (2005). The molecular machinery of autophagy: unanswered questions. Journal of cell science *118*, 7-18.

Klionsky, D.J., Abeliovich, H., Agostinis, P., Agrawal, D.K., Aliev, G., Askew, D.S., Baba, M., Baehrecke, E.H., Bahr, B.A., Ballabio, A., *et al.* (2008). Guidelines for the use and interpretation of assays for monitoring autophagy in higher eukaryotes. Autophagy *4*, 151-175.

Klionsky, D.J., Cuervo, A.M., and Seglen, P.O. (2007). Methods for monitoring autophagy from yeast to human. Autophagy *3*, 181-206.

Klionsky, D.J., and Emr, S.D. (2000). Autophagy as a regulated pathway of cellular degradation. Science *290*, 1717-1721.

Klionsky, D.J., and Ohsumi, Y. (1999). Vacuolar import of proteins and organelles from the cytoplasm. Annual review of cell and developmental biology *15*, 1-32.

Klucken, J., Shin, Y., Masliah, E., Hyman, B.T., and McLean, P.J. (2004). Hsp70 Reduces alpha-Synuclein Aggregation and Toxicity. J Biol Chem *279*, 25497-25502.

Knaevelsrud, H., and Simonsen, A. (2010). Fighting disease by selective autophagy of aggregate-prone proteins. FEBS Lett *584*, 2635-2645.

Koegl, M., Hoppe, T., Schlenker, S., Ulrich, H.D., Mayer, T.U., and Jentsch, S. (1999). A novel ubiquitination factor, E4, is involved in multiubiquitin chain assembly. Cell *96*, 635-644.

Kohno, K. (2010). Stress-sensing mechanisms in the unfolded protein response: similarities and differences between yeast and mammals. J Biochem *147*, 27-33.

Koike, M., Shibata, M., Waguri, S., Yoshimura, K., Tanida, I., Kominami, E., Gotow, T., Peters, C., von Figura, K., Mizushima, N., *et al.* (2005). Participation of autophagy in storage of lysosomes in neurons from mouse models of neuronal ceroid-lipofuscinoses (Batten disease). Am J Pathol *167*, 1713-1728.

Kokjohn, T.A., and Roher, A.E. (2009). Amyloid precursor protein transgenic mouse models and Alzheimer's disease: understanding the paradigms, limitations, and contributions. Alzheimers Dement *5*, 340-347.

Komatsu, M., Waguri, S., Chiba, T., Murata, S., Iwata, J., Tanida, I., Ueno, T., Koike, M., Uchiyama, Y., Kominami, E., *et al.* (2006). Loss of autophagy in the central nervous system causes neurodegeneration in mice. Nature *441*, 880-884.

Kozak, M. (2002). Pushing the limits of the scanning mechanism for initiation of translation. Gene *299*, 1-34.

Kroeger, H., Miranda, E., MacLeod, I., Perez, J., Crowther, D.C., Marciniak, S.J., and Lomas, D.A. (2009). Endoplasmic reticulum-associated degradation (ERAD) and autophagy cooperate to degrade polymerogenic mutant serpins. J Biol Chem *284*, 22793-22802.

Krueger, S.R., Ghisu, G.P., Cinelli, P., Gschwend, T.P., Osterwalder, T., Wolfer, D.P., and Sonderegger, P. (1997). Expression of neuroserpin, an inhibitor of tissue plasminogen activator, in the developing and adult nervous system of the mouse. J Neurosci *17*, 8984-8996.

Kruse, K.B., Brodsky, J.L., and McCracken, A.A. (2006). Characterization of an ERAD gene as VPS30/ATG6 reveals two alternative and functionally distinct protein quality control pathways: one for soluble Z variant of human alpha-1 proteinase inhibitor (A1PiZ) and another for aggregates of A1PiZ. Molecular biology of the cell *17*, 203-212.

Kuma, A., Hatano, M., Matsui, M., Yamamoto, A., Nakaya, H., Yoshimori, T., Ohsumi, Y., Tokuhisa, T., and Mizushima, N. (2004). The role of autophagy during the early neonatal starvation period. Nature *432*, 1032-1036.

Kuma, A., Mizushima, N., Ishihara, N., and Ohsumi, Y. (2002). Formation of the approximately 350-kDa Apg12-Apg5.Apg16 multimeric complex, mediated by Apg16 oligomerization, is essential for autophagy in yeast. J Biol Chem *277*, 18619-18625.

Laemmli, U.K. (1970). Cleavage of structural proteins during the assembly of the head of bacteriophage T4. Nature *227*, 680-685.

Lam, Y.A., Pickart, C.M., Alban, A., Landon, M., Jamieson, C., Ramage, R., Mayer, R.J., and Layfield, R. (2000). Inhibition of the ubiquitin-proteasome system in Alzheimer's disease. Proc Natl Acad Sci U S A *97*, 9902-9906.

Lawless, M.W., Greene, C.M., Mulgrew, A., Taggart, C.C., O'Neill, S.J., and McElvaney, N.G. (2004). Activation of endoplasmic reticulum-specific stress responses associated with the conformational disease Z alpha 1-antitrypsin deficiency. J Immunol *172*, 5722-5726.

Lawless, M.W., Mankan, A.K., White, M., O'Dwyer, M.J., and Norris, S. (2007). Expression of hereditary hemochromatosis C282Y HFE protein in HEK293 cells activates specific endoplasmic reticulum stress responses. BMC Cell Biol *8*, 30.

Lebeurrier, N., Launay, S., Macrez, R., Maubert, E., Legros, H., Leclerc, A., Jamin, S.P., Picard, J.Y., Marret, S., Laudenbach, V., *et al.* (2008). Anti-Mullerian-hormone-dependent regulation of the brain serine-protease inhibitor neuroserpin. Journal of cell science *121*, 3357-3365.

Lebeurrier, N., Liot, G., Lopez-Atalaya, J.P., Orset, C., Fernandez-Monreal, M., Sonderegger, P., Ali, C., and Vivien, D. (2005). The brain-specific tissue-type plasminogen activator inhibitor, neuroserpin, protects neurons against excitotoxicity both in vitro and in vivo. Molecular and cellular neurosciences *30*, 552-558.

Lemasters, J.J., Qian, T., He, L., Kim, J.S., Elmore, S.P., Cascio, W.E., and Brenner, D.A. (2002). Role of mitochondrial inner membrane permeabilization in necrotic cell death, apoptosis, and autophagy. Antioxidants & redox signaling *4*, 769-781.

Levine, B., and Kroemer, G. (2008). Autophagy in the pathogenesis of disease. Cell *132*, 27-42.

Lindsten, K., de Vrij, F.M., Verhoef, L.G., Fischer, D.F., van Leeuwen, F.W., Hol, E.M., Masucci, M.G., and Dantuma, N.P. (2002). Mutant ubiquitin found in neurodegenerative disorders is a ubiquitin fusion degradation substrate that blocks proteasomal degradation. The Journal of cell biology *157*, 417-427.

Liu, C.Y., Schroder, M., and Kaufman, R.J. (2000). Ligand-independent dimerization activates the stress response kinases IRE1 and PERK in the lumen of the endoplasmic reticulum. J Biol Chem *275*, 24881-24885.

Liu, C.Y., Wong, H.N., Schauerte, J.A., and Kaufman, R.J. (2002). The protein kinase/endoribonuclease IRE1alpha that signals the unfolded protein response has a luminal N-terminal ligand-independent dimerization domain. J Biol Chem *277*, 18346-18356.

Loebermann, H., Tokuoka, R., Deisenhofer, J., and Huber, R. (1984). Human alpha 1-proteinase inhibitor. Crystal structure analysis of two crystal modifications, molecular model and preliminary analysis of the implications for function. J Mol Biol *177*, 531-557.

Lomas, D.A. (2005). Molecular mousetraps, alpha1-antitrypsin deficiency and the serpinopathies. Clinical medicine (London, England) *5*, 249-257.

Lomas, D.A., Belorgey, D., Mallya, M., Miranda, E., Kinghorn, K.J., Sharp, L.K., Phillips, R.L., Page, R., Robertson, A.S., and Crowther, D.C. (2005). Molecular mousetraps and the serpinopathies. Biochem Soc Trans *33*, 321-330.

Lomas, D.A., Evans, D.L., Finch, J.T., and Carrell, R.W. (1992). The mechanism of Z alpha 1-antitrypsin accumulation in the liver. Nature *357*, 605-607.

Lomas, D.A., Lourbakos, A., Cumming, S.A., and Belorgey, D. (2002). Hypersensitive mousetraps, alpha1-antitrypsin deficiency and dementia. Biochem Soc Trans *30*, 89-92.

Lomas, D.A., and Mahadeva, R. (2002). Alpha1-antitrypsin polymerization and the serpinopathies: pathobiology and prospects for therapy. The Journal of clinical investigation *110*, 1585-1590.

Lomas, D.A.C., R. W. (2002). Serpinopathies and the conformational dementias. Nat Rev Genet *3*, 759-768.

Lunemann, J.D., Schmidt, J., Dalakas, M.C., and Munz, C. (2007a). Macroautophagy as a pathomechanism in sporadic inclusion body myositis. Autophagy *3*, 384-386.

Lunemann, J.D., Schmidt, J., Schmid, D., Barthel, K., Wrede, A., Dalakas, M.C., and Munz, C. (2007b). Beta-amyloid is a substrate of autophagy in sporadic inclusion body myositis. Annals of neurology *61*, 476-483.

Luo, W., Sun, W., Taldone, T., Rodina, A., and Chiosis, G. (2010). Heat shock protein 90 in neurodegenerative diseases. Mol Neurodegener *5*, 24.

Ma, Y., Brewer, J.W., Diehl, J.A., and Hendershot, L.M. (2002). Two distinct stress signaling pathways converge upon the CHOP promoter during the mammalian unfolded protein response. J Mol Biol *318*, 1351-1365.

Madani, R., Kozlov, S., Akhmedov, A., Cinelli, P., Kinter, J., Lipp, H.P., Sonderegger, P., and Wolfer, D.P. (2003). Impaired explorative behavior and neophobia in genetically modified mice lacking or overexpressing the extracellular serine protease inhibitor neuroserpin. Molecular and cellular neurosciences *23*, 473-494.

Magrane, J., Smith, R.C., Walsh, K., and Querfurth, H.W. (2004). Heat shock protein 70 participates in the neuroprotective response to intracellularly expressed beta-amyloid in neurons. J Neurosci *24*, 1700-1706.

Mahadeva, R., Dafforn, T.R., Carrell, R.W., and Lomas, D.A. (2002). 6-mer peptide selectively anneals to a pathogenic serpin conformation and blocks polymerization. Implications for the prevention of Z alpha(1)-antitrypsin-related cirrhosis. J Biol Chem *277*, 6771-6774.

Marciniak, S.J., and Ron, D. (2006). Endoplasmic reticulum stress signaling in disease. Physiological reviews *86*, 1133-1149.

Massey, A.C., Zhang, C., and Cuervo, A.M. (2006). Chaperone-mediated autophagy in aging and disease. Current topics in developmental biology *73*, 205-235.

McCullough, K.D., Martindale, J.L., Klotz, L.O., Aw, T.Y., and Holbrook, N.J. (2001). Gadd153 sensitizes cells to endoplasmic reticulum stress by down-regulating Bcl2 and perturbing the cellular redox state. Molecular and cellular biology *21*, 1249-1259.

McLeland, C.B., Rodriguez, J., and Stern, S.T. (2011). Autophagy monitoring assay: qualitative analysis of MAP LC3-I to II conversion by immunoblot. Methods in molecular biology (Clifton, NJ *697*, 199-206.

Meijer, A.J., and Codogno, P. (2006). Signalling and autophagy regulation in health, aging and disease. Mol Aspects Med *27*, 411-425.

Miranda, E., and Lomas, D.A. (2006). Neuroserpin: a serpin to think about. Cell Mol Life Sci *63*, 709-722.

Miranda, E., McLeod, I., Davies, M.J., Perez, J., Romisch, K., Crowther, D.C., and Lomas, D.A. (2008). The intracellular accumulation of polymeric neuroserpin explains the severity of the dementia FENIB. Hum Mol Genet.

Miranda, E., Romisch, K., and Lomas, D.A. (2004). Mutants of neuroserpin that cause dementia accumulate as polymers within the endoplasmic reticulum. J Biol Chem *279*, 28283-28291.

Mizushima, N. (2004). Methods for monitoring autophagy. The international journal of biochemistry & cell biology *36*, 2491-2502.

Mizushima, N. (2005). The pleiotropic role of autophagy: from protein metabolism to bactericide. Cell death and differentiation *12 Suppl 2*, 1535-1541.

Mizushima, N., and Hara, T. (2006). Intracellular quality control by autophagy: how does autophagy prevent neurodegeneration? Autophagy *2*, 302-304.

Mizushima, N., and Klionsky, D.J. (2007). Protein turnover via autophagy: implications for metabolism. Annu Rev Nutr *27*, 19-40.

Mizushima, N., Levine, B., Cuervo, A.M., and Klionsky, D.J. (2008). Autophagy fights disease through cellular self-digestion. Nature *451*, 1069-1075.

Mizushima, N., Yamamoto, A., Hatano, M., Kobayashi, Y., Kabeya, Y., Suzuki, K., Tokuhisa, T., Ohsumi, Y., and Yoshimori, T. (2001). Dissection of autophagosome formation using Apg5-deficient mouse embryonic stem cells. The Journal of cell biology *152*, 657-668.

Mori, K. (2000). Tripartite management of unfolded proteins in the endoplasmic reticulum. Cell *101*, 451-454.

Mori, K., Kawahara, T., Yoshida, H., Yanagi, H., and Yura, T. (1996). Signalling from endoplasmic reticulum to nucleus: transcription factor with a basic-leucine zipper motif is required for the unfolded protein-response pathway. Genes Cells *1*, 803-817.

Mori, K., Ma, W., Gething, M.J., and Sambrook, J. (1993). A transmembrane protein with a cdc2+/CDC28-related kinase activity is required for signaling from the ER to the nucleus. Cell *74*, 743-756.

Muchowski, P.J., Schaffar, G., Sittler, A., Wanker, E.E., Hayer-Hartl, M.K., and Hartl, F.U. (2000). Hsp70 and hsp40 chaperones can inhibit self-assembly of polyglutamine proteins into amyloid-like fibrils. Proc Natl Acad Sci U S A *97*, 7841-7846.

Muchowski, P.J., and Wacker, J.L. (2005). Modulation of neurodegeneration by molecular chaperones. Nat Rev Neurosci *6*, 11-22.

Naidoo, N. (2009). The endoplasmic reticulum stress response and aging. Rev Neurosci *20*, 23-37.

Nakagawa, T., Zhu, H., Morishima, N., Li, E., Xu, J., Yankner, B.A., and Yuan, J. (2000). Caspase-12 mediates endoplasmic-reticulum-specific apoptosis and cytotoxicity by amyloid-beta. Nature *403*, 98-103.

Nakatsukasa, K., and Brodsky, J.L. (2008). The recognition and retrotranslocation of misfolded proteins from the endoplasmic reticulum. Traffic (Copenhagen, Denmark) *9*, 861-870.

Nixon, R.A., Cataldo, A.M., and Mathews, P.M. (2000). The endosomal-lysosomal system of neurons in Alzheimer's disease pathogenesis: a review. Neurochem Res *25*, 1161-1172.

Noda, T., and Ohsumi, Y. (1998). Tor, a phosphatidylinositol kinase homologue, controls autophagy in yeast. J Biol Chem *273*, 3963-3966.

Normington, K., Kohno, K., Kozutsumi, Y., Gething, M.J., and Sambrook, J. (1989). S. cerevisiae encodes an essential protein homologous in sequence and function to mammalian BiP. Cell *57*, 1223-1236.

Ogata, M., Hino, S., Saito, A., Morikawa, K., Kondo, S., Kanemoto, S., Murakami, T., Taniguchi, M., Tanii, I., Yoshinaga, K., *et al.* (2006). Autophagy is activated for cell survival after endoplasmic reticulum stress. Molecular and cellular biology *26*, 9220-9231.

Okada, T., Yoshida, H., Akazawa, R., Negishi, M., and Mori, K. (2002). Distinct roles of activating transcription factor 6 (ATF6) and double-stranded RNA-activated protein kinase-like endoplasmic reticulum kinase (PERK) in transcription during the mammalian unfolded protein response. Biochem J *366*, 585-594.

Okamura, K., Kimata, Y., Higashio, H., Tsuru, A., and Kohno, K. (2000). Dissociation of Kar2p/BiP from an ER sensory molecule, Ire1p, triggers the unfolded protein response in yeast. Biochem Biophys Res Commun *279*, 445-450.

Onda, M., Belorgey, D., Sharp, L.K., and Lomas, D.A. (2005). Latent S49P neuroserpin forms polymers in the dementia familial encephalopathy with neuroserpin inclusion bodies. J Biol Chem *280*, 13735-13741.

Osterwalder, T., Cinelli, P., Baici, A., Pennella, A., Krueger, S.R., Schrimpf, S.P., Meins, M., and Sonderegger, P. (1998). The axonally secreted serine proteinase inhibitor, neuroserpin, inhibits plasminogen activators and plasmin but not thrombin. J Biol Chem *273*, 2312-2321.

Osterwalder, T., Contartese, J., Stoeckli, E.T., Kuhn, T.B., and Sonderegger, P. (1996). Neuroserpin, an axonally secreted serine protease inhibitor. The EMBO journal *15*, 2944-2953.

Pahl, H.L., and Baeuerle, P.A. (1995). A novel signal transduction pathway from the endoplasmic reticulum to the nucleus is mediated by transcription factor NF-kappa B. The EMBO journal *14*, 2580-2588.

Pahl, H.L., and Baeuerle, P.A. (1996). Activation of NF-kappa B by ER stress requires both Ca2+ and reactive oxygen intermediates as messengers. FEBS Lett *392*, 129-136.

Pahl, H.L., and Baeuerle, P.A. (1997). The ER-overload response: activation of NF-kappa B. Trends in biochemical sciences *22*, 63-67.

Palade, G. (1975). Intracellular aspects of the process of protein synthesis. Science *189*, 867.

Papa, F.R., Zhang, C., Shokat, K., and Walter, P. (2003). Bypassing a kinase activity with an ATP-competitive drug. Science *302*, 1533-1537.

Parodi, A.J. (2000). Protein glucosylation and its role in protein folding. Annual review of biochemistry *69*, 69-93.

Perlmutter, D.H., Schlesinger, M.J., Pierce, J.A., Punsal, P.I., and Schwartz, A.L. (1989). Synthesis of stress proteins is increased in individuals with homozygous PiZZ alpha 1-antitrypsin deficiency and liver disease. The Journal of clinical investigation *84*, 1555-1561.

Pfaffl, M.W. (2001). A new mathematical model for relative quantification in real-time RT-PCR. Nucleic acids research *29*, e45.

Pickart, C.M. (2001). Mechanisms underlying ubiquitination. Annual review of biochemistry *70*, 503-533.

Plemper, R.K., Deak, P.M., Otto, R.T., and Wolf, D.H. (1999). Re-entering the translocon from the lumenal side of the endoplasmic reticulum. Studies on mutated carboxypeptidase yscY species. FEBS Lett *443*, 241-245.

Ravikumar, B., Duden, R., and Rubinsztein, D.C. (2002). Aggregate-prone proteins with polyglutamine and polyalanine expansions are degraded by autophagy. Hum Mol Genet *11*, 1107-1117.

Ravikumar, B., Vacher, C., Berger, Z., Davies, J.E., Luo, S., Oroz, L.G., Scaravilli, F., Easton, D.F., Duden, R., O'Kane, C.J., *et al.* (2004). Inhibition of mTOR induces autophagy and reduces toxicity of polyglutamine expansions in fly and mouse models of Huntington disease. Nature genetics *36*, 585-595.

Reggiori, F. (2006). 1. Membrane origin for autophagy. Current topics in developmental biology *74*, 1-30.

Ricagno, S., Caccia, S., Sorrentino, G., Antonini, G., and Bolognesi, M. (2009). Human neuroserpin: structure and time-dependent inhibition. J Mol Biol *388*, 109-121.

Richter, K., Haslbeck, M., and Buchner, J. (2010). The heat shock response: life on the verge of death. Molecular cell *40*, 253-266.

Ron, D., and Walter, P. (2007). Signal integration in the endoplasmic reticulum unfolded protein response. Nat Rev Mol Cell Biol *8*, 519-529.

Rubinsztein, D.C. (2006). The roles of intracellular protein-degradation pathways in neurodegeneration. Nature *443*, 780-786.

Rubinsztein, D.C., DiFiglia, M., Heintz, N., Nixon, R.A., Qin, Z.H., Ravikumar, B., Stefanis, L., and Tolkovsky, A. (2005). Autophagy and its possible roles in nervous system diseases, damage and repair. Autophagy *1*, 11-22.

Rutkevich, L.A., and Williams, D.B. (2010). Participation of lectin chaperones and thiol oxidoreductases in protein folding within the endoplasmic reticulum. Curr Opin Cell Biol.

Ryu, S.E., Choi, H.J., Kwon, K.S., Lee, K.N., and Yu, M.H. (1996). The native strains in the hydrophobic core and flexible reactive loop of a serine protease inhibitor: crystal structure of an uncleaved alpha1-antitrypsin at 2.7 A. Structure *4*, 1181-1192.

Sakahira, H., and Nagata, S. (2002). Co-translational folding of caspase-activated DNase with Hsp70, Hsp40, and inhibitor of caspase-activated DNase. J Biol Chem *277*, 3364-3370.

Salminen, A., and Kaarniranta, K. (2010). ER stress and hormetic regulation of the aging process. Ageing Res Rev *9*, 211-217.

Scheuner, D., Song, B., McEwen, E., Liu, C., Laybutt, R., Gillespie, P., Saunders, T., Bonner-Weir, S., and Kaufman, R.J. (2001). Translational control is required for the unfolded protein response and in vivo glucose homeostasis. Molecular cell *7*, 1165-1176.

Schrimpf, S.P., Bleiker, A.J., Brecevic, L., Kozlov, S.V., Berger, P., Osterwalder, T., Krueger, S.R., Schinzel, A., and Sonderegger, P. (1997). Human neuroserpin (PI12): cDNA cloning and chromosomal localization to 3q26. Genomics *40*, 55-62.

Schroder, M., and Kaufman, R.J. (2005). The mammalian unfolded protein response. Annual review of biochemistry *74*, 739-789.

Schwartz, A.L., and Ciechanover, A. (2009). Targeting proteins for destruction by the ubiquitin system: implications for human pathobiology. Annu Rev Pharmacol Toxicol *49*, 73-96.

Scorrano, L., Oakes, S.A., Opferman, J.T., Cheng, E.H., Sorcinelli, M.D., Pozzan, T., and Korsmeyer, S.J. (2003). BAX and BAK regulation of endoplasmic reticulum Ca2+: a control point for apoptosis. Science *300*, 135-139.

Shamu, C.E., and Walter, P. (1996). Oligomerization and phosphorylation of the Ire1p kinase during intracellular signaling from the endoplasmic reticulum to the nucleus. The EMBO journal *15*, 3028-3039.

Shen, J., Chen, X., Hendershot, L., and Prywes, R. (2002). ER stress regulation of ATF6 localization by dissociation of BiP/GRP78 binding and unmasking of Golgi localization signals. Dev Cell *3*, 99-111.

Shen, X., Zhang, K., and Kaufman, R.J. (2004). The unfolded protein response--a stress signaling pathway of the endoplasmic reticulum. J Chem Neuroanat *28*, 79-92.

Shi, Y., Vattem, K.M., Sood, R., An, J., Liang, J., Stramm, L., and Wek, R.C. (1998). Identification and characterization of pancreatic eukaryotic initiation factor 2 alpha-subunit kinase, PEK, involved in translational control. Molecular and cellular biology *18*, 7499-7509.

Silverman, G.A., Bird, P.I., Carrell, R.W., Church, F.C., Coughlin, P.B., Gettins, P.G., Irving, J.A., Lomas, D.A., Luke, C.J., Moyer, R.W., *et al.* (2001). The serpins are an expanding superfamily of structurally similar but functionally diverse proteins. Evolution, mechanism of inhibition, novel functions, and a revised nomenclature. J Biol Chem *276*, 33293-33296.

Sitia, R., and Braakman, I. (2003). Quality control in the endoplasmic reticulum protein factory. Nature *426*, 891-894.

Sittler, A., Lurz, R., Lueder, G., Priller, J., Lehrach, H., Hayer-Hartl, M.K., Hartl, F.U., and Wanker, E.E. (2001). Geldanamycin activates a heat shock response and inhibits huntingtin aggregation in a cell culture model of Huntington's disease. Hum Mol Genet *10*, 1307-1315.

Sivasothy, P., Dafforn, T.R., Gettins, P.G., and Lomas, D.A. (2000). Pathogenic alpha 1-antitrypsin polymers are formed by reactive loop-beta-sheet A linkage. J Biol Chem *275*, 33663-33668.

Slot, J.W., and Geuze, H.J. (2007). Cryosectioning and immunolabeling. Nature protocols *2*, 2480-2491.

Stoeckli, E.T., Lemkin, P.F., Kuhn, T.B., Ruegg, M.A., Heller, M., and Sonderegger, P. (1989). Identification of proteins secreted from axons of embryonic dorsal-root-ganglia neurons. Eur J Biochem *180*, 249-258.

Stratikos, E., and Gettins, P.G. (1999). Formation of the covalent serpin-proteinase complex involves translocation of the proteinase by more than 70 A and full insertion of the reactive center loop into beta-sheet A. Proc Natl Acad Sci U S A *96*, 4808-4813.

Stromhaug, P.E., Berg, T.O., Fengsrud, M., and Seglen, P.O. (1998). Purification and characterization of autophagosomes from rat hepatocytes. Biochem J *335 (Pt 2)*, 217-224.

Szegezdi, E., Duffy, A., O'Mahoney, M.E., Logue, S.E., Mylotte, L.A., O'Brien, T., and Samali, A. (2006a). ER stress contributes to ischemia-induced cardiomyocyte apoptosis. Biochem Biophys Res Commun *349*, 1406-1411.

Szegezdi, E., Logue, S.E., Gorman, A.M., and Samali, A. (2006b). Mediators of endoplasmic reticulum stress-induced apoptosis. EMBO reports *7*, 880-885.

Takao, M., Benson, M.D., Murrell, J.R., Yazaki, M., Piccardo, P., Unverzagt, F.W., Davis, R.L., Holohan, P.D., Lawrence, D.A., Richardson, R., *et al.* (2000). Neuroserpin mutation S52R causes neuroserpin accumulation in neurons and is associated with progressive myoclonus epilepsy. Journal of neuropathology and experimental neurology *59*, 1070-1086.

Takasawa, A., Kato, I., Takasawa, K., Ishii, Y., Yoshida, T., Shehata, M.H., Kawaguchi, H., Mohafez, O.M., Sasahara, M., and Hiraga, K. (2008). Mutation-, aging-, and gene dosage-dependent accumulation of neuroserpin (G392E) in endoplasmic reticula and lysosomes of neurons in transgenic mice. J Biol Chem *283*, 35606-35613.

Tanida, I., Ueno, T., and Kominami, E. (2004). LC3 conjugation system in mammalian autophagy. The international journal of biochemistry & cell biology *36*, 2503-2518.

Teckman, J.H., An, J.K., Blomenkamp, K., Schmidt, B., and Perlmutter, D. (2004). Mitochondrial autophagy and injury in the liver in alpha 1-antitrypsin deficiency. Am J Physiol Gastrointest Liver Physiol *286*, G851-862.

Teckman, J.H., and Perlmutter, D.H. (2000). Retention of mutant alpha(1)-antitrypsin Z in endoplasmic reticulum is associated with an autophagic response. Am J Physiol Gastrointest Liver Physiol *279*, G961-974.

Tergaonkar, V. (2006). NFkappaB pathway: a good signaling paradigm and therapeutic target. The international journal of biochemistry & cell biology *38*, 1647-1653.

Terman, A., and Brunk, U.T. (2004). Aging as a catabolic malfunction. The international journal of biochemistry & cell biology *36*, 2365-2375.

Thrower, J.S., Hoffman, L., Rechsteiner, M., and Pickart, C.M. (2000). Recognition of the polyubiquitin proteolytic signal. The EMBO journal *19*, 94-102.

Tirasophon, W., Welihinda, A.A., and Kaufman, R.J. (1998). A stress response pathway from the endoplasmic reticulum to the nucleus requires a novel bifunctional protein kinase/endoribonuclease (Ire1p) in mammalian cells. Genes & development *12*, 1812-1824.

Towbin, H., Staehelin, T., and Gordon, J. (1979). Electrophoretic transfer of proteins from polyacrylamide gels to nitrocellulose sheets: procedure and some applications. Proc Natl Acad Sci U S A *76*, 4350-4354.

Tsai, B., Ye, Y., and Rapoport, T.A. (2002). Retro-translocation of proteins from the endoplasmic reticulum into the cytosol. Nat Rev Mol Cell Biol *3*, 246-255.

Tu, B.P., and Weissman, J.S. (2004). Oxidative protein folding in eukaryotes: mechanisms and consequences. The Journal of cell biology *164*, 341-346.

Ueno, T., Muno, D., and Kominami, E. (1991). Membrane markers of endoplasmic reticulum preserved in autophagic vacuolar membranes isolated from leupeptin-administered rat liver. J Biol Chem *266*, 18995-18999.

Urano, F., Bertolotti, A., and Ron, D. (2000). IRE1 and efferent signaling from the endoplasmic reticulum. Journal of cell science *113 Pt 21*, 3697-3702.

van Leeuwen, F.W., de Kleijn, D.P., van den Hurk, H.H., Neubauer, A., Sonnemans, M.A., Sluijs, J.A., Koycu, S., Ramdjielal, R.D., Salehi, A., Martens, G.J., *et al.* (1998). Frameshift mutants of beta amyloid precursor protein and ubiquitin-B in Alzheimer's and Down patients. Science *279*, 242-247.

Voges, D., Zwickl, P., and Baumeister, W. (1999). The 26S proteasome: a molecular machine designed for controlled proteolysis. Annual review of biochemistry *68*, 1015-1068.

Wang, X.Z., Harding, H.P., Zhang, Y., Jolicoeur, E.M., Kuroda, M., and Ron, D. (1998). Cloning of mammalian Ire1 reveals diversity in the ER stress responses. The EMBO journal *17*, 5708-5717.

Wannier-Morino, P., Rager, G., Sonderegger, P., and Grabs, D. (2003). Expression of neuroserpin in the visual cortex of the mouse during the developmental critical period. Eur J Neurosci *17*, 1853-1860.

Warrick, J.M., Chan, H.Y., Gray-Board, G.L., Chai, Y., Paulson, H.L., and Bonini, N.M. (1999). Suppression of polyglutamine-mediated neurodegeneration in Drosophila by the molecular chaperone HSP70. Nature genetics *23*, 425-428.

Webb, J.L., Ravikumar, B., Atkins, J., Skepper, J.N., and Rubinsztein, D.C. (2003). Alpha-Synuclein is degraded by both autophagy and the proteasome. J Biol Chem *278*, 25009-25013.

Welchman, R.L., Gordon, C., and Mayer, R.J. (2005). Ubiquitin and ubiquitin-like proteins as multifunctional signals. Nat Rev Mol Cell Biol *6*, 599-609.

Whisstock, J.C., and Bottomley, S.P. (2006). Molecular gymnastics: serpin structure, folding and misfolding. Current opinion in structural biology *16*, 761-768.

Wilczynska, M., Fa, M., Karolin, J., Ohlsson, P.I., Johansson, L.B., and Ny, T. (1997). Structural insights into serpin-protease complexes reveal the inhibitory mechanism of serpins. Nat Struct Biol *4*, 354-357.

Wilczynska, M., Fa, M., Ohlsson, P.I., and Ny, T. (1995). The inhibition mechanism of serpins. Evidence that the mobile reactive center loop is cleaved in the native protease-inhibitor complex. J Biol Chem *270*, 29652-29655.

Wiman, B., Almquist, A., Sigurdardottir, O., and Lindahl, T. (1988). Plasminogen activator inhibitor 1 (PAI) is bound to vitronectin in plasma. FEBS Lett *242*, 125-128.

Witt, S.N. (2010). Hsp70 molecular chaperones and Parkinson's disease. Biopolymers *93*, 218-228.

Wu, J., Echeverry, R., Guzman, J., and Yepes, M. (2010). Neuroserpin protects neurons from ischemia-induced plasmin-mediated cell death independently of tissue-type plasminogen activator inhibition. The American journal of pathology *177*, 2576-2584.

Wu, J., Rutkowski, D.T., Dubois, M., Swathirajan, J., Saunders, T., Wang, J., Song, B., Yau, G.D., and Kaufman, R.J. (2007). ATF6alpha optimizes long-term endoplasmic reticulum function to protect cells from chronic stress. Dev Cell *13*, 351-364.

Xie, Z., and Klionsky, D.J. (2007). Autophagosome formation: core machinery and adaptations. Nature cell biology *9*, 1102-1109.

Xue, L., Fletcher, G.C., and Tolkovsky, A.M. (2001). Mitochondria are selectively eliminated from eukaryotic cells after blockade of caspases during apoptosis. Curr Biol *11*, 361-365.

Yamamoto, A., Masaki, R., and Tashiro, Y. (1990). Characterization of the isolation membranes and the limiting membranes of autophagosomes in rat hepatocytes by lectin cytochemistry. J Histochem Cytochem *38*, 573-580.

Yamasaki, M., Li, W., Johnson, D.J., and Huntington, J.A. (2008). Crystal structure of a stable dimer reveals the molecular basis of serpin polymerization. Nature *455*, 1255-1258.

Yang, W., and Paschen, W. (2009). The endoplasmic reticulum and neurological diseases. Exp Neurol *219*, 376-381.

Ye, J., Rawson, R.B., Komuro, R., Chen, X., Dave, U.P., Prywes, R., Brown, M.S., and Goldstein, J.L. (2000). ER stress induces cleavage of membrane-bound ATF6 by the same proteases that process SREBPs. Molecular cell *6*, 1355-1364.

Yenari, M.A. (2002). Heat shock proteins and neuroprotection. Advances in experimental medicine and biology *513*, 281-299.

Yepes, M., and Lawrence, D.A. (2004a). Neuroserpin: a selective inhibitor of tissue-type plasminogen activator in the central nervous system. Thrombosis and haemostasis *91*, 457-464.

Yepes, M., and Lawrence, D.A. (2004b). Tissue-type plasminogen activator and neuroserpin: a well-balanced act in the nervous system? Trends Cardiovasc Med *14*, 173-180.

Yepes, M., Sandkvist, M., Coleman, T.A., Moore, E., Wu, J.Y., Mitola, D., Bugge, T.H., and Lawrence, D.A. (2002). Regulation of seizure spreading by neuroserpin and tissue-type plasminogen activator is plasminogen-independent. The Journal of clinical investigation *109*, 1571-1578.

Yorimitsu, T., and Klionsky, D.J. (2007). Endoplasmic reticulum stress: a new pathway to induce autophagy. Autophagy *3*, 160-162.

Yoshida, H., Matsui, T., Hosokawa, N., Kaufman, R.J., Nagata, K., and Mori, K. (2003). A time-dependent phase shift in the mammalian unfolded protein response. Dev Cell *4*, 265-271.

Yoshida, H., Matsui, T., Yamamoto, A., Okada, T., and Mori, K. (2001). XBP1 mRNA is induced by ATF6 and spliced by IRE1 in response to ER stress to produce a highly active transcription factor. Cell *107*, 881-891.

Yoshida, H., Okada, T., Haze, K., Yanagi, H., Yura, T., Negishi, M., and Mori, K. (2000). ATF6 activated by proteolysis binds in the presence of NF-Y (CBF) directly to the cis-acting element responsible for the mammalian unfolded protein response. Molecular and cellular biology *20*, 6755-6767.

Yoshida, H., Oku, M., Suzuki, M., and Mori, K. (2006). pXBP1(U) encoded in XBP1 pre-mRNA negatively regulates unfolded protein response activator pXBP1(S) in mammalian ER stress response. The Journal of cell biology *172*, 565-575.

Zhang, K., and Kaufman, R.J. (2006). The unfolded protein response: a stress signaling pathway critical for health and disease. Neurology *66*, S102-109.

Zhang, K., and Kaufman, R.J. (2008). Identification and characterization of endoplasmic reticulum stress-induced apoptosis in vivo. Methods in enzymology *442*, 395-419.

Zong, W.X., Li, C., Hatzivassiliou, G., Lindsten, T., Yu, Q.C., Yuan, J., and Thompson, C.B. (2003). Bax and Bak can localize to the endoplasmic reticulum to initiate apoptosis. The Journal of cell biology *162*, 59-69.

Zuber, C., Cormier, J.H., Guhl, B., Santimaria, R., Hebert, D.N., and Roth, J. (2007). EDEM1 reveals a quality control vesicular transport pathway out of the endoplasmic reticulum not involving the COPII exit sites. Proc Natl Acad Sci U S A *104*, 4407-4412.

8. Appendix

8.1 Abbreviations

%	percentage
°C	degree Celcius
µg	microgram
µl	microlitre
AD	alzheimer's disease
APS	ammoniumperoxidsulfat
ATF4	activating transcription factor-4
ATF6	activating transcription factor-6
bp	base pair
BSA	bovine serum albumin
cDNA	complementary deoxyribonucleic acid
CNS	central nervous system
CP	crossing point
DAB	diaminiobenzidine
DEPC	diethylpyrocarbonat
DMEM	Dulbecco's Modified Eagle's Medium
DMSO	dimethylsulfoxid
DNA	deoxyribonucleic acid
dNTPs	desoxynucleotide triphosphate (s)
DTT	dithiothreitol
E	efficiency
ECL	enhanced chemiluminiscence
EDTA	ethylendiamintetraacetat
eIF2α	eukaryotic initiation factor 2α
eIF2αP	eukaryotic initiation factor 2α phosphorylated
ELISA	enzyme-linked immunosorbent assay
EOR	ER overload response
ER	endoplasmic reticulum
ERAD	ER associated degradation

F	fluorescence
FBS	fetal bovine sera
FENIB	familial encephalopathy with neuroserpin inclusion bodies
Fig.	figure
g	accelaration
g	gram
GFP	green flourescent protein
h	hour
HRP	horse radish peroxidase
IRE1	inositol-requiring kinase 1
kb	kilo base (= 1000 bp)
kDa	kilo Dalton (= 1000 Da)
l	liter
M	mol
M*	intermediate
mA	mili amper
mg	miligram
min	minute
ml	mililitre
mM	milimol
MOPS	3-(N-Morpholino)propan Sulfonsäure
mRNA	messenger RNA
ng	nanogram
nm	nanometer
NS	neuroserpin
OD	optical densitiy
PAGE	polyacrylamide gel electrophoresis
PAI-1	plasminogen activator inhibitor-1
PBS	phosphate buffered saline
PBST	phosphate buffered saline with Tween
PCR	polymerase chain reaction
PD	Parkinson's disease
PERK	double-stranded RNA-activated protein kinase (PKR)-like ER kinase

pH	potentia hydrogenii
PI12	Proteinase Inhibitor 12
PVDF	polyvinylidene fluoride
qPCR	quantitative polymerase chain reaction
R	realtive expression ratio
RCL	reactive center loop
RNA	ribonucleic acid
RNA	ribonucleic acid
rpm	round per minute
RT	room temperature
rt-PCR	reverse transcriptase polymerase chain reaction
SDS	sodiumdodecyl sulfate
SDS	sodium dodecyl sulfate
sec	seconds
SP	signal peptide
STD	standard deviation
TBS	tris buffered saline
TEMED	N',N'-tetramethylethylenediamine
Tm	annealing tempertature
T_m	melting tempertur
TMB	(3,3´,5,5´-Tetramethylbenzidine
tPA	type plasminogen activator
U	unit
uPA	urokinase-type plasminogen activator
UPR	unfolded protein response
UPS	Ubiqutin proteasome system
UPS	Ubiqutin proteasome system
UV	ultra violet
V	volt
v/v	volume per volume
w/v	weight per volume
WT	wild-type
ZMNH	Zentrum für Molekulare Biologie Hamburg

8.2 List of figures

8.3 List of tables

9. Acknowledgments

First, I would like to thank Prof. Markus Glatzel for giving me the opportunity to work in his Lab. Thank you for the support and the nice atmosphere. Furthermore, I want to thank Prof. Christian Voigt for being my second reviewer.

Second, I would like to thank the evaluation committee for kindly accepting to evaluate my thesis.

Additionally, I would like to especially thank the people involved in this work as well as the collaborators, namely Prof. David Lomas (Cambridge Institute for Medical Research, University of Cambridge, Cambridge, United Kingdom), Dr. Stefan Marciniak (Cambridge Institute for Medical Research, University of Cambridge, Cambridge, United Kingdom), Dr. Elena Miranda (Departamento Biologia e Biotecnologie, Università di Roma La Sapienza, Roma, Italy), Prof. Fred van Leeuwen (Maastricht University, Department of Neuroscience, 6229ER Maastricht, The Netherlands), Dr. Michaela Schweitzer (Morphological Service Unit of the ZMNH, Hamburg; [Fig. 14]), Prof. Christian Hagel (Institute of Neuropathology, UKE, Hamburg; [Fig. 18]), Dr. Markus Geissen (Klinik und Poliklinik für Gefäßmedizin, UKE, Hamburg), the diagnostic team of Martin Haberkorn (Institute of Neuropathology, UKE, Hamburg) and Andreas Suellau (Animal Facility, UKE, Hamburg).

Additionally, I would like to thank Prof. Thomas Braulke as well as the research training group 1459 “Sorting and Interactions Between Proteins of Subcellular Compartments” for supporting my PhD training.

To all past and present members of the Glatzel Lab: thank you for being such great colleagues! I had lots of fun working with you! Thanks guys!

Last but not least and more than anything I would like to thank my family, friends and my fiancée, without whom I could not have done this. Thanks for always being there when I need you!